

2. SITE 893¹

Shore-based Scientific Party²

HOLE 893A

Date occupied: 20 November 1992
Date departed: 21 November 1992
Time on hole: 8 hr, 15 min
Position: 34°17.25'N, 120°02.19'W
Bottom felt (rig floor; m, drill-pipe measurement): 588.0
Distance between rig floor and sea level (m): 11.5
Water depth (drill-pipe measurement from sea level, m): 576.5
Total depth (rig floor; m): 784.5
Penetration (m): 196.5
Number of cores (including cores with no recovery): 21
Total length of cored section (m): 196.5
Total core recovered (m): 204.9
Core recovery (%): 104
Oldest sediment cored:
Depth (mbsf): 196.5
Nature: hemipelagic; laminated to nonlaminated silt and clay
Age: Quaternary (~150,000 yr)

HOLE 893B

Date occupied: 21 November 1992
Date departed: 21 November 1992
Time on hole: 5 hr, 25 min
Position: 34°17.25'N, 120°02.20'W
Bottom felt (rig floor; m, drill-pipe measurement): 588.2
Distance between rig floor and sea level (m): 11.5
Water depth (drill-pipe measurement from sea level, m): 576.7
Total depth (rig floor; m): 657
Penetration (m): 68.8
Number of cores (including cores with no recovery): 21
Total length of cored section (m): 68.8
Total core recovered (m): 73.5
Core recovery (%): 107
Oldest sediment cored:
Depth (mbsf): 68.8
Nature: hemipelagic; laminated to nonlaminated silt and clay
Age: Quaternary (~70,000 yr)

Principal results: Site 893 is located at 34°17.25'N, 120°02.2'W, on the floor of the Santa Barbara Basin, California, 20 km south of the Santa Barbara coastline at a water depth of 576.5 m. For the first time in ocean scientific drilling, a continuously cored Quaternary sequence has been obtained from the southern California borderland province. Modern and Holocene hemipelagic sedimentary sequences in the Santa Barbara Basin were deposited in low-oxygen environments. During the late Quaternary, an absence of burrowing organisms allowed the preservation of annual laminations caused by seasonal changes in sediment supply and character. The sediments are rich in organic carbon and microbial methane. Gas voids developed in the cores upon retrieval, but the quality and continuity of the cores was good to excellent, as voids developed largely along bedding planes.

The sequence at Site 893 represents deposition at high sedimentation rates in suboxic to oxic conditions and contains diatoms, radiolarians, foraminifers, and pollen in sufficient abundance, thus providing an important opportunity for high- to ultra-high-resolution paleoclimatic/paleoenvironmental investigations in the late Quaternary. Studies of the stable isotopes and the geochemical and micropaleontological properties will provide critical information within the context of global climatic change and the roles of the ocean in the global carbon cycle.

Hole 893A recovered a total of 21 advanced hydraulic piston cores (APC) to a depth of 196.5 m below seafloor (mbsf), and Hole 893B a total of 8 APC cores to a depth of 68.8 mbsf. The upper Quaternary sequence at Site 893 is composed primarily of olive gray silt and clay with variable biogenic components of diatoms and calcareous nannofossils. Because no major changes in bulk sediment composition were present, only one lithostratigraphic unit was recognized. This unit has been divided into six subunits based upon differences in sedimentary facies, primarily on the degree of lamination of the sediment. Laminated intervals are inferred to have been deposited at times of low-oxygen concentrations in bottom waters, whereas fully homogenized sediment intervals were deposited during well-oxygenated conditions. The laminated sequences are marked by higher abundances of biogenic material, especially calcareous nannofossils in the upper laminated sequence and diatoms throughout. Thin sand beds, interpreted as turbidites, occur at various intervals, but they are noticeably absent in the upper and lower laminated sequences. Conversely, thin gray clayey silt to silt clay layers are common in the laminated sequences. Two broadly similar sedimentary cycles are apparent, which consist in each case of a lower, intermittently laminated interval passing upward with decreasing abundance of laminations into a relatively thin homogeneous interval. This homogeneous (totally nonlaminated) interval is then succeeded abruptly by a thin interval of relatively continuous, well-laminated sediment.

Preliminary studies of the pollen content and the planktonic foraminifer biostratigraphy indicate that Site 893 sediments range from near the base of Isotope Stage 6 (~150,000 ka) to the present day. The sequence, therefore, includes two glacial maxima (Stages 6 and 2) and two interglacial episodes (Stages 5 and 1).

Changing oxygen conditions in the basin, as inferred from the degree of bioturbation and the strength and persistence of the laminations, correspond with distinct changes in the benthic foraminifer assemblages. Laminated sedimentary sequences are associated with low-diversity benthic foraminifer assemblages, dominated by *Bolivina*, and they reflect very low oxygen levels at the ocean floor. Well-homogenized sediments are associated with more diverse benthic foraminifer assemblages—those generally lacking in *Bolivina* and *Uvigerina* and including a number of rotaliid taxa.

¹ Kennett, J.P., Baldauf, J.G., et al., 1994. *Proc. ODP, Init. Repts.*, 146 (Pt. 2): College Station, TX (Ocean Drilling Program).

² Santa Barbara Basin group participants include Jack Baldauf, Richard Behl, William Bryant, Michael Fuller, Kurt Grimm, Linda Heusser, Alan Kemp, James Kennett, Carina Lange, Steve Lund, Russell Merrill, Fabrice Olivier, Evelyn Polgreen, Lisa Pratt, Frank Rack, Arndt Schimmelmann, Martha Schwartz, Niall Stowey, Rüdiger Stein, and Jürgen Thurow.

Intermittently laminated sedimentary sequences are typically associated with assemblages intermediate in character.

The sedimentary cycles and associated changes in the benthic foraminifer assemblages appear to correspond closely with glacial/interglacial oscillations during the last 150,000 yr. Each sedimentary cycle represents a progressive dominance of fully oxygenated basin waters culminating in a period of sustained basin oxygenation (Stages 6 and 2). The fully oxygenated intervals are then terminated by an abrupt return to a sustained period of low-oxygen conditions that promote lamina preservation during Stages 5 and 1. Thus, global paleoclimatic cycles are reflected by lithofacies and biofacies changes in the Santa Barbara Basin that are largely modulated through changes in oxygen concentrations.

The changes in basinal oxygen concentrations resulted from changing interplay between biogenic productivity, the depth and strength of the Oxygen Minimum Zone in relation to the basin sill depth, and changing oxygen concentrations in Pacific Intermediate Waters at the southern California continental margin. Preliminary evidence suggest that the changes in oxygen concentration of Pacific Intermediate Waters during the Quaternary were largely responsible in controlling the cycles of oxygenation/dysaerobia in the Santa Barbara Basin.

Glacial/interglacial fluctuations in the planktonic foraminifer assemblages at Site 893 range from cool temperate during the interglacial episodes to lower diversity subarctic assemblages during the glacial episodes. Surface-water temperatures in the Santa Barbara Basin during glacial maxima were as low as $\sim 8^{\circ}\text{C}$. Cooler conditions during the glacial episodes are reflected by a dominance of coniferous pollen; warmer, interglacial episodes by an abundance of oak pollen.

Small fragments of tar occurring throughout the sedimentary sequence reflect past natural oil seepages in the region. A distinct 3-mm-thick, tar-saturated layer at ~ 110 mbsf may represent a major oil seepage event. Small charcoal fragments in Site 893 are evidence for past forest fires in the coastal region.

BACKGROUND AND SCIENTIFIC OBJECTIVES

The Santa Barbara Basin (Fig. 1) is a semi-enclosed basin on the southern California continental margin with a maximum depth close to 600 m. Quaternary sediments throughout the basin are flat lying and structurally uncomplicated to the depth of penetration of the air gun (300–600 m). Site 893 ($34^{\circ}17.25'N$; $120^{\circ}02.2'W$) is positioned on the floor of this basin 20 km south of the Santa Barbara coastline, at a water depth of 576.5 m. This site was positioned toward the north of the basin as well as north of the shipping lanes that run through the Santa Barbara Channel between the southern California mainland and Santa Rosa Island. A continuous advanced hydraulic piston corer (APC) sequence was obtained to 196.5 m below the seafloor (mbsf) in Hole 893A and to 68.8 mbsf in Hole 893B (Table 1).

The Santa Barbara Basin contains suboxic (<0.1 mL/L oxygen) bottom waters deeper than sill depth at ~ 475 m. This bottom water is replaced by waters from the Oxygen Minimum Zone off California, with occasional partial turnover at a rate that prevents total stagnation (Sholkovitz and Gieskes, 1971). The small supplies of oxygen entering the basin are largely depleted through oxidation of the abundant organic material derived from the highly productive surface waters. Surface sediments in the basin are anoxic muds, containing hydrogen sulfide, that lack burrowing organisms. An absence of burrows in Holocene sediments allows the preservation of annual laminations caused by seasonal changes in the sediment supply. Bacterial mats on the basin floor also assist in stabilizing the surface sediments; in addition, they provide a framework for sediment accumulation and the preservation of annual laminations (Soutar and Crill, 1977). Hence, in combination with the high sedimentation rates (~ 10 cm/100 yr), it is possible to resolve decadal paleoclimatic changes and even inter-annual to annual climatic changes in parts of the Holocene. At depths approximately above that of the sill, in contrast, water is oxygenated and sediments are homogenized as a result of bioturbation.

The Santa Barbara Basin is the only basin in the California Borderland Province (Fig. 2) that exhibits persistent laminations throughout the Holocene, reflecting the near-zero oxygen levels in its bottom waters and the seasonal differences in local and regional meteorology (Emery and Hülsemann, 1960; Soutar, 1975; Sholkovitz and Soutar, 1975; Soutar and Crill, 1977; Pisias, 1978; Dunbar, 1981; Soutar et al., 1981; Lange et al., 1987, 1990; Schimmelmann et al., 1990, 1992; Schimmelmann and Tegner, 1991). The combination of seasonal runoff from land and seasonal surface productivity results in an accumulation of annual pairs of laminae within individual varves. Average varve thickness during the last 140 yr is ~ 2 mm (with a range between 1.1 and 3.8 mm). Each of the varves consists of a light and dark lamination (Fleischer, 1972; Soutar, 1975). The dark laminae are formed as a result of terrigenous sediment input caused by winter rains. The rate of sedimentation seems to be independent of temperature, but it is highly correlated with rainfall and rate of tree growth as determined by tree-ring studies (Soutar and Crill, 1977). The thickness of the varves is highly correlated with annual rainfall in southern California and hence can be used as an indirect tracer for annual rainfall. It is generally thought that the light laminae reflect the spring plankton bloom. However, Soutar and Crill (1977) found that the thickness of the dark and light laminae are directly related. From this, they suggested that the formation of the laminae is a result of the interaction of the seasonal rate of deposition and the growth of a *Beggiatoa* filamentous bacterial mat on the surface sediments. The growth of the mat may provide an open matrix into which the sediment particles fall and are subsequently trapped (see Grant [1991] for a review). An increase in bacterial biomass during late summer/early fall is a response to changing redox conditions in the basin's surface sediments. Reimers et al. (1990) found that oxygen supply varies seasonally in response to bottom-water changes induced by spillover into the basin. These investigators suggest that the light-colored laminae, which also contain abundant diatoms, formed during late summer and early fall. The dark laminae, in contrast, formed during winter and early spring, during times of low biomass and high terrigenous input.

Table 1. Coring summary, Site 893.

Core	Date (Nov. 1992)	Time (UTC)	Depth (mbsf)	Cored (m)	Recovered (m)	Recovery (%)
146-893A-						
1H	20	2155	0–6.5	6.5	6.57	101
2H	20	2225	6.5–16.5	9.5	10.08	106
3H	20	2250	16.5–25.5	9.5	10.20	107
4H	20	2310	25.5–35.0	9.5	10.17	107
5H	20	2330	35.0–44.5	9.5	9.60	101
6H	20	2345	44.5–54.0	9.5	10.23	108
7H	21	0000	54.0–63.5	9.5	10.34	109
8H	21	0020	63.5–73.0	9.5	10.37	109
9H	21	0040	73.0–82.5	9.5	10.50	111
10H	21	0100	82.5–92.0	9.5	10.12	107
11H	21	0125	92.0–101.5	9.5	8.81	93
12H	21	0155	101.5–111.0	9.5	10.08	106
13H	21	0215	111.0–120.5	9.5	10.30	108
14H	21	0250	120.5–130.0	9.5	10.00	105
15H	21	0315	130.0–139.5	9.5	10.17	107
16H	21	0345	139.5–149.0	9.5	10.16	107
17H	21	0420	149.0–158.5	9.5	9.70	102
18H	21	0450	158.5–168.0	9.5	9.85	104
19H	21	0515	168.0–177.5	9.5	9.25	97
20H	21	0545	177.5–187.0	9.5	9.62	101
21H	21	0610	187.0–196.5	9.5	8.79	93
146-893B-						
1H	21	1130	0–2.3	2.3	2.34	102
2H	21	1450	2.3–11.8	9.5	9.84	104
3H	21	1520	11.8–21.3	9.5	10.14	107
4H	21	1540	21.3–30.8	9.5	10.11	106
5H	21	1600	30.8–40.3	9.5	10.18	107
6H	21	1615	40.3–49.8	9.5	10.09	106
7H	21	1635	49.8–59.3	9.5	10.47	110
8H	21	1655	59.3–68.8	9.5	10.29	108

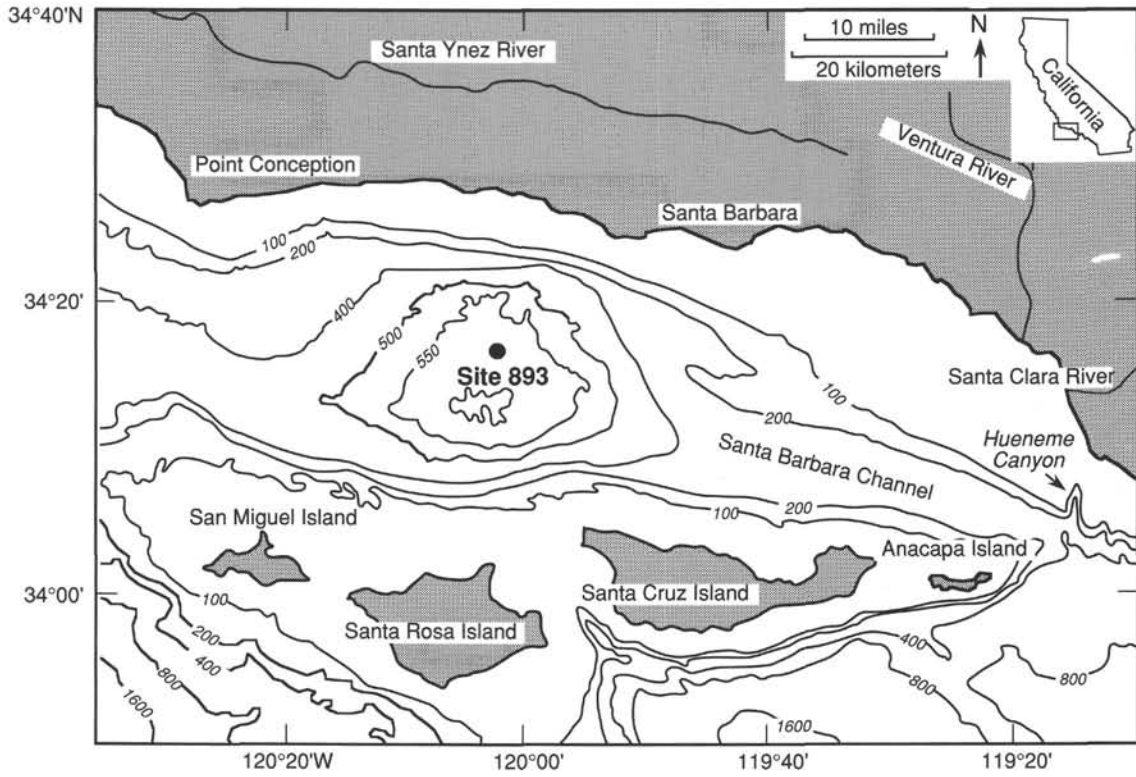


Figure 1. Map of the Santa Barbara Basin and location of Site 893. Inset shows location of enlarged view of California coast. Contours are in meters.

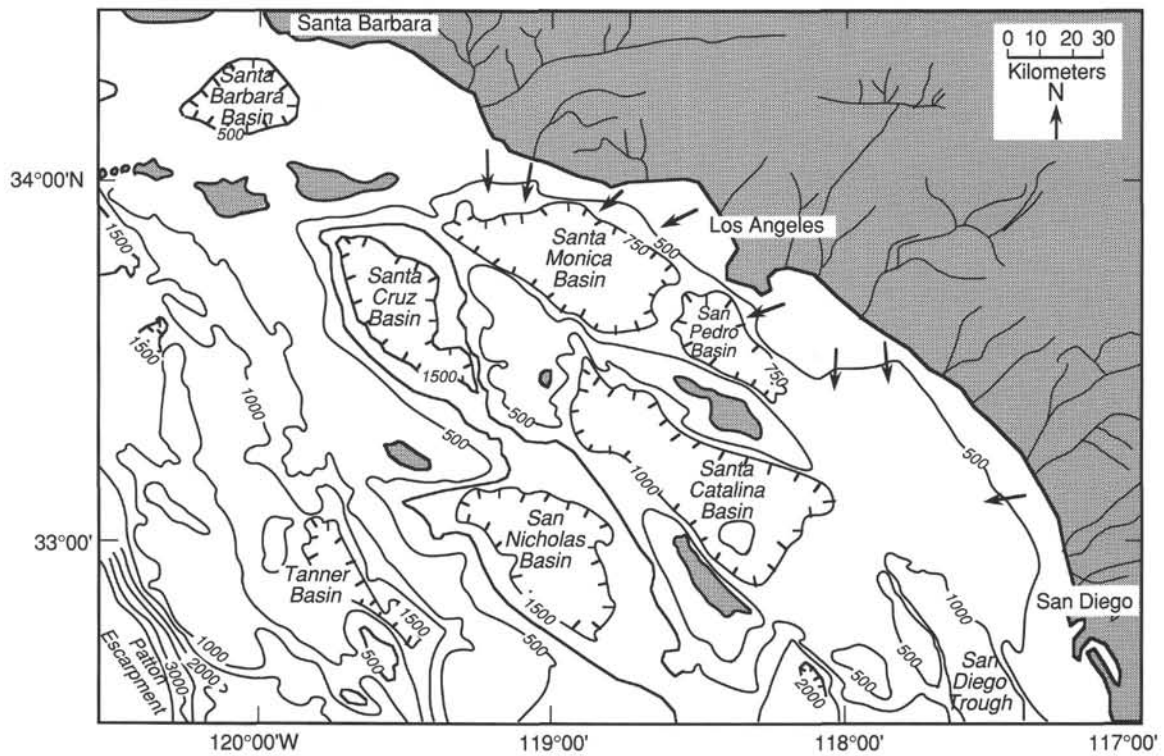


Figure 2. Regional map of the California Continental Borderland showing major basins, coastal drainage, and important submarine canyons (arrows). Contours indicate water depths in meters.

The varves form distinct stratigraphic patterns that can be correlated between cores within the Santa Barbara Basin (Soutar and Crill, 1977; Schimmelmann et al., 1990; Baumgartner et al., 1991).

Sediments recovered from the Santa Barbara Basin are important to further our understanding of climate in that they provide a rare oceanic record of climate change on time scales of a thousand years or less. In addition, Site 893 represents one of only a few sites in the world ocean in which sediments accumulated rapidly and with minimal disturbance so that a high-resolution record of climate was preserved in the geological record. For example, Soutar and Crill (1977) and Baumgartner et al. (1989) have correlated the local tree ring and Santa Barbara Basin varve records with historical precipitation records of the Santa Barbara Basin area.

Strong evidence exists that the sedimentary record in the basin may also reflect Pacific-wide fluctuations in oceanic and atmospheric conditions (Pisias, 1979; Dunbar, 1983). Decoding this record requires the development of explicit strategies for combining paleoclimatic indicators of varying precision that monitor different elements of the system. In this region, changes in oceanic circulation and water masses, including El Niño/Southern Oscillation (ENSO) events, strongly influence sea-surface temperatures, plankton composition, productivity, and rainfall. Seasonally varying precipitation is responsible for pulses of terrigenous sediment input, and regional changes in wind patterns affect seasonal changes in oceanic upwelling and productivity.

The modern basin benthic foraminifer assemblages exhibit drastic responses in relation to changes in oxygen concentrations in bottom waters (Lutze, 1964; Bernhard and Reimers, 1991). Thus, downcore changes in benthic foraminifer assemblages are expected to provide critical information about changes in the oxygenation state of basin waters during the late Quaternary.

Previous studies of the upper Quaternary sediments from the Santa Barbara Basin are confined to Holocene age sediments. Only two studies of the sediments of the Santa Barbara Basin focused on paleoclimatic records on time scales of 1000 yr or greater. Pisias (1978, 1979) documented paleoclimatic-paleoceanographic changes based on radiolarian assemblages, whereas Heusser (1978) documented changes in pollens and spores.

Pisias (1978) studied a core from the center of the Santa Barbara Basin. Age assignments were made by calculating accumulation rates based on varve counts in parts of the core. Pisias used radiolarian assemblages as a tracer of sea-surface temperature (SST) changes. He calibrated this tracer by comparing radiolarian assemblages at different sediment sites in the region with prevailing surface-water temperatures using the transfer function method (Imbrie and Kipp, 1971). Thus, he produced a record of radiolarian-based sea-surface temperatures for the past 8000 yr. This study demonstrated that significant paleoclimatic/paleoceanographic changes occurred during the Holocene.

Pisias (1979) used his data to calculate changes in the intensity of the California Current over the past 8,000 yr. He argued that the dynamic height anomaly in this area is closely related to SSTs and demonstrated that SSTs off southern California are regionally correlated. Using these two arguments, he extrapolated from a paleotemperature record at one core site (base data set) to produce a map of dynamic height anomalies and hence the character of the California Current in the region at particular time slices. Thus, Pisias (1979) was able to show, using extrapolated dynamic height maps, that the relative strengths of the cold southward-flowing California Current and the warm northward-flowing Davidson Current varied temporally and were out of phase with each other during the last 8000 yr.

The Santa Barbara Basin is ideally located to amplify global climate changes that occurred during the Quaternary. The range of estimated temperatures (12°C) in the Holocene exceeds that of the historical temperature measurements for February, but it is less than the observed range for the broader California Current region (Pisias, 1979). The climate of the area was dominantly warm (subtropical) from 8000 to 5400 yr ago and marked by warm SSTs, increased rainfall, and reduced southerly flow of the California Current. Pollen analyses from

the same core indicate a humid climate during this time in southern California (Heusser, 1978). Since 5400 yr ago, the area was cooler and underwent relatively large climatic fluctuations with a tendency for strengthening of the California Current system (Pisias, 1978).

A number of investigations on piston cores from the Santa Barbara Basin have dealt with the paleoclimatic history at high resolutions within the last 300 yr (Soutar and Crill, 1977; Dunbar, 1983; Weinheimer et al., 1986; Schimmelmann and Tegner, 1991). A number of these are pioneering, such as the study by Kennedy and Brassell (1992a, 1992b) in which a time series (1910–1987) of C₃₇ alkenones, from bulk sediment, provided a SST history that included reconstruction of El Niño events. Historic El Niño events between 1940 and 1987 are recorded in the sediment sequence by diagnostic warm-water diatom assemblages that migrated from the south (Lange et al., 1987, 1990). Relationships between fish productivity (using the fish-scale record in sediments) and climatic change are discussed by Baumgartner et al. (1992).

Dunbar (1983) produced a foraminifer oxygen isotope record of 230 yr from a box core. The 1-cm sampling strategy that he employed produced a resolution of 2 yr in the upper 20 cm of the core and a 5-yr resolution below this level. For example, the oxygen isotopic record for the planktonic foraminifer *Globigerina bulloides* exhibits good correlation with the historical record of SST in the area since 1870. The potential resolution of the climatic variation in the varved sediments is annual or even seasonal (Dunbar, 1983), allowing comparisons with modern historical records and oceanographic measurements. The amplitude of the oxygen isotopic signal is large (1.5%) and partly reflects the large temporal and seasonal variability of SSTs caused by upwelling and ENSO events. However, Dunbar (1983) noted that the isotopic range is greater than expected from historical temperature records being amplified by seasonal and/or annual differential production of *G. bulloides*. The isotopic records clearly reflect a prolonged cool period from 200 to ~230 yr ago equated with the Little Ice Age. Also of significance is a distinct post-1930 warming interval. Although Dunbar's study is temporally limited, it demonstrates that reliable records of temperature, the most critical paleoclimatic and paleoceanographic parameter, can be recovered from fossil foraminifers.

Studies of Site 893 are pioneering because no pre-Holocene sediment sequence has previously been obtained from the Santa Barbara Basin. However, the studies of the Holocene record indicate the potential of very high-resolution studies, even in bioturbated sediments of Pleistocene age. The Quaternary sediments contain diatoms, radiolarians, foraminifers, and pollen in sufficient abundance to provide an important opportunity for high-resolution paleoclimatic/paleoceanographic investigations for the late Quaternary. Studies of the stable isotopes as well as of the geochemical and micropaleontological properties will be of considerable value in providing critical information within the context of global climatic change and the role of the ocean in the global carbon cycle. Sediments from Site 893 were retrieved to conduct high-resolution studies for the late Quaternary.

Specific scientific objectives include:

1. examining the paleoclimatic history of the Santa Barbara basin region for the last 150,000 yr;
2. determining the response of this coastal region to local and global climate variation, including paleoproductivity;
3. documenting the variations in organic carbon, silica, and carbonate production as well as their preservation and diagenesis;
4. examining the biota preserved in the sediments to develop an integrated biostratigraphy and to determine the response of the faunas and floras to oceanographic, climatic, and tectonic changes;
5. investigating variations in the paleomagnetism of the sediments to develop a magnetostratigraphy, to determine the magnetic diagenesis of the sediments, and to examine secular variation; and
6. examining changes in the physical properties of sediments to develop sediment flux models and to investigate the postdepositional processes.

Such information is crucial to scientists working on the global carbon cycle. The annual layering of sediments allows earth scientists to sample oceanographic variations, including El Niño episodes, at a frequency rarely accessible. In addition, the results of Santa Barbara Basin coring may be integrated with tree-ring and other nearby continental climate reconstructions to understand coupled ocean-continents changes relevant to global environmental change.

This sediment record will also allow high-resolution studies of late Quaternary current strength, productivity, and other variations caused by sea-level and global climatic changes, including the effect of sunspot cycles (11 yr) and other solar cycles. A tie-in to deep-sea stratigraphy would greatly enhance our knowledge about the history of coastal upwelling in the Milankovitch time scale. This knowledge is necessary for the proper understanding of changes in the carbon dioxide content of the atmosphere as seen in ice cores. Valuable data related to the nature of organic carbon preservation, the diagenesis of silica and phosphate, and fluid flow in the borderland basins will also be provided by investigations of Site 893. Santa Barbara Basin sediments may provide an analog for understanding hydrocarbon generation and diagenesis in older organic-rich deposits such as the Miocene Monterey Formation. Early diagenesis of sulfur-rich kerogen that generates petroleum at substantially lower temperatures than typical marine kerogen can also be traced. A study of the role of chemosynthetic communities in carbon cycling and storage may help to understand periods of ocean history when these organisms were more widespread.

GEOLOGIC AND OCEANOGRAPHIC SETTING

The Santa Barbara Basin is a tectonic depression that constitutes the submerged southwestern part of the Transverse Ranges Province. The area is commonly referred to as the Santa Barbara Channel, and the basin is approximately 600 m deep. The basin itself consists of a very thick (>2000 m), uncomplicated, flat-lying sequence of Quaternary sediments (see "Site geophysics" section, this chapter). The sill

depth to the west of the basin is only 475 m deep, and lies within the oxygen minimum zone; hence, waters in the deeper parts of the basin are dysaerobic, leading to organic carbon preservation and to a general lack or reduction in bioturbation in the Holocene.

The dominant hydrographic features of the Santa Barbara Basin are the California Current and related countercurrents (Fig. 3; see Hickey [1992] for review). These currents control the water masses and circulation in the region and supply the nutrients necessary to maintain high biological productivity. The character and distribution of the cold California Current and nearshore warmer countercurrent (Davidson Current) are determined by ocean-atmosphere interactions over broad areas of the Pacific Ocean; in addition, they reflect the effects of present-day and past climatic variations (Douglas, 1981). A dominant feature of the surface circulation in the Santa Barbara Basin is a semipermanent cyclonic gyre that incorporates water from both the northwest and southeast (Fig. 3).

Seasonal variations in the California Current system are primarily responses to changes in wind strength and direction. Northerly winds are generally strongest between April and August (spring and summer), causing strong flow of the cold California Current toward the equator, and weak cyclonic flow into the Santa Barbara Basin. Conversely, from December to February, when the northerly winds weaken, the Davidson Current is stronger and a net poleward surface transport occurs along the coast (Pisias, 1978). This northward flow produces warmer surface-water temperatures during the winter than in the summer in the Santa Barbara region.

Seasonal changes in the strength and direction of the winds influence the intensity of upwelling near Point Conception and, in turn, biological productivity in the Santa Barbara Basin. Upwelling is strongest during the spring and summer months at times of strongest northerly winds (McGowan, 1984). The upwelled water is cold, oxygen poor, and nutrient rich in comparison with the surface waters. The upwelling of cold waters during summer and the increased northward flow in winter of the relatively warm Davidson Current

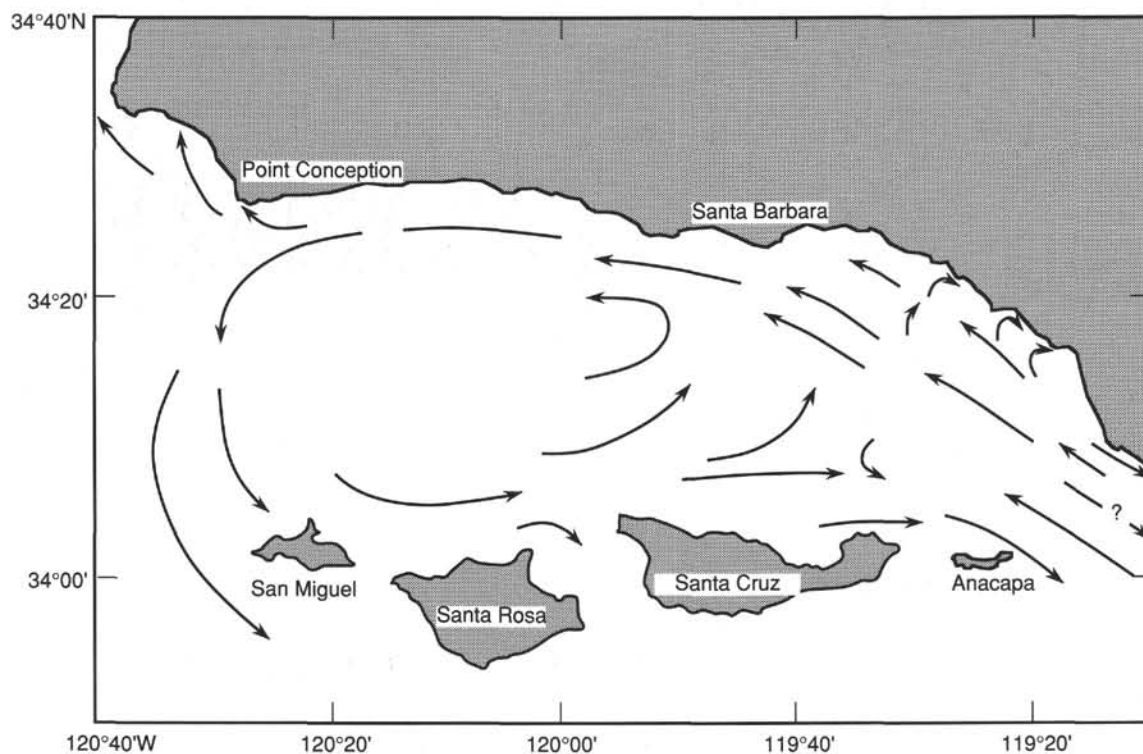


Figure 3. Map illustrating the cyclonic gyre surface circulation in the Santa Barbara Basin area. The northward-flowing Davidson current is prominent at this time of year (data taken from January 1970). Modified from Kolpack (1971).

reduces the annual temperature range in the surface waters, although this is still high at 12°C (Pisias, 1979).

Low-frequency, supra-seasonal variations in sea-level height (dynamic height) along the southern California coast correlate closely with SST anomalies in the eastern tropical Pacific. These, in turn, are related to southward or northward transport within the California Current. Low sea-level anomalies result from increased southerly flow, and high sea-level anomalies with increased northerly flow. Periods of intensification of the Davidson Countercurrent are related to ENSO events that affect the entire eastern Pacific and typically occur at intervals of ~5 to 7 yr (Enfield and Allen, 1980; Douglas, 1981). In the region of the Santa Barbara Basin, these warm events coincide with episodes of decreased plankton productivity and reduced southerly flow of the California Current. The warmer events are often associated with anomalously high rainfall in southern California (Namias, 1969). In the southern California borderland region, surface waters of several sources are mixed in varying proportions, creating rapid biogeographic gradients in planktonic assemblages. Large temporal changes that occur in the surface waters are reflected by changes in the planktonic microfossil assemblages. The planktonic microfossil assemblages that have not been mixed by bioturbation during the Holocene provide high-resolution markers for paleoceanographic change.

Rainfall in the region is seasonal, occurring almost entirely during winter storms. As a consequence, river runoff takes place almost exclusively during the winter months. Some of the associated flood sediment is transported to the basin by way of the water column, as demonstrated by Soutar and Crill (1977) and not simply as gravity flows. During historic times, abnormally high precipitation in southern California has often been associated with warm surface waters that contribute more water vapor to the atmosphere (Pisias, 1978). In contrast, dry conditions occur during times of cool surface water (Namias, 1969).

A thorough review of the available data on the biological, chemical, and physical oceanography of the Santa Barbara Basin and the Southern California Bight is in Eppley (1986). One set of observations is particularly relevant to the proposed investigations. Since the mid-1950s, data on hydrography, biology, chemistry, and meteorol-

ogy has been collected regularly at CALCOFI Station 82.47 to the west of the basin near Point Conception. The availability of such long-term data sets and the wealth of other data from the area make the Santa Barbara Basin especially desirable as a site for late Quaternary paleoceanographic and paleoclimatic investigations.

OPERATIONS

The vessel steamed away from Leg 146 (Site 892) until the seismic gear had been streamed and tested, then turned and crossed the approximate position of Hole 892B on a west-southwesterly heading. After the single short tie-in seismic line had been shot, the gear was retrieved, and the ship turned south at full speed.

Favorable weather conditions prevailed during the transit down the Oregon and California coasts. Strong following winds developed during the second day, boosting the ship's speed to over 12 kt for some time. At 0600 hr, 20 November 1992, the vessel rounded Point Conception and entered the Santa Barbara Channel. The average speed for the voyage was 11.4 kt. A brief precision depth recorder (PDR) survey over the area of Site 893 began at 0930 hr, and the ship stopped at the chosen location at 1030 hr. Thrusters and hydrophones were lowered while the position was refined. Assembly of the bottom-hole assembly (BHA) had begun before the positioning beacon was launched at 1130 hr.

Site 893 (proposed Site SB-1A) is located at 34°17.0'N, 120°02.2'W near the center of the Santa Barbara Basin. Sediments in the Santa Barbara Basin are flat lying and structurally uncomplicated to a depth of air-gun penetration of about 500 m (Fig. 4). The site location approximates the position of cross-line data (lines 92-4-3 and 92-4-6) of both single-channel and 3.5-kHz seismic data from the *Farnella* provided by the U.S. Geological Survey (Figs. 5–9).

Site 893 (Proposed Site SB-1A)— Santa Barbara Basin

The final site of Leg 146 was dedicated to objectives that were distinctly different from those of the Cascadia Margin sites. All

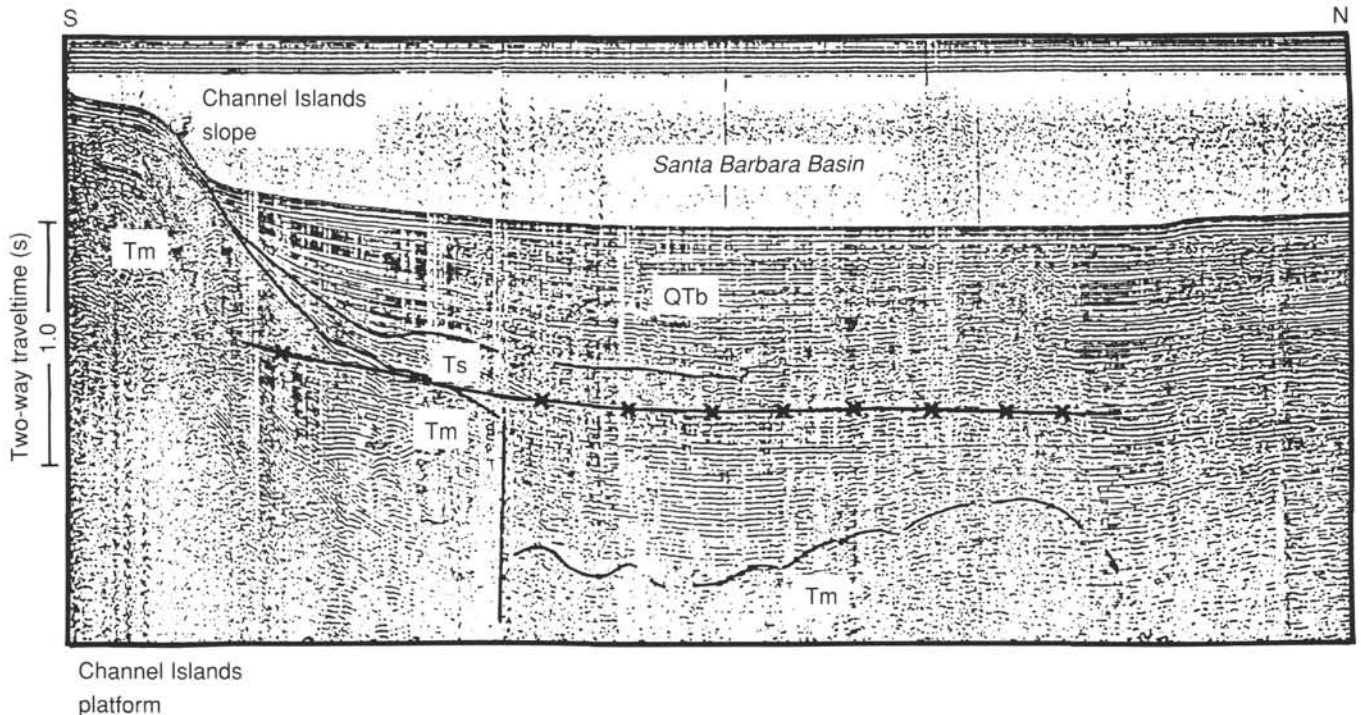


Figure 4. North to south seismic Profile K-652 across the eastern edge of the Santa Barbara Basin. See Figure 1 for location of profile. From Junger (1979).

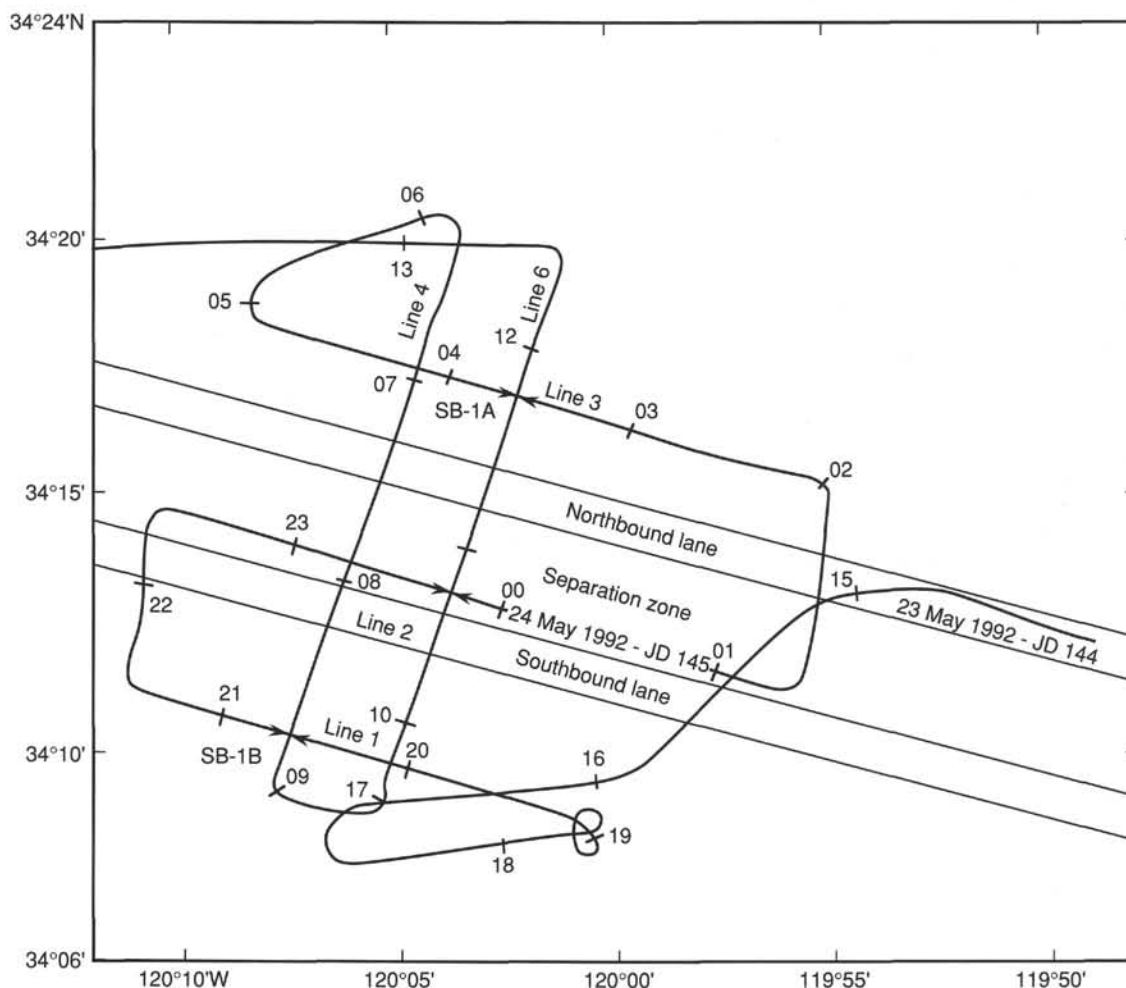


Figure 5. Location of Site 893 (proposed Site SB-1A) and proposed alternates in relation to shipping lanes and pre-cruise site survey tracklines from *Farnella* Cruise 92-4.

remaining operating time, about 24 hr, was to be used for APC-coring of upper Quaternary hemipelagic sediments in the floor of the Santa Barbara Basin for high-resolution paleoenvironmental studies. Because the area is adjacent to a commercial hydrocarbon province, penetration was limited to 200 m or APC refusal depth, whichever would be reached first.

Hole 893A

Hole 893A was spudded at 1345 hr with an APC core "shot" from 3 m above the corrected PDR depth of 588.2 m (from the rig floor). Core recovery of 6.57 m proved the PDR to be accurate. The basinal sediments were easy to core, and the hole reached 196.5 mbsf without approaching refusal conditions. Full stroke was achieved on all cores, and the maximum overpull of 40K lb was recorded on the final core. Core recovery exceeded 100% because the sediment contained a large amount of biogenic methane. The cores exhibited high gas pressure upon arrival on deck. Thus, the core liners had to be vented (by drilling small holes in the plastic casing) before they could be cut to avoid excessive loss of core. This, in turn, caused voids that disrupted the continuity of the sedimentary sequence.

When the final core had been recovered, the hole was filled with 12 lb/gal mud. Because of the shallow hole depth, the top drive was left in the string and the bit was "doubled out" to clear the seafloor.

Hole 893B

The ship was offset for a new location 10 m northwest of Hole 893A, and the APC corer was deployed for the initial core of the second hole. The bit was positioned 4 m higher to provide maximum vertical offset of core tops between the holes. All parameters were normal as the mud-line core was shot, but the APC became stuck and could not be pulled free with the coring line for retrieval.

Unsuccessful efforts to jar the APC loose took 1 hr. The exact nature of the problem was unclear, as the core barrel could have been bent during the spud-in attempt or the upper portion of the APC could have been stuck in the landing/saver sub (LSS) or the seal-bore drill collar. In either case, a round trip was required to correct the problem. Because of the shallow water, only 2 hr was required to bring the outer core barrel (OCB) assembly to the rig floor. It was then discovered that the landing shoulder of the APC was jammed hard into the restricted portion of the LSS. Efforts to free the APC from the sub were unsuccessful; thus, it was necessary to cut the sub away with a torch. With the sub replaced and the APC redressed, the bit was run back to the seafloor for continued coring.

Eight cores were recovered in the next 2½ hr before time ran out at 68.8 mbsf. The hole was filled with heavy mud before the final pipe trip of the leg was made. The vessel departed Site 893 at 1215 hr, 21 November 1992.

The *JOIDES Resolution* continued to the east end of the Santa Barbara Channel, turned south between Anacapa Island and the coast, and approached San Diego by passing between Santa Catalina and San Clemente islands. The ship docked at Berth 4, 10th Street Terminal, Port of San Diego, at 0720 hr, 22 November 1992.

LITHOSTRATIGRAPHY

The upper Quaternary sequence recovered at Site 893 is primarily composed of terrigenous silt and clay with variable biogenic contributions of calcareous nannofossils and diatoms. Much of the sediment is laminated; these laminations are preserved to varying degrees and occur principally within several restricted intervals. Because no major changes are present in the bulk sediment composition, the sediments at Site 893 are considered to form one lithostratigraphic unit. This stratigraphic sequence is divided into subunits on the basis of the sedimentary structure, primarily the presence or absence of lamination (Fig. 10). The lithostratigraphy of Holes 893A and 893B can be correlated in detail on the basis of lamination and bedding patterns (Fig. 11). This correlation is not linear, however, because of numerous, heterogeneously distributed, gas expansion voids. The descriptions given below and in the barrel sheets are intended as a guide to the average composition of the sediments; however, significant small-scale variations in composition occur over meter to submillimeter scales.

Unit I

Intervals: Core 146-893A-1H through Section 146-893A-21H-CC
Depth: Hole 893A, 0–196.5 mbsf; Hole 893B, 0–68.8 mbsf
Age: Holocene to latest Pleistocene

The sediments recovered at Site 893 are mainly olive gray (5Y 4/2) silty clay to clayey silt with subordinate quantities of diatoms and nannofossils (generally 5%–30%) and persistent traces of sponge spicules, silicoflagellates, foraminifers, mica, and framboidal pyrite (<3%) (Table 2). The sediment also contains abundant, finely disseminated amorphous organic matter. Successive intervals of the silty clay-clayey silt are either thinly laminated or massive. Interspersed throughout most of the core are distinct beds or laminations of gray (5Y 5/1) clayey silt that form a consistent minor lithology. The section is punctuated by relatively few, very thin to thick beds of sand.

Unit I is divided into six subunits, chiefly on the degree of lamination of the sediment (Fig. 10). Thin olive gray (5Y 4/2) sand beds are

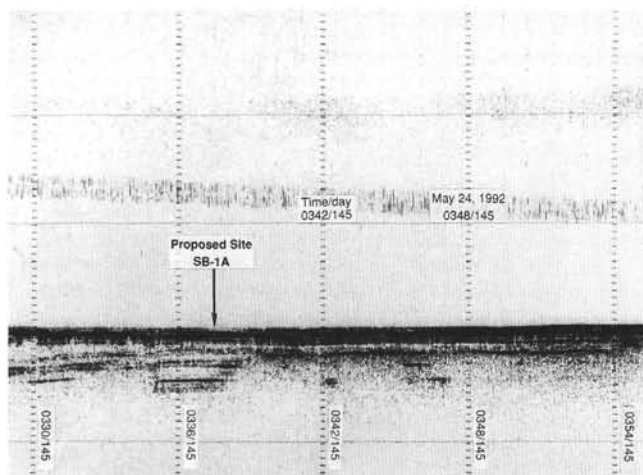


Figure 6. The 3.5-kHz record for *Farnella* line 92-4-3 over Site 893. See Figure 5 for trackline.

abundant in Subunit IB, common in Subunits IC and IF, and rare to absent in Subunits IA, ID, and IE. Thick, medium- to coarse-grained sand layers occur in Subunit IC. Thin, gray (5Y 5/1) clayey silt and silty clay layers are present throughout the laminated intervals.

Subunit IA: Upper Laminated Sequence

Intervals: Core 146-893A-1H through Section 146-893A-3H-6, 75 cm
Depth: Hole 893A, 0–24.25 mbsf; Hole 893B, 0–24.3 mbsf
Age: Holocene to latest Pleistocene

The upper laminated sequence contains 24.25 m of mainly olive gray (5Y 4/2) diatom nannofossil clayey silt and diatom nannofossil silty clay. The core is soupy in the top 30 cm, becoming firm below. Based on smear-slide analyses, the upper 5 m is more nannofossil rich, containing up to 30% nannofossils. The abundance of nannofossils decreases to values of 10% toward the base of the subunit. Diatoms are present throughout in abundances typically between 5% and 20%. Foraminifers are also persistently present in abundances of 1%–2% and radiolarians are present only in trace amounts. A small fragment of tar-saturated wood is present in Core 146-893A-3H-5, 11 cm (22.11 mbsf). The subunit is characterized by the presence of variably preserved laminations throughout most of the interval, intercalated with thin horizons of homogeneous sediment. A prominent, notably thicker, nonlaminated interval extends from 17.5 to 20.5 mbsf.

Laminations comprise a millimeter to submillimeter scale of light/dark alternation from olive gray (5Y 4/2) to very dark gray (5Y 3/1). Laminations are relatively well preserved from 0 to 3.3 mbsf, indistinct from 3.5 to 6.5 mbsf, and intermittently present between 6.5 and 15 mbsf, except for two thin intervals with better preserved laminations between 8.8 and 9.5 mbsf and between 12.1 and 12.5 mbsf. Thin (2–15 cm), nonlaminated intervals occur between 0 and 1.5 mbsf. We could not resolve the compositional differences between most laminations by smear-slide analysis, although some are notably rich in diatoms, nannofossils, or clay minerals. Horizons with very sparse to abundant shell debris occur at 0.25 mbsf and between 8 and 13.5 mbsf. Many of these shell-bearing layers contain very delicate shells that are highly fragmented; others include intact specimens of thin-shelled bivalves and gastropods, or coarse fragments of robust-shelled bivalves. The layer of intact pelecypods at 0.25 mbsf (Sample 146-893A-1H-1, 25 cm) probably represents the 1835 to 1840 A.D. “Macoma oxygenation event” of Schimmelmann et al. (1992) and indicates that initiation of APC coring probably washed away the uppermost 30 cm of sediment. From 0 to 17 mbsf, the dominant, laminated lithology is commonly interbedded with conspicuous, very thin to medium beds (1–15 cm) of gray (5Y 5/1) silty clay to clayey silt. Some of these beds have a coarser, basal silt layer that fines upward to silty clay. These gray layers are rare in the lowermost laminated interval between 20.5 and 24.2 mbsf. A thin sand bed occurs at 13.4 mbsf. Overall, evidence of bioturbation is rare.

Subunit IB: Upper Nonlaminated Sequence

Intervals: Sections 146-893A-3H-6, 75 cm, to -5H-2, 50 cm
Depth: Hole 893A, 24.25–37.0 mbsf; Hole 893B, 24.3–37.0 mbsf
Age: late Pleistocene

Subunit IB consists of 13 m of olive gray (5Y 4/2) silty clay. The subunit is characterized by a total absence of laminations. Few very thin beds or laminations of sand are present in this interval. Horizons with shell debris occur throughout but are concentrated between 32 and 35 mbsf. Diatoms range from 2% to 10% in abundance. In contrast to Subunit IA, calcareous nannofossils rarely make up more than a few percent of the sediment. Foraminifers are typically present in abundances from 1% to 2%. Most of the subunit is entirely homogeneous, and distinct bioturbation structures are rare. The dominant lithology (silty clay) continues into Subunit IC to 49 mbsf.

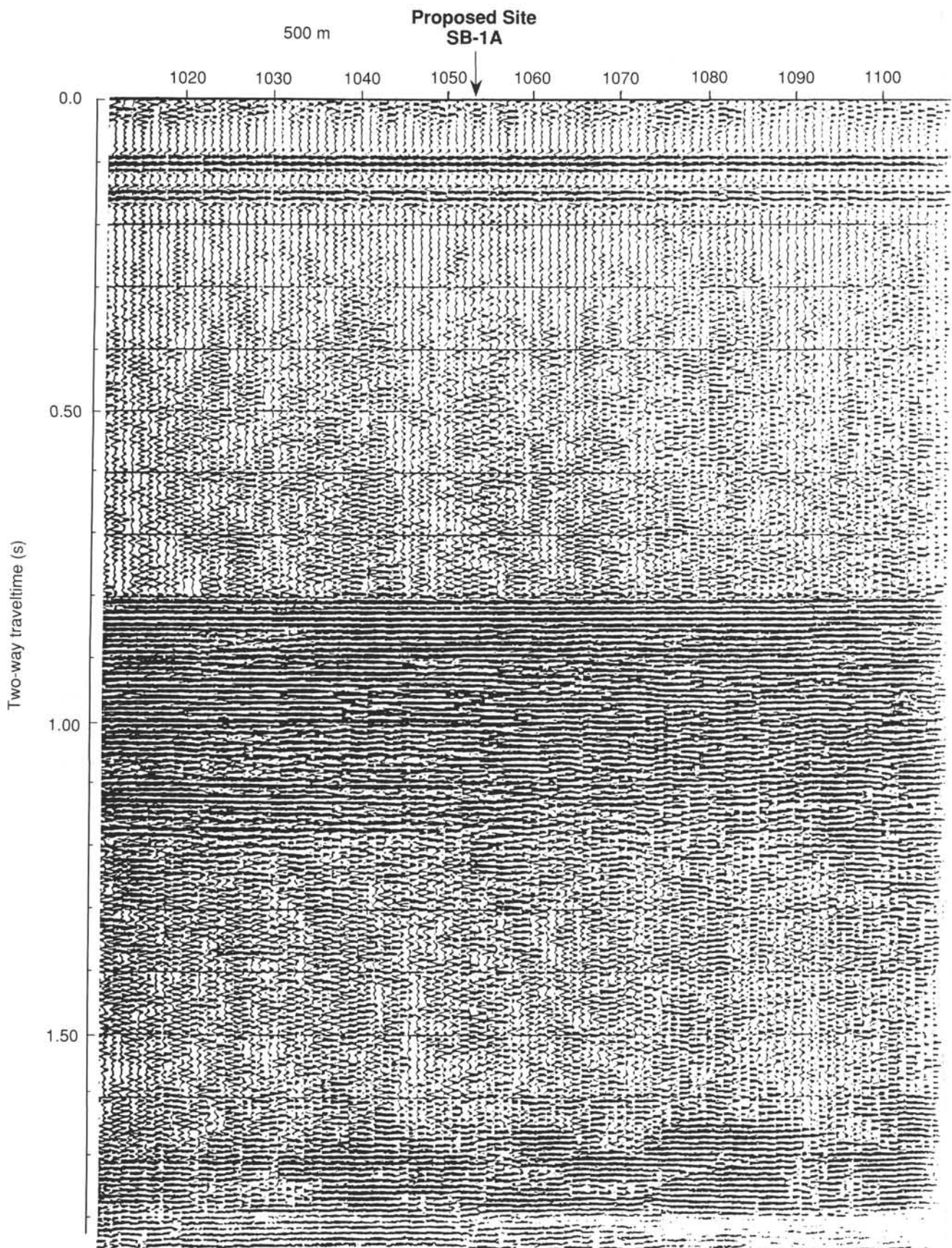


Figure 7. Single-channel seismic profile (*Farnella* cruise line 92-4-3) for Site 893 (proposed Site SB-1A). See Figure 5 for survey tracklines.

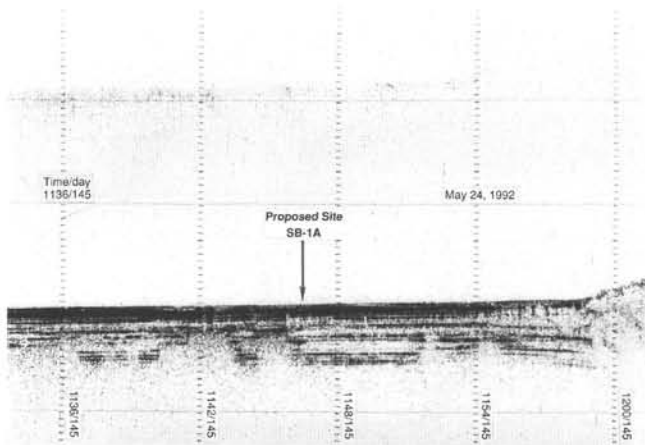


Figure 8. The 3.5-kHz record for *Farnella* line 92-4-6 over Site 893. See Figure 5 for trackline.

Subunit IC: Upper Intermittently Laminated Sequence

Intervals: Hole 893A, Sections 146-893A-5H-2, 50 cm, to -15H-1, 150 cm;
Hole 893B, Sections 146-893B-5H-5, 20 cm, to -8H-CC
Depth: Hole 893A, 37.0–131.0 mbsf; Hole 893B, 37.0–68.8 mbsf
Age: late Pleistocene

Subunit IC comprises 94 m of olive gray (5Y 4/2) silty clay and clayey silt with diatom silty clay. The subunit is characterized by the intermittent presence of laminations. Between 37 and 84 mbsf, thin packets of laminations are only locally present. From 84 to 131 mbsf, the subunit is characterized by an alternation of subordinate, 0.2–3 m packets of laminated diatom silty clay with thicker (2–15 m) intervals of structureless, nonlaminated sediment. From 37 to 49 mbsf, the dominant lithology is a silty clay. Below 49 mbsf, the dominant lithology is a diatom silty clay or diatom clayey silt. Very thin to thin beds of sand are common throughout the upper and lower thirds of the unit (37.0–82.5 and 101.8–125.6 mbsf, respectively; Fig. 10). Four medium to thick beds of sand occur between 56.5 and 64.7 mbsf and a markedly thicker, 2.5-m sand bed occurs at 114.4–116.9 mbsf. Horizons with shell debris occur throughout but are concentrated between 37–45 mbsf, 47.5–50.0 mbsf, and 74.5–113.0 mbsf. They are particularly abundant from 104 to 106 mbsf. Diatom abundances range from 2% to 10% between 37 and 49 mbsf, but they generally increase from 15% to 25% between 49 and 74.5 mbsf. Calcareous nannofossils rarely make up more than a few percent of the sediment. Several granules of siltstone, up to 5 mm in diameter, occur between 83.2 and 88.7 mbsf.

Very thin to medium (1–15 cm) beds of gray (5Y 5/1) silty clay and clayey silt principally occur within the lower unlaminated intervals between 95.5 and 129.5 mbsf. Within the laminated intervals, in addition to the light/dark laminae are occasional millimeter to submillimeter, pale olive (5Y 6/3) diatom ooze laminae, often containing low-diversity assemblages of diatom vegetative cells; laminae enriched in resting spores are also present. Diatom abundances in the dominant lithology generally range from 10%–25% but locally make up as little as 3%. Distinct burrows and mottling are observed sporadically, although much of the subunit appears homogeneous.

Subunit ID: Lower Laminated Sequence

Interval: Sections 146-893A-15H-2, 0 cm, to -16H-4, 150 cm
Depth: Hole 893A, 131.0–145.5 mbsf
Age: late Pleistocene

Subunit ID comprises 14.5 m of olive gray (5Y 4/2) diatom silty clay. The subunit is characterized by the presence of laminations throughout other than in three thin intervals of structureless sediment.

The subunit contains abundant very thin to thin (1–15 cm) interbeds of gray (5Y 5/1) silty clay and clayey silt except between 134.5 and 137 mbsf. Within the laminated intervals, in addition to the light/dark couplets, occasional millimeter to submillimeter laminations of pale olive (5Y 6/3) diatom ooze are present. A prominent interval of indistinctly laminated foraminifer diatom silty clay occurs between 139.5 and 141.2 mbsf. A thin, entirely structureless interval with no gray silty clay beds occurs between 135 and 136.9 mbsf. Diatom abundances in the dominant lithology generally range from 10% to 25%. Burrows are rarely observed. Overall, this subunit is quite similar to Subunit IA, except that the laminations have been compressed as a result of the greater burial depth.

Subunit IE: Lower Nonlaminated Sequence

Interval: Sections 146-893A-16H-5, 0 cm, to -18H-2, 40 cm
Depth: Hole 893A, 145.5–160.5 mbsf
Age: late Pleistocene

Subunit IE comprises 15 m of olive gray to pale olive (5Y 4/2 to 5Y 6/3) silty clay and clayey silt with diatom silty clay. The subunit is characterized by the complete absence of laminations. Although most beds lack sharp boundaries, distinctive color changes occur gradually over decimeter-scale intervals. Diatom abundances range from 5% to 10%. Occasional shell debris and evidence of minor bioturbation are present in this interval.

Subunit IF: Lower Intermittently Laminated Sequence

Interval: Sections 146-893A-18H-2, 40 cm, to -21H-CC
Depth: Hole 893A, 160.5–196.5 mbsf
Age: late Pleistocene

Subunit IF comprises 36 m of olive gray (5Y 4/2) silty clay and clayey silt and diatom silty clay. The subunit is characterized by an alternation of subordinate 0.2–3.0 m packets of laminated diatom silty clay with thicker (up to 5 m) intervals of structureless, nonlaminated sediment. In contrast to the stratigraphically higher laminated sediments, gray silty clay and clayey silt beds are rare. Within the dominant lithology, diatom abundances range from 3% to 10% between 169.9 and 184 mbsf and from 15% to 30% between 184 and 196.5 mbsf. Occasional very thin sand beds occur throughout. Layers containing shell debris are also present. Indistinct burrows are common in the nonlaminated sediment, with diameters typically ranging from <1 to 4 mm. Lamination becomes increasingly common and continuous in the lowest part of the subunit (below 188.5 mbsf).

SEDIMENTOLOGY

The sediments recovered at Site 893 are mostly hemipelagic in nature, being almost entirely composed of silt- and clay-sized terrigenous and biogenic grains. The biogenic component includes varying quantities of diatoms and nannofossils and persistent traces of sponge spicules, silicoflagellates, foraminifers, mica, framboidal pyrite, and amorphous organic matter (<3%) (Table 2). Successive centimeter- to meter-scale intervals of the olive-gray (5Y 4/2) sediment are either thinly laminated or massive. Layers of gray (5Y 5/1) clayey silt are intermittently interbedded with the olive-gray sediment and form a consistent minor lithology. The section is punctuated by relatively few, very thin to thick beds of sand, which are most abundant in Subunits IC and IF.

Laminated Silty Clay to Clayey Silt

Laminated sediment is most abundant in two distinct intervals (Subunits IA and ID). Laminations vary from very thin with straight and parallel fabric to thicker laminations that are discontinuous to crinkly (Fig. 12). We interpret horizons of indistinct laminations to be the result

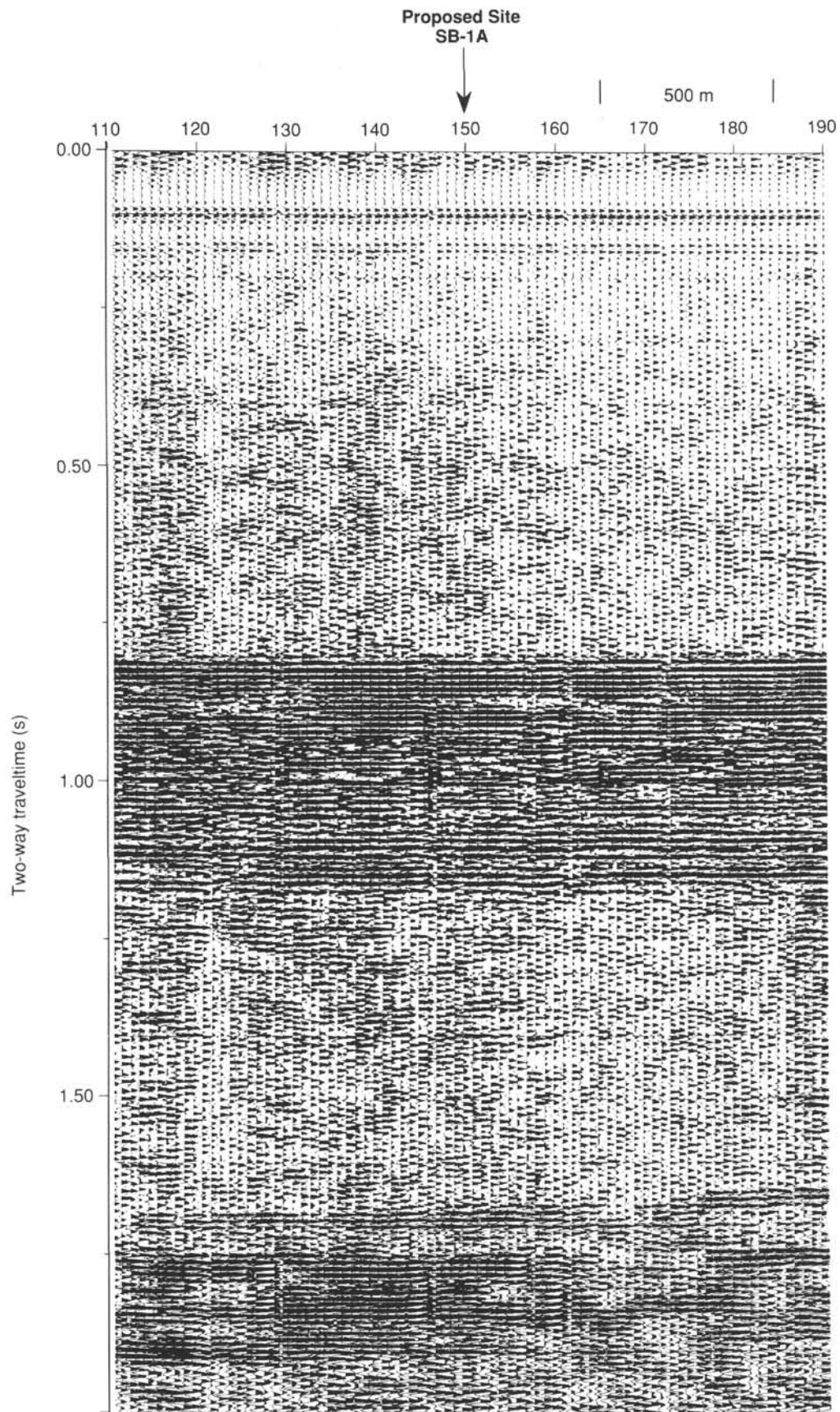


Figure 9. Single-channel seismic profile (*Farnella* cruise line 92-4-6) for Site 893 (proposed Site SB-1A). See Figure 5 for survey tracklines.

Table 2. Results of analysis of smear slides for selected samples from Site 893.

Core, section, interval (cm)	Quartz/feldspar	Rock fragments	Mica	Clay	Volcanic glass	Calcite	Dolomite	Accessory minerals	Pyrite	Foraminifers	Nannofossils	Diatoms	Radiolarians	Sponge spicules	Silicoflagellates	Bioclasts	Echinoderm spines	Plant debris	Wood fragment	Fish remains	Aggregates	Opauques	Mollusk fragments	Zeolite	Collophane	
146-893A-																										
1H-1, 65	20				60	15		1	2	Tr	1	1		Tr	Tr											
1H-1, 68	10				5	10				3	41	30	Tr	1	Tr											
1H-1, 75	20				30	2			1	Tr	36	10		1	Tr											
1H-2, 11	8				10	5			2	1	58	15		1	Tr											
1H-2, 53	39				1	4		Tr	2	1	40	5		Tr												
1H-2, 110	25		Tr		53	5			2	1	5	5			Tr											
1H-3, 37	20		1		64	2			3	Tr	5	5		Tr	Tr											
1H-4, 9	30	3			17	2		1	2	3	30	10		2	Tr											
1H-4, 47	75	5			1	3			1	2	Tr	Tr	Tr	Tr			Tr									
2H-1, 53	20		2		42	2			1	1	30	10		2	Tr											
2H-2, 63	25		1		42	3		2	2	1	10	3		Tr												
2H-5, 92	43		5		20	4			1	2	35	10		Tr	1											
2H-5, 98	66	Tr			17	3			2	2	8	1			Tr											
3H-1, 41	62		3		25	2		3	3	Tr	2	2	Tr	Tr	Tr											
3H-1, 74	15		2		73	3			2	Tr	3	2		Tr	Tr											
3H-2, 85	35				44	Tr			Tr	1	15	4		5	Tr											
3H-5, 59	30	1			20	Tr	Tr		2	2	29	15		Tr	Tr											
3H-6, 106	10		3		56	5		2	2	Tr	10	10		2	Tr											
3H-7, 18	77					3		5	5	2	5	Tr		3												
4H-3, 61	30		1		48	Tr	Tr		3	1	1	5		1	Tr		2									
4H-1, 143	62		2		5	5		4	3	2	5	5	Tr	2		3										
5H-1, 62	83		2		4	1		1	1	2	1	2		Tr		1										
5H-3, 64	20		1		59	2		2	1	Tr	10	4		1	Tr											
5H-CC, 18	67		2		15	3		3				4		3												
5H-1, 134	2		Tr		49				9		10	30	Tr													
6H-2, 98	15		Tr		36	4		2	2	Tr	15	10		1	Tr											
6H-3, 31	20		2		47	2		1	Tr	Tr	20	5		1	Tr		1									
6H-4, 44	20		3		47				2	Tr	10	15		2	1											
6H-6, 94	95				Tr	Tr																				
7H-2, 28	30				40	1				1	1	3														
7H-4, 133	90							6				25			Tr											
7H-5, 59	35				43	1	1				5	15			Tr											
7H-6, 27	86	5						5	Tr						Tr											
8H-2, 10	20		1		42	2		2		Tr	3	25		2	3											
8H-4, 86	15		2		40	3			1		5	25		2	5											
9H-1, 141	10				5						2	83														
9H-4, 66	50				20	1	5		1	2	2	25		Tr	Tr											
9H-8, 6	42				25				1	1	3	28		Tr	Tr											
9H-8, 12	40		8		25				5	1	4	15		Tr	Tr											
9H-5, 39	3					8			1	5	76			1	2											
9H-8, 25	20				41	2		3	1	Tr	5	25		Tr	3		Tr									
10H-4, 141	89				Tr			5	6		Tr	Tr		Tr												
10H-1, 54	4		1		84	Tr			1		3	5			1											
10H-6, 33	10		Tr		76	1			1	Tr	5	4		1	Tr		2									
10H-6, 54	10		1		70	2		3	1		2	5			Tr											
11H-3, 78	20		1		48	1			2	1	1	25		Tr	Tr											
11H-3, 50	10		4		68	2					1	15		Tr	Tr											
11H-4, 101	3		1		60	2			5	1	3	25	Tr	Tr	1		Tr									
11H-6, 93	30		1		40	3			1	5		20		Tr	Tr		Tr									
12H-3, 111	15		10		50	5			5		5	10		Tr												
12H-4, 37	12		1		76	2			2	1	2	3		1	Tr											
12H-7, 31	66		2		20				2	2	Tr	5			1		2									
12H-CC, 18	100	2							3		Tr															
13H-3, 63	10		1		66	2			1	Tr	5	15			Tr											
13H-4, 40	97		Tr						3																	
13H-5, 121	98		1			Tr			1																	
13H-7, 77	30		3		42				18		2	5	Tr		Tr											
13H-7, 33	2		1		15	2			1		5	74		Tr	Tr											
13H-8, 3	15		2		54				15		3	10		Tr	Tr											
14H-1, 118	10		6		59				2	Tr	1	20		Tr	Tr											
14H-3, 68	96		1						1			2			Tr											

of incomplete mixing by low-oxygen benthic meiofauna. Scattered, entirely homogeneous layers represent episodic bottom-water oxygenation with extensive sediment mixing. In much of the sequence, laminated sediment is contained in decimeter-scale packets that alternate with homogeneous (bioturbated) sediment, suggesting alternation between oxygen-depleted and -enriched depositional environments.

The laminations encountered at Site 893 generally take the form of ca. 0.5–1 mm pale/dark alternations of olive gray (5Y 4/2) and very dark gray (5Y 3/1). Locally, the thickness of individual laminations exceeds 2 mm, especially in the less compacted Holocene sediments. Changes in major sediment components within the pale/dark laminations cannot be assessed by smear-slide analyses and must await detailed electron microscope analyses. Two other distinct lamina types occur besides the pale/dark alternations. In certain laminated

intervals, millimeter- to submillimeter-scale, pale olive (5Y 6/4) diatom ooze laminations occur that commonly contain abundant *Chaetoceros* resting spores. These diatom-ooze laminations appear with an irregular centimeter-scale spacing within the regular pale dark laminations. In some laminated intervals, millimeter-scale laminations of gray clayey silt occur that may have similar origins to the thicker distinctive “gray layers” (see below).

Massive Beds of Olive Gray (5Y 4/2) Silty Clay to Clayey Silt

Most massive beds are similar in average color and composition to well-laminated intervals, with the exception of local intervals containing fewer diatoms and nannofossils (Fig. 13). Evidence for

Table 2 (continued).

Core, section, interval (cm)	Quartz/feldspar	Rock fragments	Mica	Clay	Volcanic glass	Calcite	Dolomite	Accessory minerals	Pyrite	Foraminifers	Nannofossils	Diatoms	Radiolarians	Sponge spicules	Silicoflagellates	Bioclasts	Echinoderm spines	Plant debris	Wood fragment	Fish remains	Aggregates	Opauques	Mollusk fragments	Zeolite	Collophane
146-893A-																									
14H-4, 87	10			53		3			2		5	25		1	Tr										1
14H-7, 22.5	5		2	83		1			2		2	5													1
15H-1, 99	15		2	66		1			5		8	2		1											Tr
15H-2, 137	1		1	57		2			3		2	30		2	1										1
15H-2, 74	91		5						3	Tr	3	1		Tr	Tr										
15H-4, 44	5		3	59		Tr			3	Tr	2	25		Tr	1										1
15H-6, 73	6		2	76		3			10		Tr	1		Tr	Tr										2
16H-1, 53	30			37		Tr			2	10	Tr	20		Tr											
16H-2, 59	8			87		3			Tr	1	1														
16H-2, 70	53	Tr	Tr	43		1		Tr	3		Tr	Tr		Tr											
16H-3, 60	30		Tr	55		2	Tr		1	2	Tr	10		Tr	Tr										
16H-6, 74	25		Tr	54		4	Tr	Tr	1	3	2	10		Tr	1										
17H-1, 78	20		Tr	72		2	Tr	Tr	1		1	5		Tr	Tr			Tr							
17H-2, 44			2	89					3		3	1													2
17H-2, 77				58							40	1													1
17H-5, 44	67		5			2			1	1	15	4		Tr		Tr									1
18H-3, 75	3		2	75		5			1		2	10		1											1
18H-5, 72	90		Tr						8	2															
19H-4, 17			1	81					1		12	4		Tr											1
19H-5, 74	1		Tr	85					3	1	2	5		1	Tr										2
19H-51, 28				Tr	67				2		17	3		Tr	Tr										1
20H-3, 76	5		2	68					2		12	10		Tr	Tr										1
20H-5, 132	15		1	55					4		1	15		2	Tr										2
20H-6, 51	2		1	78		5			1		1	10													2
21H-2, 106	10		Tr	53		2			2		6	25		Tr	Tr										2
21H-4, 21	10			35					1		2	50		Tr	Tr										3
21H-61, 10	10		Tr	55					2			30													3
146-893B-																									
1H-2, 18	20		1	67					1		10	2		Tr											Tr
1H-2, 43	1			63					Tr		20	5		Tr	Tr										1
1H-1, 124	1		Tr	70					3		10	15													1
2H-1, 96	2			50		1			1		30	15		Tr	Tr										1
2H-5, 53	10		1	62					1		20	5		Tr											1
2H-2, 94	3		Tr	86					1		5	1													4
3H-2, 45	3		Tr	43	Tr				2		40	10		Tr											2
3H-3, 83	4		Tr	88		Tr			1	Tr	Tr	5		Tr	Tr										2
3H-4, 127	2		Tr	49		Tr			2	Tr	30	15		Tr	Tr										1
4H-1, 45	15			56		Tr			2	Tr	10	15		Tr	Tr										2
4H-3, 43	20		Tr	67					Tr		5	5		Tr											3
4H-4, 70	63			15		Tr			5	Tr	3	3		Tr											1
4H-5, 10	79		2						14		4	1													
5H-4, 55	20		1	53		Tr			1		10	4		Tr											1
6H-2, 56	15			63		1			Tr		5	4		Tr											2
6H-3, 118	100	Tr	Tr						Tr	Tr															
6H-4, 101	5		Tr						5	Tr	15	Tr		Tr											5
6H-6, 140	15			63		1			1	Tr	10	10		Tr	Tr										20
7H-2, 40	15		1	61					3		Tr	10		Tr											Tr
7H-2, 67	40			51					2	Tr	Tr	2													5
8H-5, 131	98		2						Tr																Tr
8H-1, 79	10		1	56					4		3	25													1
8H-4, 97												100													Tr
8H-3, 91	10		Tr	74					2			9													5
8H-6, 82	15		Tr						2		2	5													1

Note: Values are in percent (%). Tr = trace or less than 1%.

bioturbation ranges from indistinct color mottling to sharply defined burrows, typically 5–15 mm thick, and rarely extending more than a few centimeters in length. The massive fabric may be a primary or penecontemporaneous feature in some beds; however, numerous gradational contacts with underlying gray layers indicate that, in part, homogenization resulted from deeper biologic mixing. Some massive intervals contain scattered shell-bearing layers with very delicate bivalves and gastropods that probably could not survive intact significant turbulent or bedload transport. Consequently, we consider these macro-organism to have lived where they were deposited, on or beneath an oxygenated basin floor.

Gray Layers and Sands

Distinctive layers of gray (5Y 5/1) silty clay to clayey silt are scattered throughout the section except in Subunits IB and IE. Individual gray strata range from millimeters to decimeters in thickness, but

most are between 1 and 5 cm thick (Fig. 13). Gray layers are chiefly sharp-based and visually massive; however, many display one or two cycles of normal grading, suggesting event deposition. Similar gray beds in box and piston cores correlate with historical floods and storms in California (Fleischer, 1972; Thornton, 1981, 1984) and are thought to record 50- to 100-yr and rarer storm events. These deposits can be attributed to low-density turbidity currents or settling of flood-related nepheloid suspensions. Although distinct gray layers are not present in the two nonlaminated sequences (Subunits IB and IE), diffuse changes in color suggest that some deposits were homogenized by bioturbation. Therefore, it is difficult to assess the quantitative contribution of gray bed-type event deposition in the late Quaternary sedimentary record of the Santa Barbara Basin.

Very thin to thin (1–5 cm) beds of olive gray to gray (5Y 4/2 to 5Y 5/1), fine- to very fine-grained sand are unevenly distributed through the section, being exceedingly rare within the two principal laminated sequences (Subunits IA and ID). A few notably thicker (up

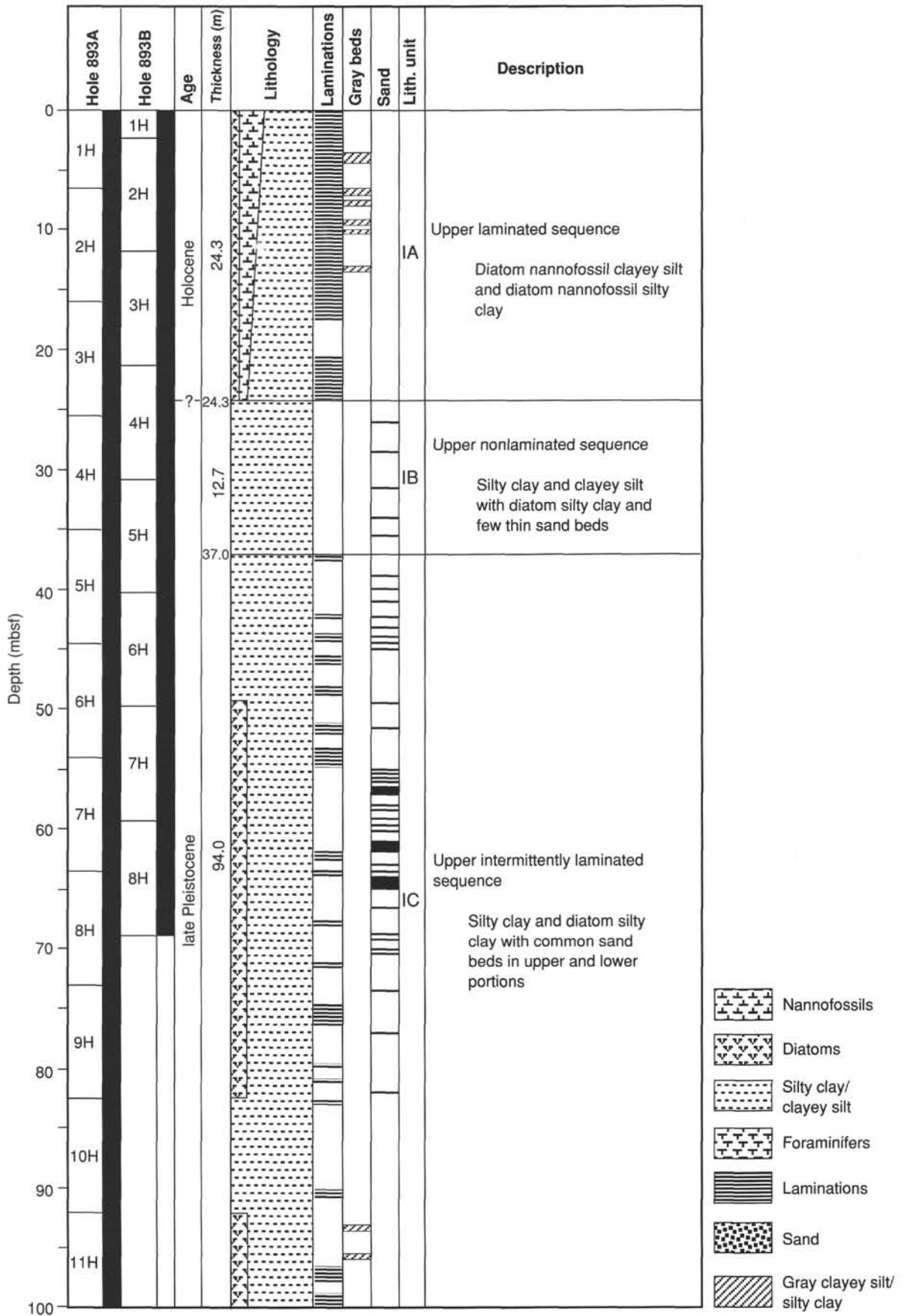


Figure 10. Lithostratigraphic summary of Holes 893A and 893B, illustrating average compositions and locations of intervals bearing laminations, sand beds, and gray layers.

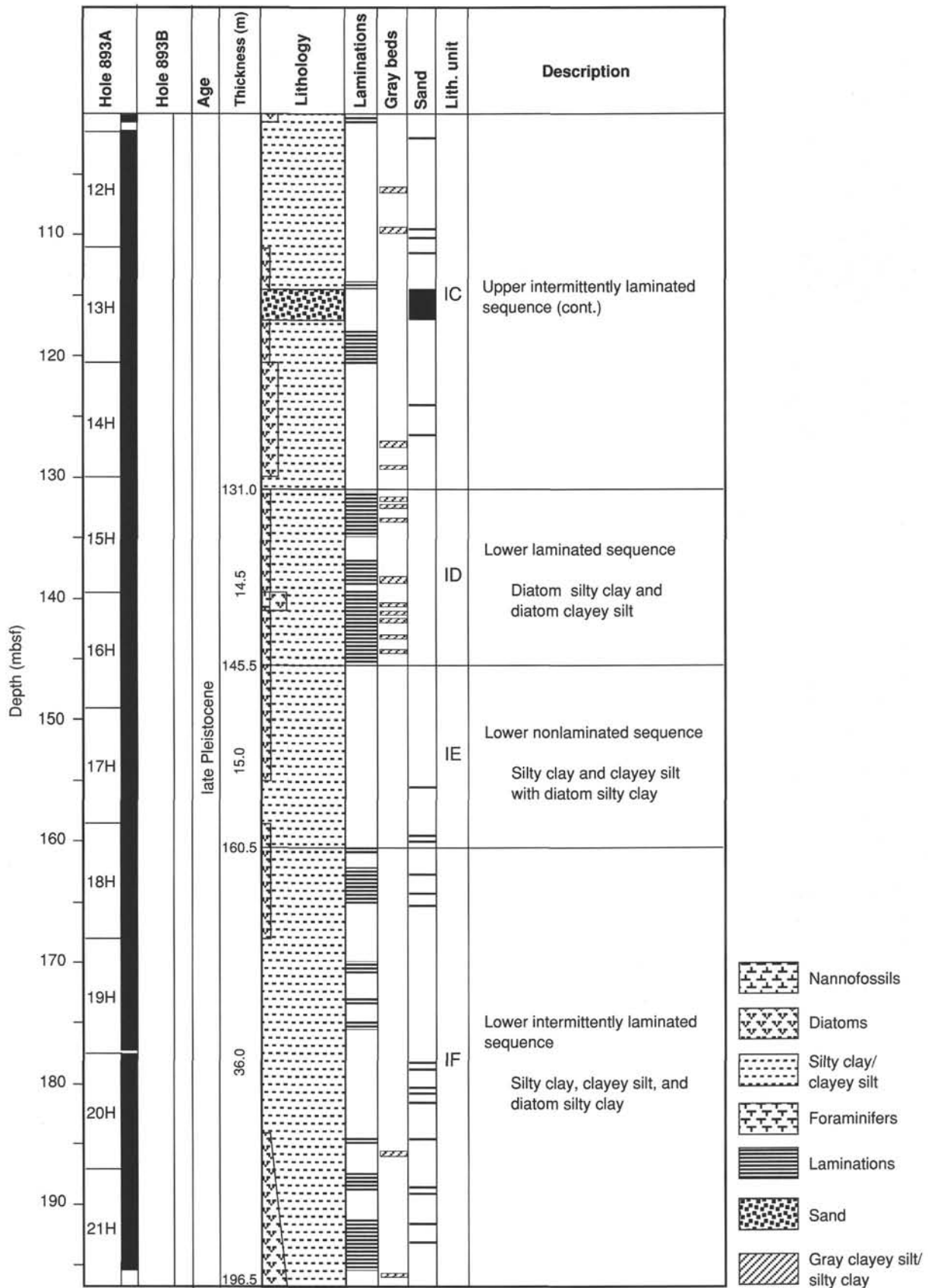


Figure 10 (continued).

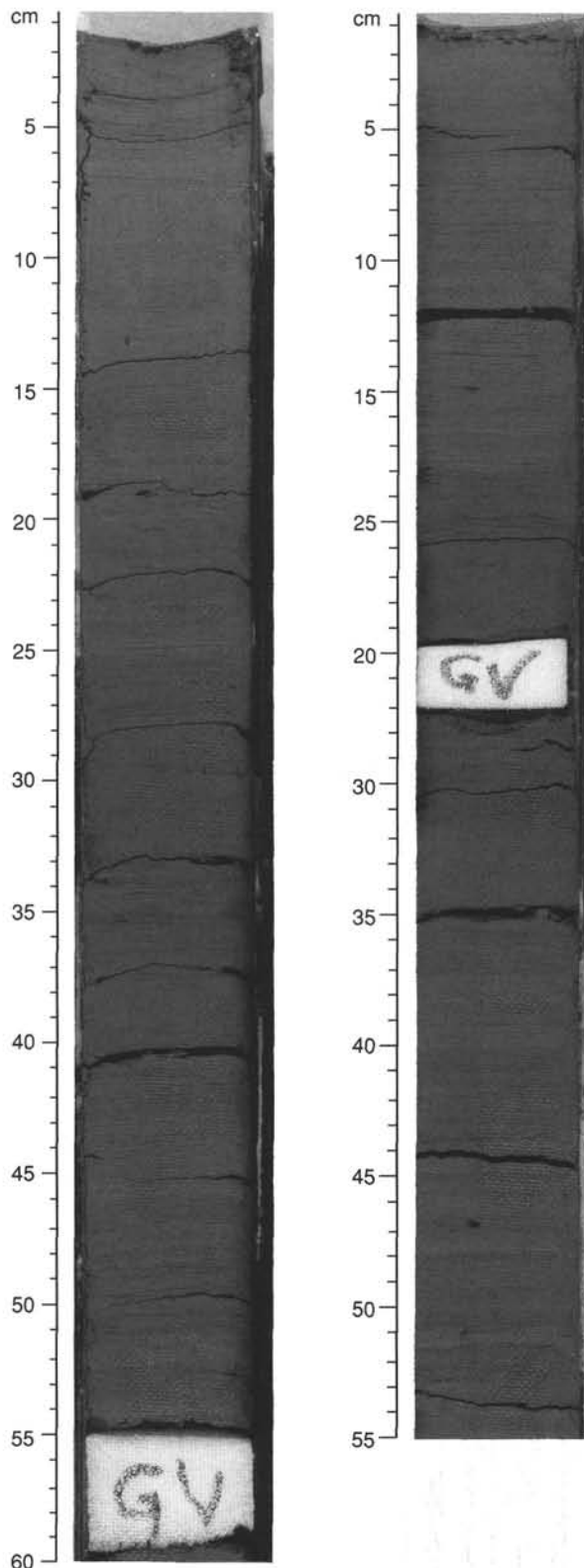


Figure 11. Fine-scale stratigraphic correlation between Holes 893A and 893B in Subunit IC. Note the close similarity between massive clay-rich beds of olive silty clay and the "bar code" similarity between the laminated portions of the core. Similar correlations are commonplace for shallow box and piston cores in the Santa Barbara Basin (cf. Soutar and Crill, 1977; Schimmelmann et al., 1990). Offset between the two holes is caused by the different rates of recovery and degrees of gas expansion in the cores. Left, Section 146-893A-6H-6, 0–60 cm; right, Section 146-893B-7H-2, 0–55 cm.

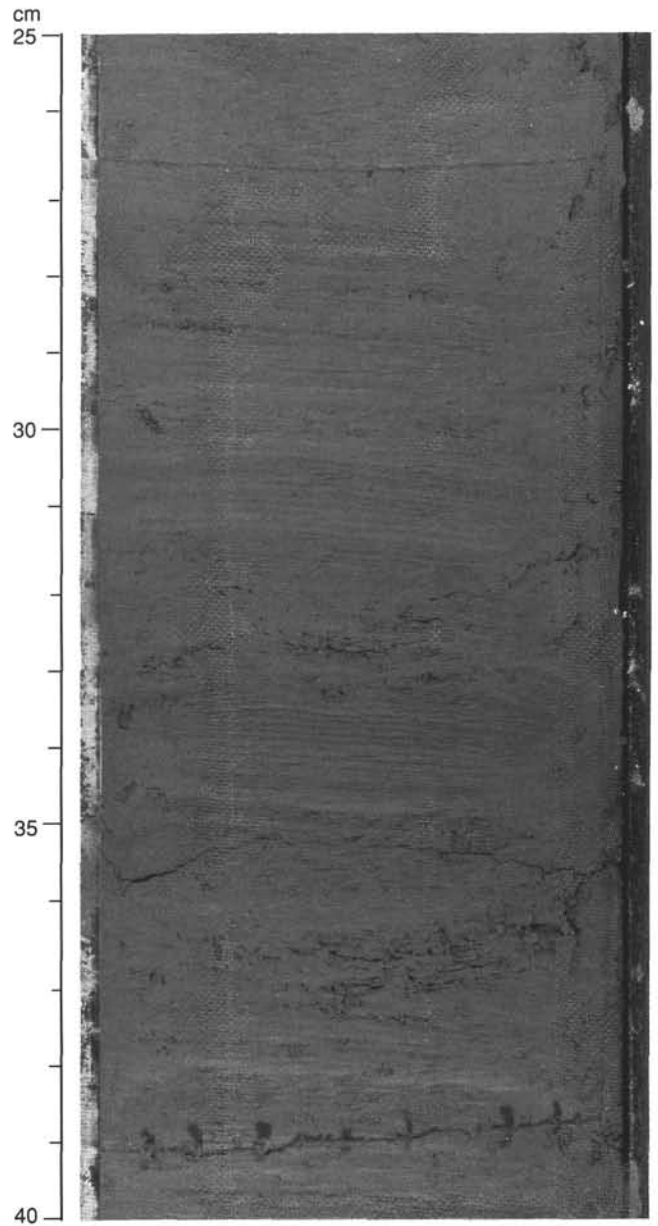


Figure 12. Millimeter- to submillimeter-scale lamination in Section 146-893A-21H-5, 25–40 cm, varies in style between a very fine, straight, and parallel fabric (31–36 cm) and thicker laminae with a slightly crinkly and commonly discontinuous fabric (36–41 and 25–31 cm). Many thicker and crinkly laminated intervals appear to be clay-enriched compared with finely laminated intervals. Note the upward transition from very fine, parallel laminae to thicker, crinkly, and more clay-rich laminae. At Site 893, this trend is part of the generally transitional contact observed between some laminated units and the massive silty clay units that locally overlie them.

to 2.5 m) and coarser (medium- to coarse-grained) beds are present between 55 and 70 mbsf and at 115, 124, and 178 mbsf. The sand is chiefly composed of quartz and feldspars, with minor lithic grains, shell fragments, and sponge spicules. Most siliciclastic grains are partially encrusted with pyrite, and some sands contain distinctive red coccoliths in their finest fraction, which probably were stained in their previous depositional or diagenetic environments. Sand beds are normally graded or massive and almost all have sharp bases: thus, we consider these to be turbidites, although they could be basin-floor channel deposits.

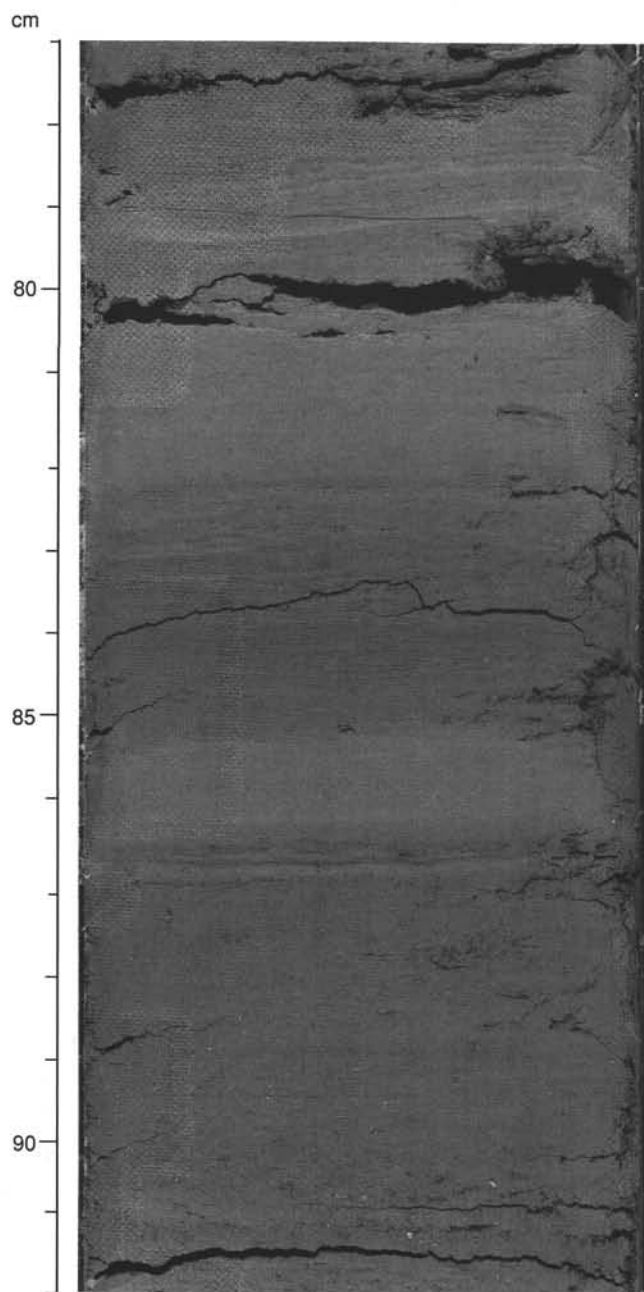


Figure 13. Gray layers are best developed or preserved within the laminated interval in Section 146-893A-13H-7, 77–92 cm. Note how gray beds (79–82 and 85–86.5 cm) are sharply based and are overlain by laminated sediment. Many gray layers display subtle normal grading. Bottom of core interval (87–91 cm) is a massive olive silty clay bed.

Diagenesis

Pyrite

Framboidal pyrite is a trace to major constituent of all sediment types at Site 893 and indicates pervasive remineralization of organic matter during diagenesis in the zone of sulfate reduction. The morphology of the framboids is uniformly spherical but varies widely in size, ranging from $<1\ \mu\text{m}$ to $>10\ \mu\text{m}$ in diameter. Two distinct facies of pyrite seem to be present in these sediments. Framboidal pyrite is either uniformly $<1\ \mu\text{m}$ in diameter or aggregated into masses of framboids with appendages and coatings of smaller pyrite spherules. Tests of diatoms and foraminifers frequently contain pyrite aggregates.

The origin of the disseminated vs. aggregate pyrite is not clear. Based on smear-slide observations, no clear association can be made between the two types of pyrite with distinct organic facies as virtually all organic matter in the Santa Barbara sediments is amorphous in optical character. It is possible that the two types of pyrite reflect the depth and intensity of initial sulfate reduction within the sediment column; this hypothesis will be tested by a comparison of sulfur isotopes within the laminated and bioturbated/massive sediment.

Methane

The high concentration of methane gas in the cores at Site 893 suggest substantial remineralization of organic matter by methanogenesis, although, with abundant natural seeps of Tertiary oil and gas in the Santa Barbara Basin, a deeper stratigraphic origin is not completely ruled out. In either case, sustained diagenesis of organic matter after onset of anoxic conditions was a major diagenetic process, reflecting both the highly metabolizable composition of organic matter in this sediment and a complex microbial community. The large amounts of framboidal pyrite in most sand beds imply high concentrations of soluble organic matter in pore waters during early anoxic diagenesis.

Sediment History

Late Quaternary Sedimentary History of the Santa Barbara Basin

The sediments recovered at Site 893 record two broadly similar sedimentary cycles. In each of these a thick, intermittently laminated interval of diatom silty clay (Subunits IF and IC) passes upward with decreasing abundance of laminations into a relatively thin (ca. 15 m) interval of homogeneous, silty clay devoid of laminations (Subunits IE and IB; Fig. 14). This homogeneous interval is then succeeded abruptly by a thin interval of relatively continuous, well-laminated sediment (Subunits ID and IA). The uppermost laminated sequence (Subunit IA) is punctuated by a short, massive, bioturbated interval that may correlate with the Younger Dryas cooling event. Low oxygen conditions inferred from the preservation of laminations are confirmed by the presence of benthic foraminifer assemblages indicative of low levels of oxygenation (see "Paleontology" section, this chapter). These cycles, therefore, represent a progression of increased dominance of oxygenated bottom waters culminating in a period of sustained basin oxygenation. The fully oxygenated intervals are then terminated by an abrupt return to a sustained period of low oxygen conditions promoting lamina preservation.

This cyclic variation of basin conditions indicated by laminations and fauna is amplified by the record of terrigenous transport into the basin. Sand beds are thickest and most numerous within the intermittently laminated intervals at the base of each cycle (Fig. 10). They are fewer and more widely spaced in the middle, fully oxygenated, non-laminated intervals, and almost completely absent in the low-oxygen laminated sequences at the top of each cycle. The cycle stages are likewise reflected in the stratigraphic distribution of gray event beds that are most numerous and densely spaced in the laminated sequence, sparse in the intermittently laminated sequences, and absent or obliterated in the bioturbated, massive sequences.

Furthermore, these cycles correlate with changes in planktonic foraminifer and pollen assemblages, suggesting that sedimentation in the late Quaternary Santa Barbara Basin was a sensitive indicator of climatic and oceanographic oscillation (see "Paleontology" section, this chapter). Foraminifers indicate two cycles of variable, yet gradually cooling water (intermittently laminated to nonlaminated sequences) sharply followed by warm water conditions (laminated sequence). This paleoceanographic record is mirrored by changes in terrestrial pollen, recording the shifting from pine-dominated (cold) to oak-dominated (warm) terrestrial vegetation.

These cyclic changes in basin oxygenation, water temperature, terrigenous input, climate, and onshore vegetation describe a distinctive sawtooth pattern that we interpret as reflecting Quaternary glacial

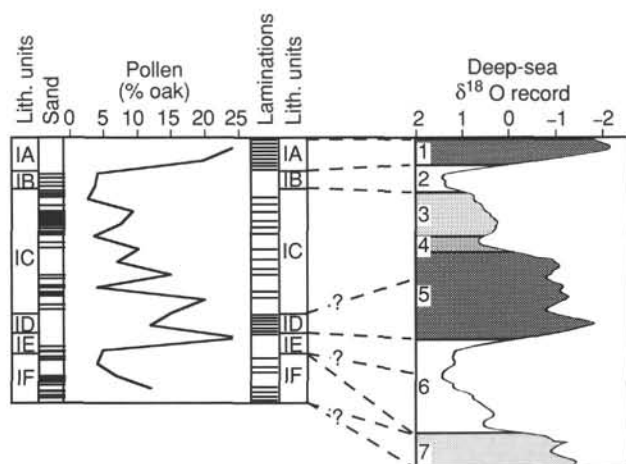


Figure 14. Preliminary correlation of cyclic variation at Site 893 with the composite deep-sea oxygen isotope record. The presence of laminations, sand turbidites, and foraminifer and pollen assemblages define two similar stratigraphic cycles in the Santa Barbara Basin that likely reflect climatic and oceanographic modulation during the past two glacial cycles of the Quaternary.

oscillations (Fig. 14). Lacking precise biostratigraphic resolution or radiometric age controls, the depositional history cannot be rigidly constrained in time. Nevertheless, we can make a tentative correlation with the last two glacial cycles of the Quaternary as follows:

Late Pleistocene interglacial warm and cool intervals (Stage 6 and possibly latest Stage 7)—lower intermittently laminated sequence/Subunit IF. Deposition of alternating stratigraphic packages of laminated and massive silty clay to clayey silt with diatom silty clay, intercalated with common sand turbidites, and a few fine-grained gray layer flood/turbidity deposits.

Late Pleistocene glacial maximum (Stage 6 and possibly earliest Stage 5)—lower nonlaminated sequence/Subunit IE. Deposition of massive, bioturbated silty clay to clayey silt with diatom silty clay, which accumulated within oxygenated waters, including relatively few thin sand turbidites and no distinct fine-grained gray layer flood/turbidity deposits.

Late Pleistocene interglacial (Stage 5)—lower laminated sequence/Subunit ID. Accumulation of well-laminated diatom silty clay, deposited under anoxic bottom waters. Intercalated with common fine-grained gray layer flood/turbidity deposits and lacking in sand turbidites.

Latest Pleistocene interstadial warm and cool intervals (Stages 4 and 3)—upper intermittently laminated sequence/Subunit IC. Deposition of alternating intervals of laminated and massive silty clay to clayey silt with diatom silty clay, intercalated with common, locally thick, sand turbidites and a few fine-grained gray layer flood/turbidity deposits.

Last glacial maximum (Stage 2)—upper nonlaminated sequence/Subunit IB. Accumulation of massive, bioturbated silty clay to clayey silt, deposited within fully oxygenated waters, with relatively few thin sand turbidites and no distinct fine-grained gray layer flood/turbidity deposits.

Latest Pleistocene to Holocene postglacial (Stage 1)—upper laminated sequence/Subunit IA. Accumulation of well-laminated diatom nannofossil silty clay to diatom nannofossil clayey silt, deposited under anoxic bottom waters with frequent fine-grained gray layer flood/turbidity deposits. No sand turbidites.

The described changes in sedimentation can be related to Quaternary climatic oscillation by a variety of mechanisms. Whereas anoxia in the modern Santa Barbara Basin is jointly produced by the interception of the Oxygen Minimum Zone at sill depth and by high primary productivity, Quaternary changes in the basin's bottom-water oxygenation were probably controlled by a combination of the following

end-member mechanisms (Fig. 15): (1) lowering of the impinging Oxygen Minimum Zone below sill depth by falling eustatic sea levels during periods of continental ice-sheet growth; (2) increased oxygen content of the Pacific Intermediate Water mass that intercepts the deeper, western sill of the modern Santa Barbara Basin, resulting from decreased production of North Atlantic Deep Water during glaciation (cf. Keigwin and Jones, 1990); and (3) shifting of high surface productivity offshore of the Santa Barbara Basin during lowered sea levels or altered wind regimes. Thus, the position and oxygen content of impinging water masses comprise the key controls of the oxygenation of the Santa Barbara Basin bottom water. This level of oxygenation is, in turn, further modified by the strength of primary productivity in the overlying surface waters. Most likely, all three mechanisms acted in conjunction during the Quaternary (Fig. 16), yet the importance of each individual mechanism varied in a complex, interdependent fashion. For example, steep latitudinal thermal gradients probably increased coastal upwelling during glacial periods, yet export productivity may still have been restricted by simultaneous development of nutrient-poor, intermediate waters (Mechanism #2). Likewise, the effect of expansion or contraction of the Oxygen Minimum Zone (Mechanism #2) could be modulated by changes in sea level with respect to the basin's sill depth (Mechanism #1). Presently, the oxygen content of Pacific Intermediate Water is too high to exclude macroinfauna and allow preservation of lamination except where depleted by the bacterial degradation of organic matter exported from productive surface waters. Yet the increased oxygen content of Pacific Intermediate Water (Mechanism #2) may have been chiefly responsible for the interval of nonlaminated sediment that is tentatively correlated with the Younger Dryas Event, in which oxygenated bottom water was present in the Santa Barbara Basin without a corresponding fall in sea level (Mechanism #1).

Variations in sand turbidite frequency can be directly related to sea level. At highstands (interglacials), sand was apparently sequestered on the shallow shelf and sandy turbidites were not deposited in the basin center. The greatest numbers and thicknesses of sand turbidites accumulated in response to falling sea levels during gradually intensified glaciation. Finally, deposition of sandy turbidites decreased during glacial maxima, reflecting either the depletion of the narrow shelfal sand reservoirs or the bypassing of sediment around the Santa Barbara Basin by the routing of Santa Clara and Ventura rivers sand down the Hueneme Canyon to the east and the transport of Santa Ynez River sediment down the Arguello submarine canyon to the west (Fig. 17).

The frequency of distinct gray layers chiefly reflects their degree of preservation or bioturbation. Gray layers are most common in laminated sequences and least frequent in the massive subunits; thus, we feel that their presence reflects levels of bottom-water oxygenation and biological mixing. Gray layer deposition may also reflect, however, the strength of the northwest-flowing Davidson/Anacapa Current, which is the principal agent for the transport of terrigenous silt and clay from the Santa Clara and Ventura rivers to the Santa Barbara Basin today (Drake et al., 1972; Thornton, 1981). The eastern sill of the Santa Barbara Basin, through which the Davidson/Anacapa current flows, is presently only ~230 m deep. Shoaling to ~110 m at maximum lowstands may be sufficient to deflect or slow the Davidson/Anacapa current, effectively blocking or severely reducing the suspended transport of river-derived silt and clay into the Santa Barbara Basin (Fig. 17). Alternately, and probably less likely, shoaling and narrowing of the eastern sill (Anacapa Passage) may have accelerated the through-going current, jetting suspended fine-grained sediments through the basin before deposition.

PALEOMAGNETISM

Multisensor Track and Discrete Measurements

Sensors mounted on the multisensor (MST) track on board *JOIDES Resolution* were used to collect closely spaced measurements of bulk

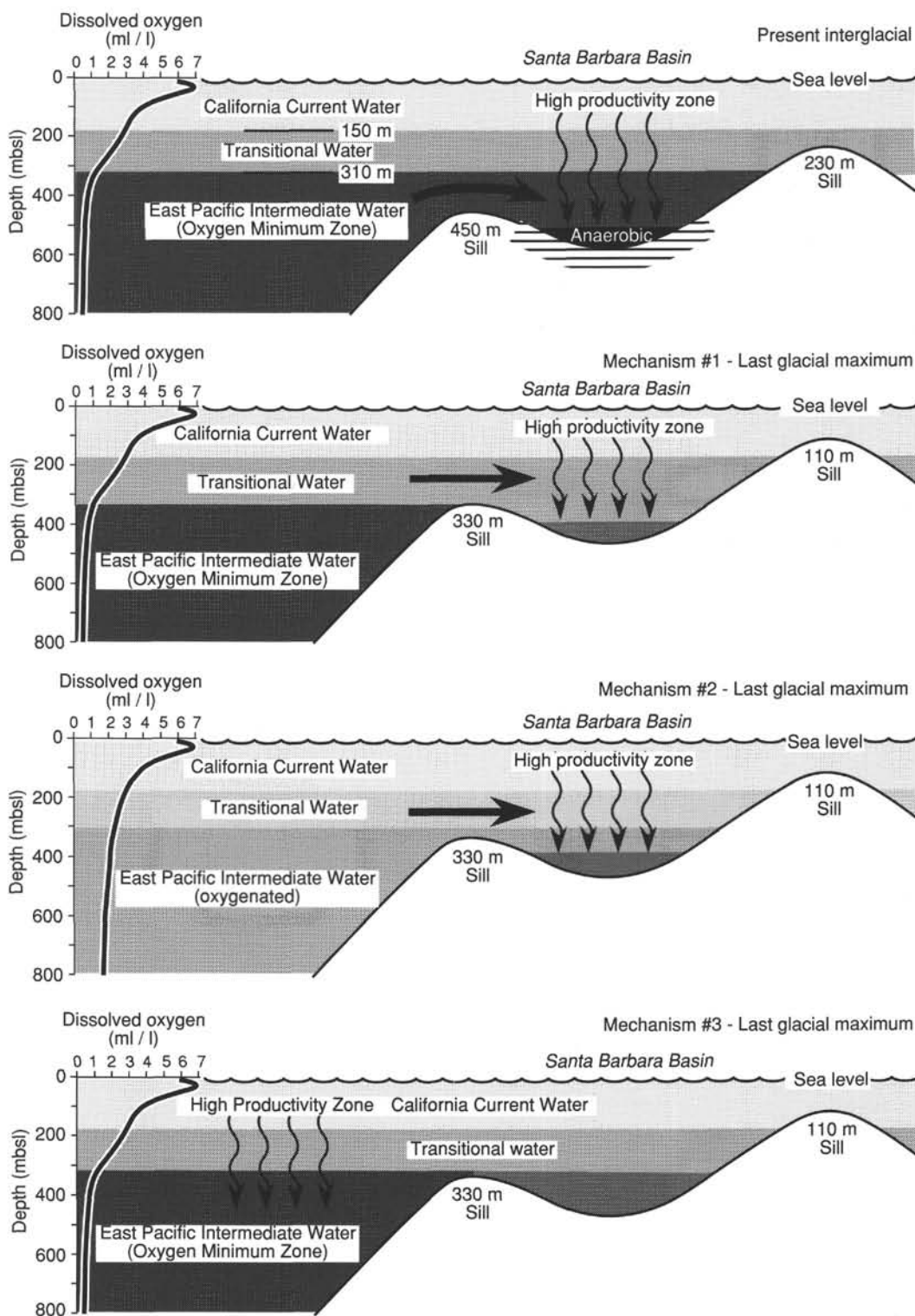


Figure 15. Model for present (interglacial) anaerobic bottom water in the center of the Santa Barbara Basin and end-member mechanisms that may have contributed to the development of aerobic bottom waters during previous glacial intervals. Darker shades of water masses reflect decreased oxygen content. Mechanism #1 = lowering of the impinging Oxygen Minimum Zone below sill depth. Mechanism #2 = increased oxygen content of the Pacific Intermediate Water mass that intercepts the deeper, western sill of the modern Santa Barbara Basin during glaciation. Mechanism #3 = shifting of high surface productivity off the shore of the Santa Barbara Basin.

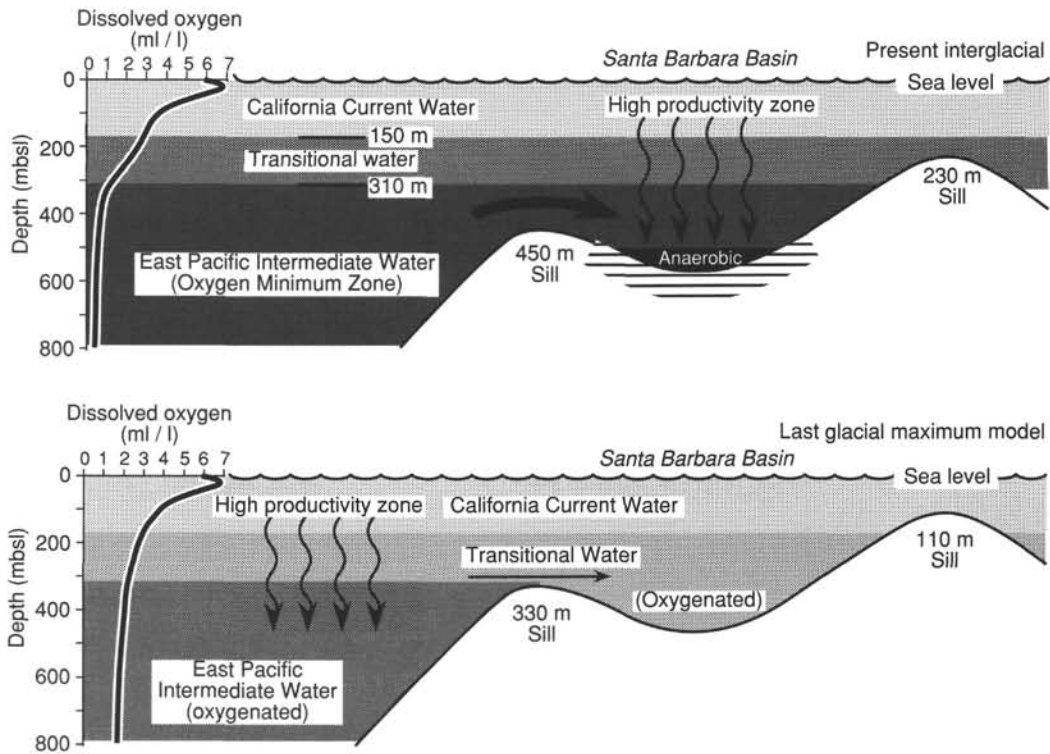


Figure 16. Preferred model for oxygenated bottom water in the Santa Barbara Basin during glacial maxima differs from present situation by lowered position (with respect to sill depth) and increased oxygen content of Pacific Intermediate Water, in conjunction with offshore shift of high surface productivity.

density and magnetic susceptibility over five cored intervals in Hole 893A. The five measured intervals include Core 146-893A-1H through Section 146-893A-3H-1 (0–17.5 mbsf; Fig. 18A), Core 146-893A-5H (35.0–44.5 mbsf; Fig. 18B), Core 146-893A-10H (82.5–92.0 mbsf; Fig. 18C), Core 146-893A-15H (130.0–139.5 mbsf; Fig. 18D), and Core 146-893A-20H (168.0–177.5 mbsf; Fig. 18E), respectively.

The presence of voids, caused by gas expansion in the cores from Site 893, caused difficulties in obtaining high-quality data within some of the intervals measured with the MST sensors, but careful comparisons of core photographs and the plotted data allow one to extract meaningful information from most of these intervals. The data from Cores 146-893A-2H and -5H were significantly degraded by the presence of numerous voids. Discrete measurements of magnetic susceptibility were obtained from variable-volume sample plugs (Table 3) that were placed inside a 36-mm inner diameter (ID) loop attached to a Bartington MS-2 magnetic susceptibility meter. Duplicate measurements collected from each sample are shown to be very consistent. These data have been scaled to a constant sample volume for comparison with the MST susceptibility data; the use of a constant sample volume should minimize the effects of the varying water content in different sediment samples relative to the wet sample weight. Discrete measurements of susceptibility from these cores exhibit general property trends that are similar to those observed in the MST susceptibility data. The discrete data are plotted along with the MST data in Figure 18.

Distinct layers of gray, silty clay to clayey silt are observed throughout much of the cored interval (see “Sedimentology” section, this chapter, and core photographs). Many of these discrete gray layers are associated with increases in bulk density and increases in magnetic susceptibility. These beds may represent “event” deposits related to storms or historical floods in California (Fleischer, 1972; Thornton, 1981, 1984; also see “Sedimentology” section, this chapter).

A detailed comparison of the bulk density and magnetic susceptibility curves generated by the MST for the upper 8 m of the sedimentary section (Fig. 18A), shows that where 2- to 5-cm-thick gray layers

are present in core photographs, they are associated with magnetic susceptibility and bulk density maxima that are located near the base, or just below the basal surface, of individual gray layers. Other, thinner gray layers may also exhibit this type of relationship, but the relative maxima may be more subtle. Measurements of magnetic susceptibility on discrete samples from these cores illustrate the general trends that are observed in the MST susceptibility data. An increase in susceptibility in Core 146-893A-1H is clearly observed; this increase may reflect an increase in the accumulation of terrigenous material relative to biogenic accumulation in the silty clay and clayey silt in the lower part of Lithologic Subunit IA.

Core 146-893A-5H exhibits a large number of gas-related voids that serve to degrade the quality of the MST data (Fig. 18B; also see core photograph). Voids are clearly observed as abrupt decreases in bulk density and magnetic susceptibility values in Figure 18B. The boundary between Lithologic Subunits IB and IC is located just below a number of voids in the upper part of Section 146-893A-5H-2, at 50 cm.

A gradual decrease in bulk density and magnetic susceptibility is observed near the base of Section 146-893A-5H-5, from 134 to 150 cm. This gradual change may reflect an increasing amount of low-density diatom skeletons in this interval of well-laminated nannofossil diatom silty clay. A sandy bed in Section 146-893A-5H-6, at 14–19 cm, is observed as a distinct bulk density peak in the GRAPE record. As noted previously, the trends that are observed in the discrete measurements of magnetic susceptibility compare favorably with the overall trend of the MST susceptibility data.

The MST magnetic susceptibility data from Sections 146-893A-10H-3 through -5 exhibit a large number of relative peaks (Fig. 18C). These peaks may be related to the presence of small siltstone pebbles and thin sand layers within the structureless silty clay comprising this core (see core photograph). A gray layer in Section 146-893A-10H-6, at 47–60 cm, is clearly observed as a susceptibility peak in the MST data.

The MST data from Core 146-893A-15H reflect the presence of a relatively dense, nonlaminated interval of silty clay extending from

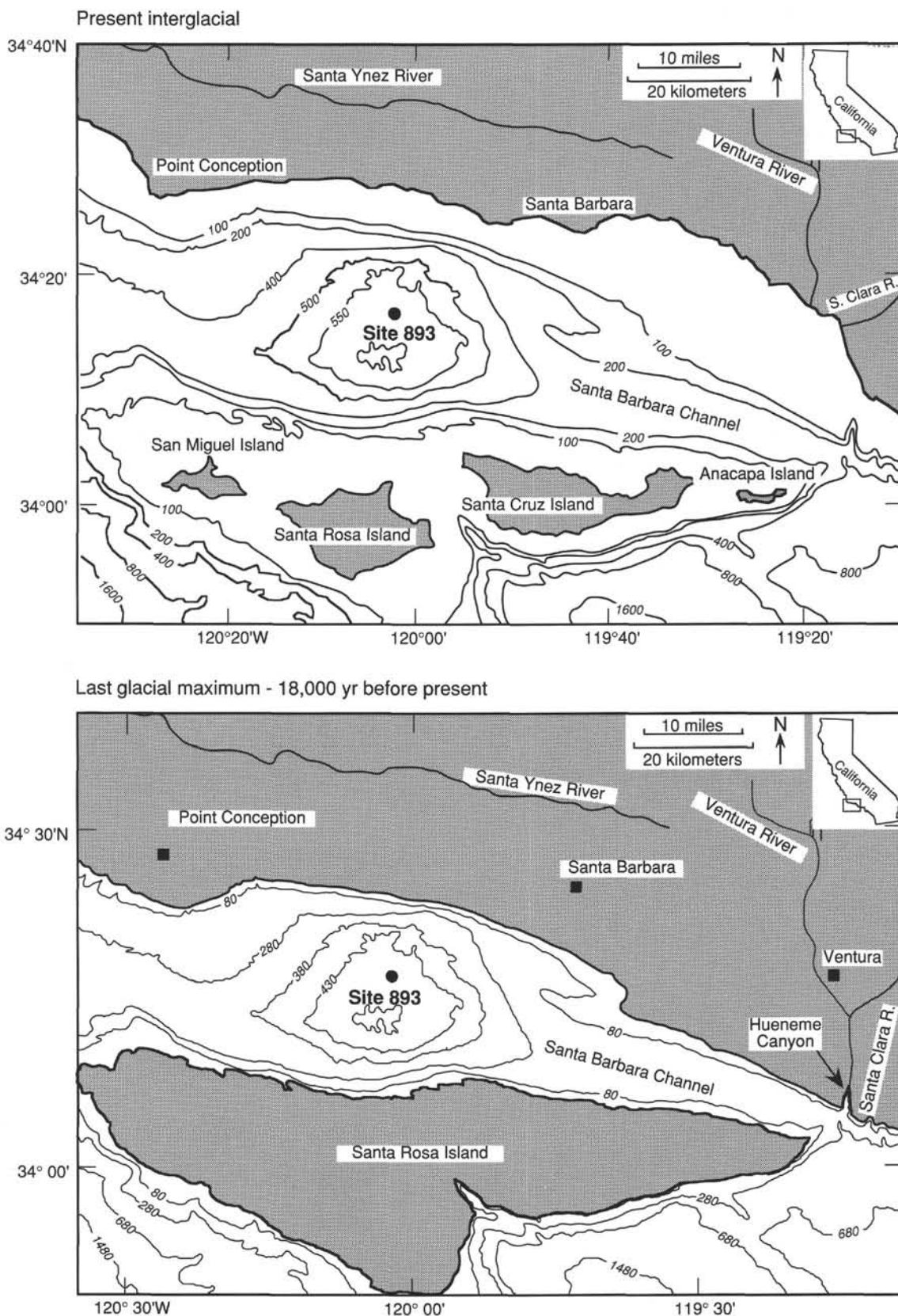


Figure 17. Comparison of physiography between present interglacial and last glacial maximum (18,000 ka). Shoreline at last glacial maximum based on sea-level drop of 120 m from present. Note coalescence of the four northern channel islands into a single, sheltering landmass, decreased sill depths, narrowing of eastern and western passages, and proposed capture of Santa Clara and Ventura rivers by the Hueneme Canyon.

Table 3. Magnetic susceptibility of cylindrical sample plugs, Hole 893A.

Core, section, interval (cm)	Depth (mbsf)	Cylinder length (cm)	Volume (cm ³)	Wet weight				Background	Core, section, interval (cm)	Depth (mbsf)	Cylinder length (cm)	Volume (cm ³)	Wet weight				Background
				(g)	Mag ₁	Mag ₂	Background						(g)	Mag ₁	Mag ₂	Background	
146-893A-																	
1H-1, 57-59	0.57	2.70	11.716	14.73	5.9	5.9	-0.2	8H-3, 58-60	65.76	3.10	13.452	21.24	45.1	45.1	0.0		
1H-1, 132-134	1.32	2.50	10.848	14.31	4.6	4.5	-0.2	8H-3, 134-136	66.52	3.00	13.018	19.71	13.7	13.6	-0.2		
1H-2, 58-60	2.08	2.60	11.282	14.89	4.3	4.3	-0.1	8H-4, 57-59	67.25	3.00	13.018	19.66	13.9	13.9	-0.1		
1H-2, 132-134	2.82	2.40	10.414	14.92	4.2	4.1	-0.1	8H-4, 132-134	68.00	3.00	13.018	19.41	11.0	11.0	-0.1		
1H-3, 58-60	3.60	2.70	11.716	18.16	6.7	6.6	-0.1	8H-5, 60-62	68.78	2.10	9.1126	15.04	8.0	7.9	-0.1		
1H-3, 132-134	4.34	2.70	11.716	19.24	9.6	9.6	-0.1	8H-5, 132-134	69.50	3.00	13.018	21.67	13.7	13.7	0.0		
1H-4, 58-60	5.10	3.00	13.018	20.10	9.5	9.5	0.0	8H-6, 53-55	70.21	2.60	11.282	19.17	11.1	10.9	-0.3		
1H-4, 132-134	5.84	2.90	12.584	18.46	8.1	8.1	-0.1	8H-6, 132-134	71.00	3.10	13.452	21.41	12.3	12.3	0.0		
2H-1, 57-59	7.07	3.00	13.018	18.44	9.9	9.8	-0.1	8H-7, 59-61	71.77	2.70	11.716	17.23	10.1	10.1	0.0		
2H-1, 133-135	7.83	2.60	11.282	19.30	22.7	22.6	0.0	8H-7, 132-134	72.50	3.20	13.886	21.05	13.4	13.4	0.0		
2H-2, 57-59	8.61	2.70	11.716	17.71	7.7	7.6	-0.2	8H-8, 57-59	73.25	3.00	13.018	21.35	14.7	14.8	0.0		
2H-2, 133-135	9.37	2.60	11.282	17.76	8.5	8.5	0.2	9H-1, 56-58	73.56	3.00	13.018	21.78	11.0	11.0	0.1		
2H-3, 57-59	10.11	2.90	12.584	16.54	10.6	10.6	0.1	9H-1, 131-133	74.31	3.00	13.018	18.91	9.1	9.0	-0.2		
2H-3, 133-135	10.87	2.80	12.150	19.51	8.5	8.4	0.0	9H-2, 56-58	75.06	2.20	9.5465	15.57	7.3	7.3	-0.2		
2H-4, 57-59	11.62	2.80	12.150	19.48	8.8	8.8	0.0	9H-2, 131-133	75.81	3.00	13.018	19.72	10.4	10.5	-0.1		
2H-4, 133-135	12.38	2.90	12.584	18.00	7.5	7.5	-0.2	9H-3, 56-58	76.56	2.90	12.584	19.07	9.2	9.2	0.1		
2H-5, 62-64	13.17	2.50	10.848	17.66	8.7	8.8	0.0	9H-3, 124-126	77.24	3.00	13.018	21.35	10.6	10.5	-0.2		
2H-5, 133-135	13.88	2.30	9.9804	16.28	6.8	6.9	-0.2	9H-4, 56-58	78.06	2.70	11.716	18.76	11.3	11.4	0.0		
2H-6, 57-59	14.62	2.50	10.848	16.90	7.0	7.1	0.0	9H-4, 131-133	78.81	2.90	12.584	18.74	11.9	11.9	0.1		
2H-6, 133-135	15.38	2.40	10.414	16.63	6.7	6.7	0.0	9H-5, 131-133	79.56	2.90	12.584	20.28	12.9	12.9	0.0		
2H-7, 57-59	16.12	2.60	11.282	16.64	6.6	6.6	0.0	9H-5, 56-58	80.31	2.90	12.584	19.86	10.9	10.9	0.2		
3H-1, 64-66	16.64	2.40	10.414	16.19	14.9	14.9	0.0	9H-7, 56-58	81.27	3.10	13.452	19.26	9.9	9.9	0.0		
3H-1, 132-134	17.32	2.50	10.848	17.03	8.6	8.5	-0.2	9H-7, 131-133	82.02	3.00	13.018	19.57	28.8	28.8	0.0		
3H-2, 58-60	18.08	2.10	9.1126	16.00	16.6	16.6	0.0	9H-8, 56-58	82.77	3.00	13.018	19.34	11.3	11.2	0.1		
3H-2, 132-134	18.82	2.50	10.848	18.17	14.8	14.7	-0.1	10H-1, 57-59	83.07	3.20	13.886	23.01	15.7	15.6	-0.1		
3H-3, 64-66	19.64	2.50	10.848	17.77	15.1	15.1	0.1	10H-1, 128-130	83.78	2.90	12.584	20.05	14.5	14.4	-0.3		
3H-3, 126-128	20.26	2.30	9.9804	15.56	11.1	11.0	0.1	10H-2, 57-59	84.57	3.00	13.018	21.10	14.4	14.4	-0.2		
3H-4, 65-67	21.15	2.90	12.584	19.65	9.2	9.2	0.1	10H-2, 132-134	85.32	3.00	13.018	21.44	15.5	15.5	-0.1		
3H-4, 132-134	21.82	3.00	13.018	20.62	8.6	8.6	-0.1	10H-3, 57-59	86.07	2.80	12.150	20.05	14.6	14.6	-0.2		
3H-5, 51-53	22.51	3.10	13.452	21.79	9.8	9.9	0.1	10H-3, 132-134	86.82	3.00	13.018	21.10	26.9	26.9	-0.1		
3H-5, 143-145	23.43	3.00	13.018	21.45	10.3	10.3	0.1	10H-4, 59-61	87.69	2.50	10.848	17.62	12.9	12.8	0.0		
3H-6, 63-65	24.13	2.80	12.150	19.68	10.1	10.1	0.1	10H-4, 132-134	88.42	2.60	11.282	18.53	16.8	16.7	-0.2		
3H-6, 132-134	24.82	3.00	13.018	21.78	12.8	12.8	0.1	10H-5, 57-59	89.17	2.90	12.584	18.87	16.9	16.9	-0.1		
3H-7, 55-57	25.55	2.80	12.150	18.33	13.9	13.9	0.1	10H-5, 132-134	89.92	2.90	12.584	18.01	15.0	14.9	-0.2		
4H-1, 60-62	26.10	3.10	13.452	22.25	13.9	13.9	-0.1	10H-6, 54-56	90.64	2.00	8.6786	13.99	18.0	17.9	-0.2		
4H-1, 132-134	26.82	2.90	12.584	20.64	13.7	13.6	-0.3	10H-7, 57-59	91.50	2.80	12.150	17.08	11.8	11.6	-0.1		
4H-2, 58-60	27.58	2.90	12.584	22.43	14.8	14.8	-0.1	10H-7, 132-134	92.25	3.20	13.886	22.51	16.4	16.3	0.1		
4H-2, 134-136	28.33	3.00	13.018	20.55	13.0	13.0	-0.1	11H-1, 57-59	92.57	3.30	14.320	24.63	15.7	15.7	0.1		
4H-3, 57-59	29.07	2.80	12.150	20.98	15.0	15.0	-0.1	11H-1, 132-134	93.32	2.80	12.150	20.83	13.6	13.6	0.1		
4H-3, 131-133	29.81	3.00	13.018	21.46	13.7	13.6	0.1	11H-2, 57-59	94.07	3.20	13.886	23.27	14.3	14.3	0.0		
4H-4, 47-49	30.47	3.00	13.018	20.78	13.1	13.1	-0.2	11H-2, 127-129	94.77	3.10	13.452	22.02	12.8	12.8	0.0		
4H-4, 124-126	31.24	3.20	13.886	21.08	12.6	12.7	0.0	11H-3, 57-59	95.57	3.10	13.452	22.01	11.2	11.2	-0.1		
4H-5, 57-59	32.07	3.20	13.886	23.06	14.3	14.3	-0.1	11H-3, 127-129	96.27	3.00	13.018	22.38	13.3	13.4	0.1		
4H-5, 126-128	32.76	2.80	12.150	18.25	11.0	11.0	0.0	11H-4, 57-59	97.07	2.70	11.716	16.64	6.2	6.2	0.0		
4H-6, 62-64	33.62	2.90	12.584	15.57	7.7	7.6	-0.2	11H-4, 127-129	97.77	2.90	12.584	21.14	10.7	10.7	0.0		
4H-6, 134-136	34.34	2.90	12.584	18.90	11.6	11.6	-0.2	11H-5, 57-59	98.57	3.30	14.320	23.62	13.7	13.7	0.0		
4H-7, 57-59	35.07	3.00	13.018	19.70	9.1	9.1	0.0	11H-6, 57-59	99.34	3.10	13.452	22.65	12.8	12.8	0.1		
5H-1, 57-59	35.57	3.00	13.018	22.98	12.4	12.4	-0.1	11H-6, 132-134	100.09	3.10	13.452	18.31	9.6	9.6	0.0		
5H-1, 132-134	36.32	2.90	12.584	18.28	9.0	9.0	0.1	12H-1, 57-59	102.07	3.10	13.452	22.75	13.3	13.3	0.0		
5H-2, 57-59	37.07	3.00	13.018	21.07	13.6	13.6	0.0	12H-1, 132-134	102.82	3.00	13.018	22.05	17.9	17.9	0.0		
5H-2, 132-134	37.82	3.00	13.018	20.85	12.4	12.4	-0.2	12H-2, 57-59	103.57	2.90	12.584	20.43	12.4	12.3	0.0		
5H-3, 57-59	38.57	2.70	11.716	18.01	11.8	11.8	-0.1	12H-2, 132-134	104.32	3.10	13.452	21.98	13.4	13.4	0.0		
5H-3, 132-134	39.32	2.80	12.150	17.78	12.2	12.2	-0.1	12H-3, 57-59	105.14	2.90	12.584	21.15	13.3	13.4	0.1		
5H-4, 57-59	40.07	3.00	13.018	21.35	13.2	13.2	-0.1	12H-3, 133-135	105.90	3.10	13.452	22.66	14.7	14.7	0.0		
5H-4, 132-134	40.82	3.20	13.886	22.36	12.8	12.7	-0.1	12H-4, 64-66	106.73	3.00	13.018	21.12	12.9	13.0	0.0		
5H-5, 57-59	41.57	2.60	11.282	18.94	11.2	11.1	-0.1	12H-4, 132-134	107.41	3.00	13.018	20.96	11.2	11.2	-0.1		
5H-5, 132-134	42.32	2.80	12.150	18.51	8.5	8.4	0.0	12H-6, 57-59	108.62	2.90	12.584	20.08	12.8	12.8	0.0		
5H-6, 57-59	43.07	3.20	13.886	20.30	10.6	10.5	-0.3	12H-6, 132-134	109.37	2.90	12.584	19.02	10.6	10.6	0.1		
5H-6, 132-134	43.82	2.50	10.848	17.36	9.4	9.2	-0.3	12H-8, 58-60	110.54	3.10	13.452	21.04	13.4	13.5	0.1		
5H-7, 57-59	44.57	2.80	12.150	21.11	13.9	13.9	0.2	12H-8, 128-130	111.24	3.00	13.018	22.90	16.7	16.8	0.0		
6H-1, 57-59	45.07	3.00	13.018	20.23	13.7	13.6	0.0	13H-1, 59-61	111.59	2.80	12.150	17.20	10.4	10.4	-0.1		
6H-1, 132-134	45.82	2.80	12.150	20.85	14.5	14.5	-0.1	13H-1, 131-133	112.31	2.70	11.716	19.57	14.4	14.3	-0.1		
6H-2, 57-59	46.57	3.00	13.018	20.64	12.3	12.4	-0.1	13H-3, 56-58	113.28	2.50	10.848	17.48	11.9	11.8	-0.1		
6H-2, 132-134	47.32	2.90	12.584	17.06	10.1	10.1	0.0	13H-3, 131-133	114.03	3.00	13.018	18.07	10.6	10.4	0.0		
6H-3, 57-59	48.07	3.10	13.452	20.28	13.0	13.0	0.1	13H-4, 56-58	114.71	3.00	13.018	22.61	9.8	9.8	0.0		
6H-3, 132-134	48.82	3.10	13.452	21.06	12.5	12.5	-0.1	13H-4, 131-133	115.46	2.80	12.150	18.67	8.5	8.5	0.1		
6H-4, 55-57	49.55	3.10	13.452	14.14	8.2	8.1	-0.1	13H-5, 131-133	116.96	2.80	12.150	20.14	12.6	12.6	0.0		
6H-4, 132-134	50.32	2.70	11.716	19.66	12.3	12.2	-0.1	13H-6, 56-58	117.71	2.80	12.150	20.03	15.8	15.8	0.0		
6H-5, 57-59	51.07	3.10	13.452	22.35	16.5	16.4	-0.2	13H-6, 131-133	118.46	3.20	13.886	18.10	8.2	8.1	-0.2		
6H-5, 132-134	51.82	3.10	13.452	19.46	11.7	11.7	0.0	13H-7, 56-58	119.21	2.60	11.282	16.76	8.1	8.0	-0.3		
6H-6, 58-60</																	

Table 3 (continued).

Core, section, interval (cm)	Depth (mbsf)	Cylinder length (cm)	Volume (cm ³)	Wet weight (g)		Background	
				Mag ₁	Mag ₂		
15H-1, 131-133	131.31	2.50	10.848	19.11	12.2	12.1	-0.2
15H-3, 55-57	133.58	2.40	10.414	17.22	8.5	8.5	-0.1
15H-3, 131-133	134.34	2.50	10.848	18.46	8.9	8.8	-0.1
15H-4, 55-57	135.12	2.40	10.414	18.18	11.0	10.9	-0.2
15H-4, 131-133	135.88	3.00	13.018	19.62	35.7	35.6	-0.1
15H-5, 56-58	136.74	2.50	10.848	18.75	15.2	15.2	0.0
15H-5, 131-133	137.49	2.40	10.414	17.08	9.2	9.1	-0.2
15H-6, 56-58	138.36	2.20	9.5465	14.09	6.0	5.9	-0.3
15H-6, 131-133	139.11	2.60	11.282	17.75	9.1	9.1	0.1
15H-7, 56-58	139.86	2.50	10.848	17.82	9.6	9.6	-0.1
16H-1, 60-62	140.10	3.10	13.452	19.32	11.6	11.6	-0.1
16H-1, 131-133	140.81	3.10	13.452	17.82	9.8	9.6	-0.1
16H-2, 57-59	141.57	2.80	12.150	15.64	6.9	6.9	-0.2
16H-2, 131-133	142.31	2.90	12.584	19.37	11.8	11.7	-0.1
16H-3, 60-62	143.10	3.00	13.018	19.51	10.0	9.9	-0.2
16H-3, 131-133	143.81	3.10	13.452	20.52	10.0	10.0	-0.2
16H-4, 55-57	144.69	3.50	15.188	23.69	33.4	33.4	-0.1
16H-4, 130-132	145.44	3.20	13.886	24.48	14.4	14.3	-0.1
16H-5, 57-59	146.25	3.20	13.886	24.19	14.4	14.4	0.0
16H-5, 131-133	146.99	2.90	12.584	21.10	12.8	12.8	-0.1
16H-6, 57-59	147.78	2.70	11.716	18.87	11.0	11.0	0.0
16H-6, 133-135	148.54	3.10	13.452	21.10	12.5	12.5	0.0
16H-7, 57-59	149.28	2.90	12.584	21.18	12.8	12.7	0.0
17H-1, 57-59	149.57	3.10	13.452	23.23	16.6	16.7	0.0
17H-1, 131-133	150.31	3.10	13.452	23.75	18.1	18.2	-0.1
17H-2, 56-58	151.06	2.90	12.584	21.76	17.6	17.6	-0.1
17H-2, 131-133	151.81	3.10	13.452	23.21	22.9	22.9	0.0
17H-3, 57-59	152.60	2.60	11.282	18.53	12.7	12.7	-0.2
17H-3, 131-133	153.34	2.90	12.584	21.75	15.0	14.9	-0.1
17H-4, 56-58	154.19	2.70	11.716	20.07	13.7	13.7	-0.1
17H-4, 131-133	154.94	3.10	13.452	22.99	15.7	15.7	0.0
17H-5, 56-58	155.79	2.20	9.5465	15.93	9.6	9.6	-0.2
17H-5, 131-133	156.54	3.10	13.452	22.87	15.6	15.6	0.0
17H-6, 56-58	157.29	3.10	13.452	21.63	16.1	16.1	-0.1
17H-6, 131-133	158.04	3.00	13.018	21.24	14.1	14.1	0.0
18H-1, 53-55	159.03	3.40	14.754	21.74	14.7	14.7	0.0
18H-1, 132-134	159.82	3.30	14.320	24.72	17.5	17.5	0.0
18H-2, 57-59	160.57	3.20	13.886	24.18	13.1	13.0	0.0
18H-2, 132-134	161.32	3.30	14.320	22.71	13.6	13.6	-0.1
18H-3, 57-59	162.07	3.10	13.452	17.96	10.5	10.4	0.0
18H-3, 132-134	162.82	3.10	13.452	22.61	12.5	12.5	0.0
18H-4, 57-59	163.65	3.00	13.018	22.95	14.6	14.6	0.0
18H-4, 132-134	164.40	2.10	9.1126	15.67	9.1	9.0	-0.1
18H-5, 56-58	165.14	3.00	13.018	14.10	7.8	7.7	0.0
18H-5, 132-134	165.90	2.70	11.716	21.97	15.2	15.2	0.2
18H-6, 57-59	166.65	3.20	13.886	23.22	55.7	55.7	0.1
18H-6, 132-134	167.40	3.00	13.018	19.36	12.3	12.3	0.1
18H-7, 37-39	167.95	3.00	13.018	22.48	14.5	14.5	0.2
19H-1, 62-64	168.62	2.90	12.584	19.05	10.2	10.3	-0.2
19H-1, 132-134	169.32	3.20	13.886	24.43	17.5	17.5	-0.1
19H-2, 57-59	170.09	2.80	12.150	18.48	11.3	11.3	-0.1
19H-2, 127-129	170.79	3.30	14.320	22.99	14.0	13.9	0.0
19H-3, 57-59	171.59	2.70	11.716	18.47	15.2	15.1	-0.2
19H-3, 132-134	172.34	2.90	12.584	21.99	16.8	16.8	-0.2
19H-4, 57-59	173.09	2.20	9.5465	16.18	9.6	9.5	-0.2
19H-4, 132-134	173.84	3.10	13.452	21.23	16.3	16.3	-0.1
19H-5, 57-59	174.65	2.80	12.150	21.92	19.8	19.9	-0.1
19H-5, 132-134	175.40	2.80	12.150	16.07	10.0	10.0	0.0
19H-6, 57-59	176.15	2.90	12.584	18.96	13.6	13.6	-0.3
19H-6, 131-133	176.89	3.00	13.018	20.95	15.8	15.8	0.0
20H-1, 55-57	178.05	2.60	11.282	19.59	13.4	13.4	0.2
20H-1, 132-134	178.82	3.30	14.320	23.71	15.9	15.8	0.1
20H-2, 57-59	179.57	2.50	10.848	18.68	12.7	12.7	0.0
20H-2, 137-139	180.37	3.20	13.886	23.83	14.9	15.0	0.0
20H-3, 57-59	181.07	3.20	13.886	24.14	18.3	18.3	0.0
20H-3, 132-134	181.82	3.20	13.886	24.14	17.5	17.5	-0.1
20H-4, 57-59	182.57	3.40	14.754	25.50	17.2	17.2	-0.1
20H-4, 132-134	183.32	3.20	13.886	24.03	17.5	17.5	-0.2
20H-5, 57-59	184.07	2.60	11.282	19.34	14.3	14.2	-0.1
20H-5, 133-135	184.83	3.10	13.452	22.19	12.5	12.6	0.0
20H-6, 57-59	185.57	3.00	13.018	23.00	27.3	27.3	0.1
20H-6, 132-134	186.32	3.30	14.320	23.21	16.7	16.6	0.0
20H-7, 51-53	187.03	2.50	10.848	13.26	7.9	7.9	-0.1

the middle of Section 146-893A-15H-4 to the middle of Section 146-893A-15H-5, with increased levels of magnetic susceptibility in both MST and discrete data (Fig. 18D; also see core photo). Sharp peaks in GRAPE bulk density and magnetic susceptibility in Sections 146-893A-15H-3, at 60-68 cm, and -15H-6, at 69-75 and 135-139 cm, respectively, correspond to gray, silty clay layers. An interval of

diatom ooze laminae in the upper part of Section 146-893A-15H-6 is indicated by a number of sharp variations in GRAPE bulk density. Additional low-density intervals in this core may correspond to relative increases in the accumulation of diatom skeletons.

The dominant feature of the MST data collected from Core 146-893A-20H is the presence of a large increase in magnetic susceptibility in the middle of Section 146-893A-20H-6. This increase may be associated with the presence of a shell-bearing bed at Section 146-893A-20H-6, 55 cm, and two gray, silty clay beds at 40-45 and 64-73 cm, respectively.

Although time constraints at the end of Leg 146 prevented the routine collection of MST data and the presence of gas voids in the cores degraded the quality of data in some intervals, it is clear from the five examples presented here that these data have merit and can effectively contribute (in the future) to the task of hole-to-hole correlation through the identification of discrete "event" horizons.

A variety of rock magnetic measurements were also conducted on discrete samples taken from Cores 146-893A-3H, -4H, and 11H. Magnetic susceptibilities (χ) were measured before demagnetization and anhysteretic remanent magnetizations (ARMs; 0.05-mT bias, 100-mT alternating field [AF]) were acquired, measured, and then stepwise demagnetized to 100 mT after NRM demagnetizations were completed. The ARM coercivity spectra are shown for three typical horizons in Figure 19. In all cases, the ARM coercivity spectra were significantly harder (higher MDFs) than the NRMs. This pattern is quite similar to rock magnetic data noted in detailed studies of Santa Catalina Basin (Brandma et al., 1989; S.P. Lund, unpubl. data).

The ARM and χ data have been used in several previous studies of surficial marine sediments in the borderland to identify major changes in the relative grain size and amount of magnetic material in the sediments. For example, Lund et al. (1992) have plotted ARM vs. χ of surface sediments from more than 30 box cores in the Santa Barbara Basin region (Fig. 20, solid circles). The distance from the origin to each data point can be used as a measure of the amount of rock magnetic material in each sample, and the higher the slope (ARM/ χ), the finer the overall magnetic grain-size distribution (King et al., 1982). As can be noted in Figure 20, surface sediments on the shelf surrounding Santa Barbara Basin are rich in coarse-grained magnetic material whereas surface sediments closer to the basin are richer in fine-grained magnetic material. In the very center of the basin and especially with increasing depth below the sediment/water interface, the ARM and χ values diminish systematically toward the origin of the plot in Figure 20 because of magnetic mineral dissolution.

Our new ARM and χ results from Hole 893A, plotted as open circles in Figure 20, suggest that the sediment throughout the core has undergone a similar degree of magnetic mineral dissolution. The remaining NRMs, as can be deduced from their low MDFs, reside primarily in detrital magnetic material that has escaped dissolution because of its coarse-grained nature. The similarity of NRM, ARM, and χ intensities in Cores 146-893A-3H, -4H, and -11H (Fig. 21) suggests that the magnetic material contributing to the NRMs has withstood early dissolution near the sediment/water interface and is not undergoing further dissolution with increasing depth in the core.

One complication to this rock magnetic analysis is the possibility that a small part (ca. 10%) of the NRMs resides in an authigenic magnetic sulfide, such as greigite or pyrrhotite. This would help to explain the small NRM contribution noted in some samples above 50-mT AF demagnetization (Fig. 19), and the much higher coercivity of the ARMs as compared with the NRMs (Fig. 19). We cannot say at this time whether such authigenic phases are present. Several rock magnetic experiments are planned to test this possibility.

These initial paleomagnetic and rock magnetic results indicate that a stable NRM, which appears to preserve a serially correlatable paleosecular variation (PSV) record, is present in the sediments at Site 893. The NRM resides primarily in relatively coarse-grained detrital magnetic material (mostly magnetite), which has withstood an interval of magnetic mineral dissolution, probably in the uppermost 50 cm

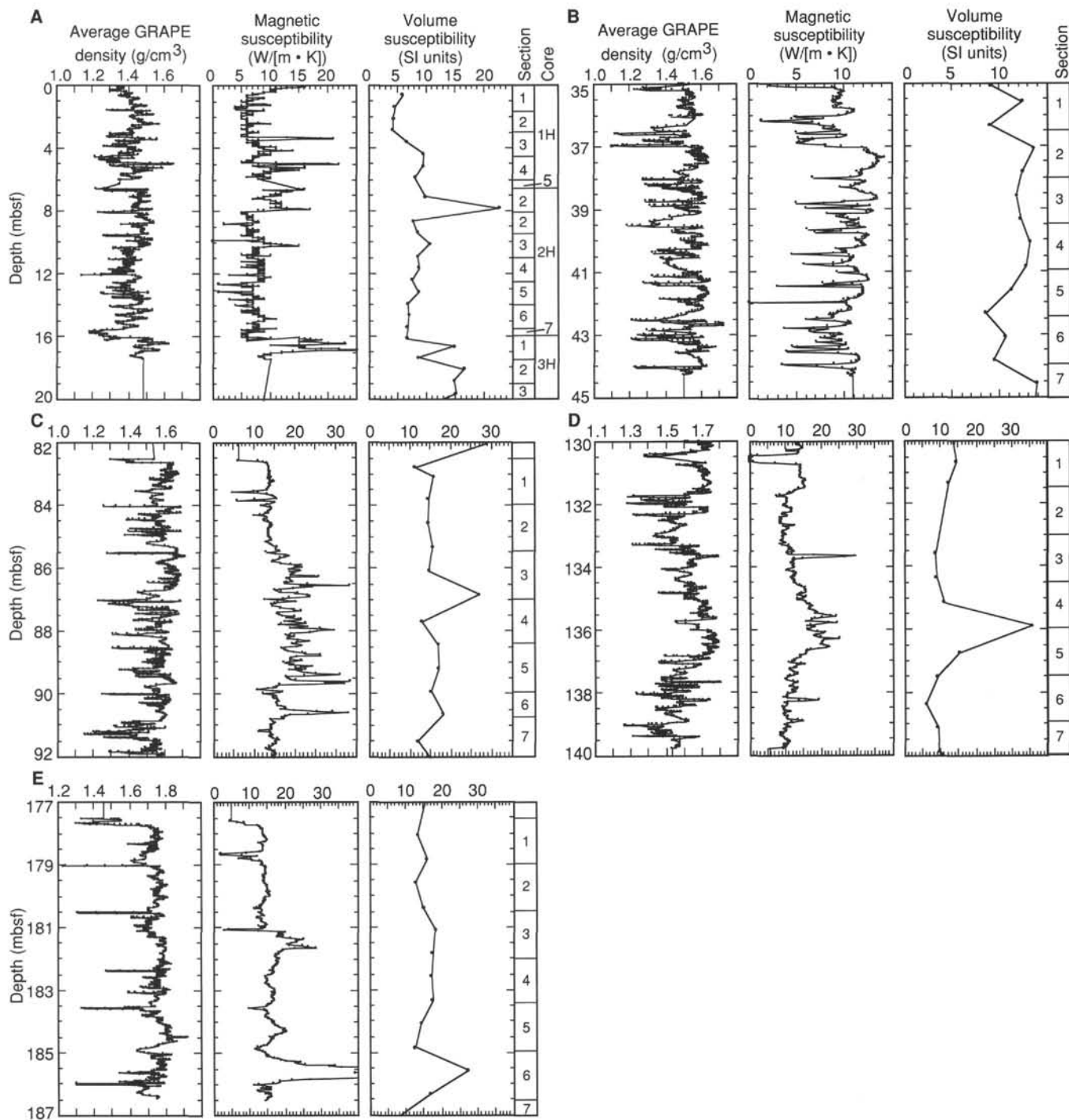


Figure 18. Smoothed GRAPE bulk density and magnetic susceptibility data vs. depth, Site 893. The MST data are compared to measurements of magnetic susceptibility using discrete sample plugs (the data is scaled to a constant sample volume). Also shown are core and section lengths to orient the reader. Note the similarities in the general trends of magnetic susceptibility measurements. Also note changes in scale for each set of figures. **A.** MST data collected from whole-round core sections of Cores 146-893A-1H and -2H and Section 146-893A-3H-1 using sensors on the multisensor (MST) track onboard the *JOIDES Resolution*. Several of the magnetic susceptibility peaks are identified in the core photos as gray-colored sedimentary layers. Susceptibility generally increases at the top of Core 146-893A-3H, relative to the upper two cores. **B.** MST data from Core 146-893A-5H. A large number of voids that degrade the quality of MST measurements are observed in this core (see core photo). **C.** MST data from Core 146-893A-10H. A number of small pebbles that were visually observed in this core in Sections 146-893A-10H-3, -4, and -5 (see core photo) are also indicated by the fluctuations in magnetic susceptibility from approximately 86 to 90 mbsf. Discrete measurements indicate increased magnetic susceptibility near the base of Section 146-893A-10H-3. **D.** MST data from Core 146-893A-15H. A peak in magnetic susceptibility in Section 146-893A-15H-3, 60–68 cm, is observed as a gray-colored sediment layer (see core photo). Laminated intervals of diatom ooze/silty clay are observed as decreased GRAPE density values in Sections 146-893A-15H-2 and -15H-3, and in Section 146-893A-15H-6. A nonlaminated interval from Section 146-893A-15H-4, 100 cm, to -15H-5, 90 cm, is observed as an increase in magnetic susceptibility by MST and discrete measurement techniques. **E.** MST data from Core 146-893A-20H. Voids within the core are observed in the MST data (see core photo).

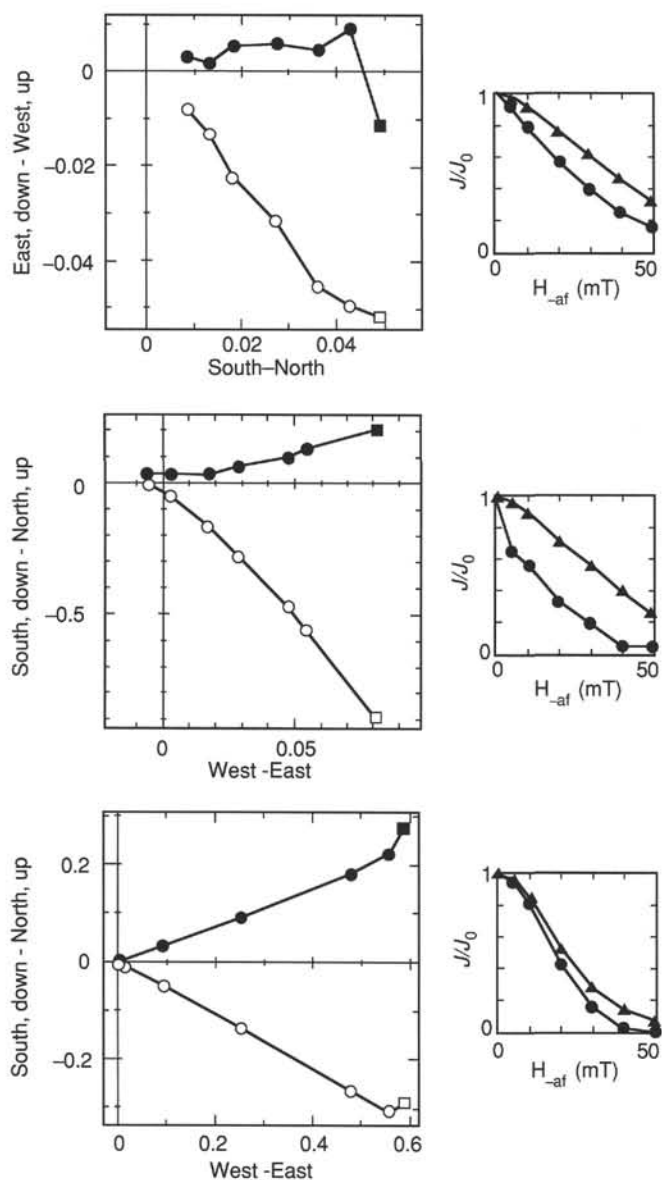


Figure 19. Results of NRM and ARM demagnetization for selected samples from Hole 893A in the Santa Barbara Basin. At left are Zijderveld diagrams that display the changes in NRM vector direction during alternating-field (AF) demagnetization. The closed circles in the Zijderveld diagrams represent the tip of the horizontal NRM component (in the X-Y plane) at each step of AF demagnetization; the open circles represent the tip of the vertical NRM component (in the X-Z plane) at each demagnetization step. At right are demagnetization curves that display the relative decrease of NRM and ARM intensity during AF demagnetization.

of the sediment column. No evidence is present that the dissolution process is continuing at a slower rate with increasing depth in the sediment column. It is possible that a small part of the NRM resides in an authigenic magnetic sulfide that grew during the dissolution process; however, further rock magnetic study is needed to test this possibility. Site 893 sediments span a time interval in which more PSV records are badly needed. The PSV record of this core, therefore, is potentially important, especially if it can be correlated with other records to form a high-resolution chronology.

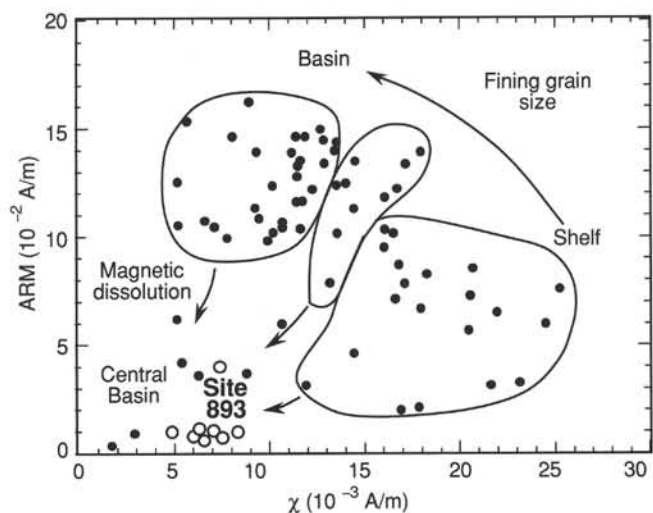


Figure 20. ARM vs. χ in the Santa Barbara Basin. The solid circles are results from box-cored surface sediments, whereas the open circles are from piston-cored sediments at Site 893. See text for further discussion. (After Lund et al., 1992.)

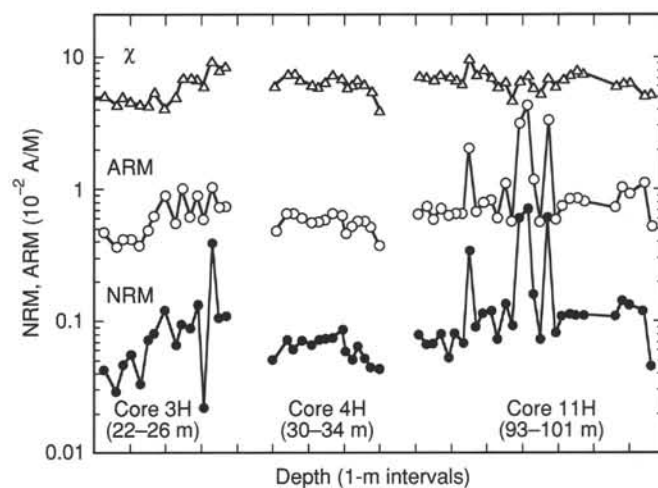


Figure 21. NRM, ARM, and χ intensity variations in three segments of cores taken from Hole 893A. Notice the lack of large-scale intensity changes over an 80-m range of sediments.

PHYSICAL PROPERTIES

Index properties (wet- and dry-bulk density, grain density, porosity, and water content) were calculated for 242 discrete sediment samples taken in cylindrical plastic plugs from the cores in Hole 893A. The raw data collected from these samples (weight and volume relationships) are given in Table 4. The calculated index properties are given in Table 5 and are graphically illustrated in Figure 22.

Fifty-six of the discrete samples were selected from the main group to determine their respective index properties using a Penta pycnometer located at the ODP Gulf Coast Repository. These data are given in Table 6 and are illustrated in Figure 23. Data provided by recent laboratory determinations of the percent calcium carbonate contained in these same samples (F. Rack, unpubl. data) are also included in Figures 22 and 23 for comparison with the index property trends.

Table 4. Raw data for calculating index properties from cylindrical sample plugs (10 cm3) in Hole 893A.

Core, section, interval (cm)	Depth (mbsf)	Cylinder height (cm)	Volume ₁ (cm ³)	Volume ₂ (cm ³)	Wet weight (g)	Dry weight (g)	Cylinder weight (g)	Wet sample weight (g)	Dry sample weight (g)	Water weight (g)	Water weight (corrected) (g)	Salt weight (g)
146-893A-												
1H-1, 57-59	0.57	2.70	12.21	11.22	19.10		4.41	14.73	4.77	9.96	10.32	0.36
1H-1, 132-134	1.32	2.50	11.31	10.39	18.86	11.38	4.55	14.31	6.82	7.49	7.76	0.27
1H-2, 58-60	2.08	2.60	11.76	10.80	19.44		4.55	14.89	5.85	9.04	9.37	0.33
1H-2, 132-134	2.82	2.40	10.86	9.97	19.40	11.99	4.48	14.92	7.51	7.41	7.68	0.27
1H-3, 58-60	3.60	2.70	12.21	11.22	22.64		4.48	18.16	7.96	10.20	10.57	0.37
1H-3, 132-134	4.34	2.70	12.21	11.22	23.90	15.67	4.66	19.24	11.01	8.23	8.53	0.30
1H-4, 58-60	5.10	3.00	13.57	12.46	24.51		4.41	20.10	9.10	11.00	11.40	0.40
1H-4, 132-134	5.84	2.90	13.12	12.05	22.94	13.23	4.48	18.46	8.75	9.71	10.06	0.35
2H-1, 57-59	7.07	3.00	13.57	12.46	22.89		4.45	18.44	8.68	9.76	10.11	0.35
2H-1, 133-135	7.83	2.60	11.76	10.80	23.83	16.71	4.53	19.30	12.18	7.12	7.38	0.26
2H-2, 57-59	8.61	2.70	12.21	11.22	22.35		4.64	17.71	8.85	8.86	9.18	0.32
2H-2, 133-135	9.37	2.60	11.76	10.80	22.39	15.06	4.63	17.76	10.43	7.33	7.60	0.27
2H-3, 57-59	10.11	2.90	13.12	12.05	20.91		4.38	16.54	9.31	7.23	7.49	0.26
2H-3, 133-135	10.87	2.80	12.67	11.63	24.04	15.01	4.53	19.51	10.48	9.03	9.36	0.33
2H-4, 57-59	11.62	2.80	12.67	11.63	23.96		4.48	19.48	9.88	9.60	9.95	0.35
2H-4, 133-135	12.38	2.90	13.12	12.05	22.62	14.18	4.62	18.00	9.56	8.44	8.75	0.31
2H-5, 62-64	13.17	2.50	11.31	10.39	22.03		4.37	17.66	12.08	5.58	5.78	0.20
2H-5, 133-135	13.88	2.30	10.40	9.56	20.90	14.37	4.62	16.28	9.75	6.53	6.77	0.24
2H-6, 57-59	14.62	2.50	11.31	10.39	21.43		4.53	16.90	8.43	8.47	8.78	0.31
2H-6, 133-135	15.38	2.40	10.86	9.97	21.19	13.57	4.56	16.63	9.01	7.62	7.90	0.28
2H-7, 57-59	16.12	2.60	11.76	10.80	21.17	13.74	4.53	16.64	9.21	7.43	7.70	0.27
3H-1, 64-66	16.64	2.40	10.86	9.97	20.75		4.56	16.19	8.27	7.92	8.21	0.29
3H-1, 132-134	17.32	2.50	11.31	10.39	21.51	14.10	4.48	17.03	9.61	7.42	7.69	0.27
3H-2, 58-60	18.08	2.10	9.50	8.72	20.64		4.64	16.00	8.99	7.01	7.26	0.25
3H-2, 132-134	18.82	2.50	11.31	10.39	22.72	15.58	4.56	18.17	11.03	7.14	7.40	0.26
3H-3, 64-66	19.64	2.50	11.31	10.39	22.25	14.84	4.47	17.77	10.36	7.41	7.68	0.27
3H-3, 126-128	20.26	2.30	10.40	9.56	19.96	13.49	4.40	15.56	9.09	6.47	6.70	0.23
3H-4, 65-67	21.15	2.90	13.12	12.05	24.12		4.47	19.65	10.29	9.36	9.70	0.34
3H-4, 132-134	21.82	3.00	13.57	12.46	25.03	15.52	4.40	20.62	11.12	9.50	9.84	0.34
3H-5, 51-53	22.51	3.10	14.02	12.88	26.28	16.51	4.49	21.79	12.02	9.77	10.12	0.35
3H-5, 143-145	23.43	3.00	13.57	12.46	25.94	17.83	4.49	21.45	13.34	8.11	8.40	0.29
3H-6, 63-65	24.13	2.80	12.67	11.63	24.34		4.66	19.68	10.79	8.89	9.21	0.32
3H-6, 132-134	24.82	3.00	13.57	12.46	26.44	17.80	4.66	21.78	13.14	8.64	8.95	0.31
3H-7, 55-57	25.55	2.80	12.67	11.63	22.82	15.11	4.48	18.33	10.63	7.70	7.98	0.28
4H-1, 60-62	26.10	3.10	14.02	12.88	26.90	17.62	4.64	22.25	12.98	9.27	9.61	0.34
4H-1, 132-134	26.82	2.90	13.12	12.05	25.29		4.65	20.64	11.58	9.06	9.39	0.33
4H-2, 58-60	27.58	2.90	13.12	12.05	26.83	17.72	4.40	22.43	13.31	9.12	9.45	0.33
4H-2, 134-136	28.33	3.00	13.57	12.46	25.10	16.44	4.55	20.55	11.88	8.67	8.98	0.31
4H-3, 57-59	29.07	2.80	12.67	11.63	25.64	17.09	4.66	20.98	12.43	8.55	8.86	0.31
4H-3, 131-133	29.81	3.00	13.57	12.46	25.94		4.48	21.46	12.65	8.81	9.13	0.32
4H-4, 47-49	30.47	3.00	13.57	12.46	25.25	16.93	4.47	20.78	12.46	8.32	8.62	0.30
4H-4, 124-126	31.24	3.20	14.48	13.30	25.63	17.12	4.55	21.08	12.57	8.51	8.82	0.31
4H-5, 57-59	32.07	3.20	14.48	13.30	27.53	18.29	4.48	23.06	13.81	9.25	9.59	0.34
4H-5, 126-128	32.76	2.80	12.67	11.63	22.66		4.41	18.25	10.58	7.67	7.95	0.28
4H-6, 62-64	33.62	2.90	13.12	12.05	20.04	13.50	4.47	15.57	9.03	6.54	6.78	0.24
4H-6, 134-136	34.34	2.90	13.12	12.05	23.46	16.11	4.56	18.90	11.55	7.35	7.62	0.27
4H-7, 57-59	35.07	3.00	13.57	12.46	24.10	15.46	4.41	19.70	11.05	8.65	8.96	0.31
5H-1, 57-59	35.57	3.00	13.57	12.46	27.54	18.72	4.55	22.98	14.17	8.81	9.13	0.32
5H-1, 132-134	36.32	2.90	13.12	12.05	22.70		4.42	18.28	10.39	7.89	8.18	0.29
5H-2, 57-59	37.07	3.00	13.57	12.46	25.47	16.88	4.40	21.07	12.48	8.59	8.90	0.31
5H-2, 132-134	37.82	3.00	13.57	12.46	25.49	17.27	4.64	20.85	12.62	8.23	8.53	0.30
5H-3, 57-59	38.57	2.70	12.21	11.22	22.41	15.61	4.40	18.01	11.21	6.80	7.05	0.25
5H-3, 132-134	39.32	2.80	12.67	11.63	22.17		4.40	17.78	10.43	7.35	7.62	0.27
5H-4, 57-59	40.07	3.00	13.57	12.46	25.76	17.43	4.41	21.35	13.03	8.32	8.62	0.30
5H-4, 132-134	40.82	3.20	14.48	13.30	26.76	18.13	4.39	22.36	13.73	8.63	8.94	0.31
5H-5, 57-59	41.57	2.60	11.76	10.80	23.42	16.08	4.47	18.94	11.61	7.33	7.60	0.27
5H-5, 132-134	42.32	2.80	12.67	11.63	23.16		4.65	18.51	10.40	8.11	8.40	0.29
5H-6, 57-59	43.07	3.20	14.48	13.30	24.77	16.83	4.47	20.30	12.35	7.95	8.24	0.29
5H-6, 132-139	43.82	2.50	11.31	10.39	21.91	15.08	4.55	17.36	10.53	6.83	7.08	0.25
5H-7, 57-59	44.57	2.80	12.67	11.63	25.58	17.23	4.47	21.11	12.76	8.35	8.65	0.30
6H-1, 57-59	45.07	3.00	13.57	12.46	24.62	16.95	4.39	20.23	12.56	7.67	7.95	0.28
6H-1, 132-134	45.82	2.80	12.67	11.63	25.26		4.41	20.85	13.01	7.84	8.12	0.28
6H-2, 57-59	46.57	3.00	13.57	12.46	25.27	17.30	4.64	20.64	12.66	7.98	8.27	0.29
6H-2, 132-134	47.32	2.90	13.12	12.05	21.70	14.80	4.64	17.06	10.16	6.90	7.15	0.25
6H-3, 57-59	48.07	3.10	14.02	12.88	24.83	16.76	4.55	20.28	12.21	8.07	8.36	0.29
6H-3, 132-134	48.82	3.10	14.02	12.88	25.61		4.55	21.06	12.49	8.57	8.88	0.31
6H-4, 55-57	49.55	3.10	14.02	12.88	18.78	12.94	4.64	14.14	8.30	5.84	6.05	0.21
6H-4, 132-134	50.32	2.70	12.21	11.22	24.30	16.45	4.64	19.66	11.81	7.85	8.13	0.28
6H-5, 57-59	51.07	3.10	14.02	12.88	27.00	18.53	4.65	22.35	13.89	8.46	8.77	0.31
6H-5, 132-134	51.82	3.10	14.02	12.88	23.88		4.41	19.46	11.10	8.36	8.66	0.30
6H-6, 58-60	52.58	2.90	13.12	12.05	22.37	14.72	4.55	17.83	10.17	7.66	7.94	0.28
6H-6, 123-134	53.32	2.90	13.12	12.05	23.23	15.66	4.40	18.83	11.26	7.57	7.84	0.27
6H-7, 57-59	54.07	2.90	13.12	12.05	25.44	17.18	4.39	21.05	12.79	8.26	8.56	0.30
7H-3, 57-59	56.15	3.00	13.57	12.46	25.94		4.37	21.57	13.58	7.99	8.28	0.29
7H-3, 132-134	56.90	3.10	14.02	12.88	24.18	16.83	4.47	19.71	12.36	7.35	7.62	0.27
7H-4, 57-59	57.65	3.00	13.57	12.46	24.35	16.71	4.62	19.73	12.09	7.64	7.92	0.28
7H-5, 57-59	59.22	2.70	12.21	11.22	22.45		4.38	18.07	10.67	7.40	7.67	0.27
7H-6, 57-59	60.72	3.20	14.48	13.30	26.30	17.55	4.64	21.67	12.91	8.76	9.08	0.32
7H-6, 132-134	61.47	2.90	13.12	12.05	23.25	16.40	4.61	18.63	11.78	6.85	7.10	0.25
7H-7, 57-59	62.22	2.50	11.31	10.39	20.47		4.38	16.09	9.65	6.44	6.67	0.23
7H-7, 132-134	62.97	2.80	12.67	11.63	22.43	15.29	4.37	18.06	10.92	7.14	7.40	0.26
7H-8, 57-59	63.72	3.10	14.02	12.88	23.84	20.22	4.56	19.28	15.66	3.62	3.75	0.13
8H-2, 24-26	63.92	2.90	13.12	12.05	24.27	16.50	4.64	19.64	11.86	7.78	8.06	0.28

Table 4 (continued).

Core, section, interval (cm)	Depth (mbsf)	Cylinder height (cm)	Volume ₁ (cm ³)	Volume ₂ (cm ³)	Wet weight (g)	Dry weight (g)	Cylinder weight (g)	Wet sample weight (g)	Dry sample weight (g)	Water weight (g)	Water weight (corrected g)	Salt weight (g)
8H-2, 132-134	65.00	3.00	13.57	12.46	26.09	17.60	4.50	21.59	13.10	8.49	8.80	0.31
8H-3, 58-60	65.76	3.10	14.02	12.88	25.65	18.38	4.41	21.24	13.97	7.27	7.53	0.26
8H-3, 134-136	66.52	3.00	13.57	12.46	24.06		4.34	19.71	11.97	7.74	8.02	0.28
8H-4, 57-59	67.25	3.00	13.57	12.46	24.15	16.46	4.49	19.66	11.96	7.70	7.98	0.28
8H-4, 132-134	68.00	3.00	13.57	12.46	23.94	16.25	4.53	19.41	11.72	7.69	7.97	0.28
8H-5, 60-62	68.78	2.10	9.50	8.72	19.54	12.96	4.49	15.04	8.47	6.57	6.81	0.24
8H-5, 132-134	69.50	3.00	13.57	12.46	26.04	17.69	4.37	21.67	13.32	8.35	8.65	0.30
8H-6, 53-55	70.21	2.60	11.76	10.80	23.79	16.63	4.62	19.17	12.01	7.16	7.42	0.26
8H-6, 132-134	71.00	3.10	14.02	12.88	25.91	17.92	4.50	21.41	13.43	7.98	8.27	0.29
8H-7, 59-61	71.77	2.70	12.21	11.22	21.62		4.39	17.23	10.23	7.00	7.25	0.25
8H-7, 132-134	72.50	3.20	14.48	13.30	25.69	17.75	4.64	21.05	13.11	7.94	8.23	0.29
8H-8, 57-59	73.25	3.00	13.57	12.46	25.79	18.08	4.45	21.35	13.63	7.72	8.00	0.28
9H-1, 56-58	73.56	3.00	13.57	12.46	26.30		4.52	21.78	13.28	8.50	8.81	0.31
9H-1, 131-133	74.31	3.00	13.57	12.46	23.40	15.76	4.49	18.91	11.27	7.64	7.92	0.28
9H-2, 56-58	75.06	2.20	9.95	9.14	20.21	13.97	4.64	15.57	9.33	6.24	6.47	0.23
9H-2, 131-133	75.81	3.00	13.57	12.46	24.36	16.71	4.64	19.72	12.07	7.65	7.93	0.28
9H-3, 56-58	76.56	2.90	13.12	12.05	23.52	16.31	4.45	19.07	11.86	7.21	7.47	0.26
9H-3, 124-126	77.24	3.00	13.57	12.46	25.73	17.61	4.38	21.35	13.23	8.12	8.41	0.29
9H-4, 56-58	78.06	2.70	12.21	11.22	23.34		4.58	18.76	11.82	6.94	7.19	0.25
9H-4, 131-133	78.81	2.90	13.12	12.05	23.12	16.12	4.38	18.74	11.74	7.00	7.25	0.25
9H-5, 131-133	79.56	2.90	13.12	12.05	24.80	17.55	4.53	20.28	13.02	7.26	7.52	0.26
9H-5, 56-58	80.31	2.90	13.12	12.05	24.50	16.85	4.64	19.86	12.22	7.64	7.92	0.28
9H-7, 56-58	81.27	3.10	14.02	12.88	23.67	16.07	4.41	19.26	11.66	7.60	7.88	0.28
9H-7, 131-133	82.02	3.00	13.57	12.46	24.13	16.94	4.56	19.57	12.38	7.19	7.45	0.26
9H-8, 56-58	82.77	3.00	13.57	12.46	23.79		4.45	19.34	11.67	7.67	7.95	0.28
10H-1, 57-59	83.07	3.20	14.48	13.30	27.65	19.50	4.64	23.01	14.86	8.15	8.45	0.30
10H-1, 128-130	83.78	2.90	13.12	12.05	24.45	17.45	4.40	20.05	13.06	6.99	7.24	0.25
10H-2, 57-59	84.57	3.00	13.57	12.46	25.75	18.27	4.65	21.10	13.62	7.48	7.75	0.27
10H-2, 132-134	85.32	3.00	13.57	12.46	25.91		4.47	21.44	13.77	7.67	7.95	0.28
10H-3, 57-59	86.07	2.80	12.67	11.63	24.61	17.35	4.56	20.05	12.80	7.25	7.51	0.26
10H-3, 132-134	86.82	3.00	13.57	12.46	25.74	18.30	4.64	21.10	13.65	7.45	7.72	0.27
10H-4, 59-61	87.69	2.50	11.31	10.39	22.02	15.84	4.40	17.62	11.44	6.18	6.40	0.22
10H-4, 132-134	88.42	2.60	11.76	10.80	23.18	16.57	4.64	18.53	11.93	6.60	6.84	0.24
10H-5, 57-59	89.17	2.90	13.12	12.05	23.34	16.71	4.47	18.87	12.24	6.63	6.87	0.24
10H-5, 132-134	89.92	2.90	13.12	12.05	22.55	16.03	4.55	18.01	11.48	6.53	6.77	0.24
10H-6, 54-56	90.64	2.00	9.05	8.31	18.38		4.39	13.99	8.68	5.31	5.50	0.19
10H-7, 57-59	91.50	2.80	12.67	11.63	21.63	15.52	4.54	17.08	10.97	6.11	6.33	0.22
10H-7, 132-134	92.25	3.20	14.48	13.30	26.99	19.14	4.48	22.51	14.66	7.85	8.13	0.28
11H-1, 57-59	92.57	3.30	14.93	13.71	29.28		4.65	24.63	15.50	9.13	9.46	0.33
11H-1, 132-134	93.32	2.80	12.67	11.63	25.22	17.86	4.39	20.83	13.47	7.36	7.63	0.27
11H-2, 57-59	94.07	3.20	14.48	13.30	27.82	19.43	4.55	23.27	14.88	8.39	8.69	0.30
11H-2, 127-129	94.77	3.10	14.02	12.88	26.67	18.64	4.64	22.02	14.00	8.02	8.31	0.29
11H-3, 57-59	95.57	3.10	14.02	12.88	26.65	18.20	4.64	22.01	13.56	8.45	8.76	0.31
11H-3, 127-129	96.27	3.00	13.57	12.46	26.92	19.12	4.55	22.38	14.58	7.80	8.08	0.28
11H-4, 57-59	97.07	2.70	12.21	11.22	21.19		4.55	16.64	9.52	7.12	7.38	0.26
11H-4, 127-129	97.77	2.90	13.12	12.05	25.53	18.47	4.39	21.14	14.08	7.06	7.32	0.26
11H-5, 57-59	98.57	3.30	14.93	13.71	28.26	19.65	4.64	23.62	15.01	8.61	8.92	0.31
11H-6, 57-59	99.34	3.10	14.02	12.88	27.12	18.78	4.47	22.65	14.32	8.33	8.63	0.30
11H-6, 132-134	100.09	3.10	14.02	12.88	22.95		4.64	18.31	10.33	7.98	8.27	0.29
12H-1, 57-59	102.07	3.10	14.02	12.88	27.30	19.35	4.55	22.75	14.80	7.95	8.24	0.29
12H-1, 132-134	102.82	3.00	13.57	12.46	26.60	19.18	4.55	22.05	14.63	7.42	7.69	0.27
12H-2, 57-59	103.57	2.90	13.12	12.05	25.07		4.64	20.43	12.95	7.48	7.75	0.27
12H-2, 132-134	104.32	3.10	14.02	12.88	26.45	18.88	4.47	21.98	14.42	7.56	7.83	0.27
12H-3, 57-59	105.14	2.90	13.12	12.05	25.69	18.31	4.55	21.15	13.77	7.38	7.65	0.27
12H-3, 133-135	105.90	3.10	14.02	12.88	27.05	19.37	4.40	22.66	14.97	7.69	7.97	0.28
12H-4, 64-66	106.73	3.00	13.57	12.46	25.51	18.25	4.39	21.12	13.86	7.26	7.52	0.26
12H-4, 132-134	107.41	3.00	13.57	12.46	25.43	17.81	4.47	20.96	13.34	7.62	7.90	0.28
12H-6, 57-59	108.62	2.90	13.12	12.05	24.73	17.62	4.64	20.08	12.98	7.10	7.36	0.26
12H-6, 132-134	109.37	2.90	13.12	12.05	23.57		4.55	19.02	11.59	7.43	7.70	0.27
12H-8, 58-60	110.54	3.10	14.02	12.88	25.59	17.86	4.55	21.04	13.31	7.73	8.01	0.28
12H-8, 128-130	111.24	3.00	13.57	12.46	27.45	20.02	4.55	22.90	15.47	7.43	7.70	0.27
13H-1, 59-61	111.59	2.80	12.67	11.63	21.84	16.40	4.64	17.20	11.75	5.45	5.65	0.20
13H-1, 131-133	112.31	2.70	12.21	11.22	24.21	16.89	4.65	19.57	12.24	7.33	7.60	0.27
13H-3, 56-58	113.28	2.50	11.31	10.39	21.95		4.47	17.48	10.72	6.76	7.01	0.25
13H-3, 131-133	114.03	3.00	13.57	12.46	22.55	15.93	4.47	18.07	11.46	6.61	6.85	0.24
13H-4, 56-58	114.71	3.00	13.57	12.46	27.09	22.45	4.48	22.61	17.98	4.63	4.80	0.17
13H-4, 131-133	115.46	2.80	12.67	11.63	23.14	19.34	4.47	18.67	14.87	3.80	3.94	0.14
13H-5, 131-133	116.96	2.80	12.67	11.63	24.62	16.29	4.48	20.14	11.80	8.34	8.64	0.30
13H-6, 56-58	117.71	2.80	12.67	11.63	24.50	17.30	4.47	20.03	12.83	7.20	7.46	0.26
13H-6, 131-133	118.46	3.20	14.48	13.30	22.75	15.78	4.65	18.10	11.13	6.97	7.22	0.25
13H-7, 56-58	119.21	2.60	11.76	10.80	21.17	15.03	4.40	16.76	10.63	6.13	6.35	0.22
13H-7, 129-131	119.94	2.90	13.12	12.05	23.63		4.56	19.08	11.60	7.48	7.75	0.27
13H-8, 56-58	120.71	2.50	11.31	10.39	19.79	13.46	4.47	15.31	8.98	6.33	6.56	0.23
14H-1, 57-59	121.07	3.40	15.38	14.13	26.70	18.30	4.52	22.18	13.78	8.40	8.70	0.30
14H-1, 133-135	121.83	3.00	13.57	12.46	26.75	18.81	4.61	22.13	14.19	7.94	8.23	0.29
14H-2, 57-59	122.64	3.00	13.57	12.46	26.31	18.44	4.39	21.92	14.04	7.88	8.17	0.29
14H-2, 132-134	123.39	3.20	14.48	13.30	26.78	18.96	4.49	22.29	14.47	7.82	8.10	0.28
14H-3, 57-59	124.21	2.90	13.12	12.05	27.02	21.00	4.62	22.41	16.39	6.02	6.24	0.22
14H-3, 133-135	124.97	3.20	14.48	13.30	26.21		4.55	21.66	13.86	7.80	8.08	0.28
14H-4, 57-59	125.71	3.20	14.48	13.30	26.75	18.77	4.43	22.32	14.34	7.98	8.27	0.29
14H-4, 133-135	126.47	3.10	14.02	12.88	26.33	19.07	4.56	21.77	14.51	7.26	7.52	0.26
14H-7, 57-59	127.64	2.60	11.76	10.80	23.44		4.37	19.07	12.39	6.68	6.92	0.24
14H-7, 132-134	128.39	3.10	14.02	12.88	25.75	18.53	4.45	21.30	14.08	7.22	7.48	0.26
14H-8, 57-59	129.14	3.20	14.48	13.30	23.18	16.83	4.52	18.66	12.31	6.35	6.58	0.23

Table 4 (continued).

Core, section, interval (cm)	Depth (mbsf)	Cylinder height (cm)	Volume ₁ (cm ³)	Volume ₂ (cm ³)	Wet weight (g)	Dry weight (g)	Cylinder weight (g)	Wet sample weight (g)	Dry sample weight (g)	Water weight (g)	Water weight (corrected g)	Salt weight (g)
14H-8, 132-134	129.89	3.00	13.57	12.46	26.22	18.85	4.35	21.88	14.50	7.38	7.65	0.27
15H-1, 65-67	130.65	3.10	14.02	12.88	25.74	18.50	4.47	21.27	14.03	7.24	7.50	0.26
15H-1, 131-133	131.31	2.50	11.31	10.39	23.76	17.41	4.65	19.11	12.76	6.35	6.58	0.23
15H-3, 55-57	133.58	2.40	10.86	9.97	21.86	15.65	4.64	17.22	11.02	6.20	6.42	0.22
15H-3, 131-133	134.34	2.50	11.31	10.39	22.86	16.13	4.40	18.46	11.73	6.73	6.97	0.24
15H-4, 55-57	135.12	2.40	10.86	9.97	22.66		4.47	18.18	12.52	5.66	5.87	0.21
15H-4, 131-133	135.88	3.00	13.57	12.46	24.27	18.34	4.64	19.62	13.70	5.92	6.13	0.21
15H-5, 56-58	136.74	2.50	11.31	10.39	23.31	17.04	4.56	18.75	12.48	6.27	6.50	0.23
15H-5, 131-133	137.49	2.40	10.86	9.97	21.73	15.60	4.65	17.08	10.95	6.13	6.35	0.22
15H-6, 56-58	138.36	2.20	9.95	9.14	18.65		4.55	14.09	8.88	5.21	5.40	0.19
15H-6, 131-133	139.11	2.60	11.76	10.80	22.14	15.75	4.39	17.75	11.36	6.39	6.62	0.23
15H-7, 56-58	139.86	2.50	11.31	10.39	22.37	15.87	4.55	17.82	11.32	6.50	6.74	0.24
16H-1, 60-62	140.10	3.10	14.02	12.88	23.77	17.25	4.45	19.32	12.80	6.52	6.76	0.24
16H-1, 131-133	140.81	3.10	14.02	12.88	22.44	16.22	4.62	17.82	11.60	6.22	6.45	0.23
16H-2, 57-59	141.57	2.80	12.67	11.63	20.25	14.39	4.61	15.64	9.78	5.86	6.07	0.21
16H-2, 131-133	142.31	2.90	13.12	12.05	23.70	17.12	4.34	19.37	12.78	6.59	6.83	0.24
16H-3, 60-62	143.10	3.00	13.57	12.46	23.92		4.41	19.51	12.42	7.09	7.35	0.26
16H-3, 131-133	143.81	3.10	14.02	12.88	24.97	17.38	4.45	20.52	12.94	7.58	7.85	0.27
16H-4, 55-57	144.69	3.50	15.83	14.54	28.33	22.44	4.63	23.69	17.81	5.88	6.09	0.21
16H-4, 130-132	145.44	3.20	14.48	13.30	29.07	21.23	4.59	24.48	16.64	7.84	8.12	0.28
16H-5, 57-59	146.25	3.20	14.48	13.30	28.64	20.69	4.45	24.19	16.24	7.95	8.24	0.29
16H-5, 131-133	146.99	2.90	13.12	12.05	25.66	18.48	4.56	21.10	13.92	7.18	7.44	0.26
16H-6, 57-59	147.78	2.70	12.21	11.22	23.40		4.52	18.87	13.00	5.87	6.08	0.21
16H-6, 133-135	148.54	3.10	14.02	12.88	25.72	18.56	4.62	21.10	13.94	7.16	7.42	0.26
16H-7, 57-59	149.28	2.90	13.12	12.05	25.80	18.65	4.61	21.18	14.03	7.15	7.41	0.26
17H-1, 57-59	149.57	3.10	14.02	12.88	27.89	19.78	4.66	23.23	15.12	8.11	8.40	0.29
17H-1, 131-133	150.31	3.10	14.02	12.88	28.23	20.17	4.48	23.75	15.69	8.06	8.35	0.29
17H-2, 56-58	151.06	2.90	13.12	12.05	26.32	19.00	4.56	21.76	14.44	7.32	7.59	0.27
17H-2, 131-133	151.81	3.10	14.02	12.88	27.77		4.57	23.21	15.44	7.77	8.05	0.28
17H-3, 57-59	152.60	2.60	11.76	10.80	23.18	16.46	4.65	18.53	11.81	6.72	6.96	0.24
17H-3, 131-133	153.34	2.90	13.12	12.05	26.15	18.41	4.40	21.75	14.01	7.74	8.02	0.28
17H-4, 56-58	154.19	2.70	12.21	11.22	24.54	17.57	4.47	20.07	13.10	6.97	7.22	0.25
17H-4, 131-133	154.94	3.10	14.02	12.88	27.46	19.44	4.47	22.99	14.97	8.02	8.31	0.29
17H-5, 56-58	155.79	2.20	9.95	9.14	20.41	14.77	4.48	15.93	10.29	5.64	5.84	0.20
17H-5, 131-133	156.54	3.10	14.02	12.88	27.52		4.65	22.87	15.15	7.72	8.00	0.28
17H-6, 56-58	157.29	3.10	14.02	12.88	26.11	18.78	4.48	21.63	14.31	7.32	7.59	0.27
17H-6, 131-133	158.04	3.00	13.57	12.46	25.80	18.54	4.56	21.24	13.98	7.26	7.52	0.26
18H-1, 53-55	159.03	3.40	15.38	14.13	26.30	18.86	4.55	21.74	14.30	7.44	7.71	0.27
18H-1, 132-134	159.82	3.30	14.93	13.71	29.21	20.67	4.48	24.72	16.19	8.53	8.84	0.31
18H-2, 57-59	160.57	3.20	14.48	13.30	28.66	19.91	4.47	24.18	15.44	8.74	9.06	0.32
18H-2, 132-134	161.32	3.30	14.93	13.71	27.25	19.54	4.54	22.71	14.99	7.72	8.00	0.28
18H-3, 57-59	162.07	3.10	14.02	12.88	22.43		4.48	17.96	11.96	6.00	6.22	0.22
18H-3, 132-134	162.82	3.10	14.02	12.88	27.16	19.60	4.55	22.61	15.05	7.56	7.83	0.27
18H-4, 57-59	163.65	3.00	13.57	12.46	27.49	20.27	4.54	22.95	15.73	7.22	7.48	0.26
18H-4, 132-134	164.40	2.10	9.50	8.72	20.22	15.04	4.55	15.67	10.50	5.17	5.36	0.19
18H-5, 56-58	165.14	3.00	13.57	12.46	18.67	13.97	4.56	14.10	9.41	4.69	4.86	0.17
18H-5, 132-134	165.90	2.70	12.21	11.22	26.52		4.56	21.97	14.89	7.08	7.34	0.26
18H-6, 57-59	166.65	3.20	14.48	13.30	27.62	20.23	4.40	23.22	15.82	7.40	7.67	0.27
18H-6, 132-134	167.40	3.00	13.57	12.46	23.76	17.25	4.41	19.36	12.85	6.51	6.75	0.24
18H-7, 37-39	167.95	3.00	13.57	12.46	27.03	19.78	4.55	22.48	15.23	7.25	7.51	0.26
19H-1, 62-64	168.62	2.90	13.12	12.05	23.70	16.76	4.66	19.05	12.11	6.94	7.19	0.25
19H-1, 132-134	169.32	3.20	14.48	13.30	29.09	20.91	4.66	24.43	16.25	8.18	8.48	0.30
19H-2, 57-59	170.09	2.80	12.67	11.63	23.14		4.66	18.48	11.74	6.74	6.98	0.24
19H-2, 127-129	170.79	3.30	14.93	13.71	27.65	19.52	4.66	22.99	14.86	8.13	8.42	0.29
19H-3, 57-59	171.59	2.70	12.21	11.22	23.13	17.12	4.66	18.47	12.46	6.01	6.23	0.22
19H-3, 132-134	172.34	2.90	13.12	12.05	26.40	19.31	4.41	21.99	14.90	7.09	7.35	0.26
19H-4, 57-59	173.09	2.20	9.95	9.14	20.83	15.48	4.65	16.18	10.82	5.36	5.55	0.19
19H-4, 132-134	173.84	3.10	14.02	12.88	25.89	19.00	4.66	21.23	14.34	6.89	7.14	0.25
19H-5, 57-59	174.65	2.80	12.67	11.63	26.32	19.40	4.40	21.92	15.00	6.92	7.17	0.25
19H-5, 132-134	175.40	2.80	12.67	11.63	20.72		4.65	16.07	10.41	5.66	5.87	0.21
19H-6, 57-59	176.15	2.90	13.12	12.05	23.43	17.28	4.47	18.96	12.80	6.16	6.38	0.22
19H-6, 131-133	176.89	3.00	13.57	12.46	25.36	18.77	4.41	20.95	14.36	6.59	6.83	0.24
20H-1, 55-57	178.05	2.60	11.76	10.80	24.25		4.66	19.59	12.47	7.12	7.38	0.26
20H-1, 132-134	178.82	3.30	14.93	13.71	28.16	20.28	4.45	23.71	15.84	7.87	8.16	0.29
20H-2, 57-59	179.57	2.50	11.31	10.39	23.26	17.01	4.58	18.68	12.43	6.25	6.48	0.23
20H-2, 137-139	180.37	3.20	14.48	13.30	28.38	20.35	4.56	23.83	15.80	8.03	8.32	0.29
20H-3, 57-59	181.07	3.20	14.48	13.30	28.64	20.68	4.50	24.14	16.18	7.96	8.25	0.29
20H-3, 132-134	181.82	3.20	14.48	13.30	28.67		4.52	24.14	15.84	8.30	8.60	0.30
20H-4, 57-59	182.57	3.40	15.38	14.13	29.98	21.74	4.48	25.50	17.26	8.24	8.54	0.30
20H-4, 132-134	183.32	3.20	14.48	13.30	28.53	20.89	4.49	24.03	16.40	7.63	7.91	0.28
20H-5, 57-59	184.07	2.60	11.76	10.80	23.68	17.50	4.34	19.34	13.15	6.19	6.41	0.22
20H-5, 133-135	184.83	3.10	14.02	12.88	26.65		4.45	22.19	13.82	8.37	8.67	0.30
20H-6, 57-59	185.57	3.00	13.57	12.46	27.41	20.38	4.41	23.00	15.98	7.02	7.27	0.25
20H-6, 132-134	186.32	3.30	14.93	13.71	27.82	20.68	4.61	23.21	16.07	7.14	7.40	0.26
20H-7, 51-53	187.03	2.50	11.31	10.39	17.78		4.51	13.26	9.63	3.63	3.76	0.13

Table 5. Index properties calculated from raw data, Hole 893A.

Core, section, interval (cm)	Depth (mbsf)	Wet-bulk density (g/cm ³)	Dry-bulk density (g/cm ³)	Porosity (%)	Water content (wet wt %)	Water content (dry wt %)	Core, section, interval (cm)	Depth (mbsf)	Wet-bulk density (g/cm ³)	Dry-bulk density (g/cm ³)	Porosity (%)	Water content (wet wt %)	Water content (dry wt %)
146-893A-							8H-3, 58-60	65.76	1.58	1.02	54.66	35.47	54.97
1H-1, 57-59	0.57	1.26	0.38	85.98	70.07	234.11	8H-3, 134-136	66.52	1.51	0.90	60.14	40.69	68.62
1H-1, 132-134	1.32	1.32	0.60	69.83	54.24	118.53	8H-4, 57-59	67.25	1.51	0.90	59.83	40.59	68.31
1H-2, 58-60	2.08	1.32	0.49	81.04	62.91	169.64	8H-4, 132-134	68.00	1.49	0.88	59.75	41.06	69.65
1H-2, 132-134	2.82	1.43	0.70	71.97	51.47	106.04	8H-5, 60-62	68.78	1.65	0.90	72.92	45.27	82.71
1H-3, 58-60	3.60	1.55	0.65	88.06	58.20	139.26	8H-5, 132-134	69.50	1.67	1.00	64.88	39.93	66.47
1H-3, 132-134	4.34	1.64	0.91	71.05	44.33	79.62	8H-6, 53-55	70.21	1.70	1.04	64.19	38.70	63.14
1H-4, 58-60	5.10	1.54	0.67	85.47	56.71	131.01	8H-6, 132-134	71.00	1.59	0.98	60.00	38.62	62.93
1H-4, 132-134	5.84	1.47	0.67	78.04	54.51	119.82	8H-7, 59-61	71.77	1.47	0.85	60.43	42.10	72.71
2H-1, 57-59	7.07	1.42	0.64	75.83	54.85	121.47	8H-7, 132-134	72.50	1.52	0.92	57.84	39.09	64.17
2H-1, 133-135	7.83	1.71	1.06	63.83	38.23	61.89	8H-8, 57-59	73.25	1.64	1.03	59.98	37.47	59.93
2H-2, 57-59	8.61	1.51	0.73	76.49	51.84	107.65	9H-1, 56-58	73.56	1.67	1.00	66.04	40.44	67.90
2H-2, 133-135	9.37	1.57	0.90	65.71	42.77	74.73	9H-1, 131-133	74.31	1.45	0.84	59.36	41.87	72.02
2H-3, 57-59	10.11	1.31	0.72	58.11	45.30	82.81	9H-2, 56-58	75.06	1.63	0.95	66.11	41.53	71.03
2H-3, 133-135	10.87	1.61	0.84	75.17	47.96	92.17	9H-2, 131-133	75.81	1.52	0.91	59.44	40.20	67.22
2H-4, 57-59	11.62	1.60	0.78	79.92	51.07	104.37	9H-3, 56-58	76.56	1.52	0.92	57.95	39.18	64.42
2H-4, 133-135	12.38	1.43	0.74	67.84	48.59	94.51	9H-3, 124-126	77.24	1.64	0.99	63.09	39.41	65.05
2H-5, 62-64	13.17	1.63	1.10	52.03	32.74	48.68	9H-4, 56-58	78.06	1.60	0.99	59.91	38.34	62.17
2H-5, 133-135	13.88	1.63	0.95	66.18	41.57	71.13	9H-4, 131-133	78.81	1.49	0.91	56.26	38.71	63.15
2H-6, 57-59	14.62	1.56	0.75	78.97	51.94	108.06	9H-5, 131-133	79.56	1.61	1.01	58.35	37.10	58.98
2H-6, 133-135	15.38	1.60	0.84	74.01	47.48	90.41	9H-5, 56-58	80.31	1.58	0.95	61.41	39.86	66.29
2H-7, 57-59	16.12	1.48	0.79	66.61	46.27	86.12	9H-7, 56-58	81.27	1.43	0.85	57.14	40.89	69.18
3H-1, 64-66	16.64	1.56	0.77	76.92	50.69	102.81	9H-7, 131-133	82.02	1.50	0.93	55.86	38.07	61.48
3H-1, 132-134	17.32	1.57	0.86	69.18	45.15	82.32	9H-8, 56-58	82.77	1.49	0.88	59.59	41.10	69.77
3H-2, 58-60	18.08	1.76	0.96	77.81	45.40	83.16	10H-1, 57-59	83.07	1.66	1.05	59.37	36.70	57.99
3H-2, 132-134	18.82	1.68	0.99	66.57	40.72	68.69	10H-1, 128-130	83.78	1.59	1.02	56.18	36.13	56.56
3H-3, 64-66	19.64	1.64	0.93	69.09	43.21	76.09	10H-2, 57-59	84.57	1.62	1.03	58.12	36.74	58.07
3H-3, 126-128	20.26	1.56	0.89	65.57	43.09	75.71	10H-2, 132-134	85.32	1.65	1.04	59.59	37.07	58.91
3H-4, 65-67	21.15	1.56	0.79	75.23	49.36	97.48	10H-3, 57-59	86.07	1.65	1.03	60.35	37.47	59.93
3H-4, 132-134	21.82	1.58	0.83	73.81	47.74	91.36	10H-3, 132-134	86.82	1.62	1.03	57.88	36.59	57.70
3H-5, 51-53	22.51	1.62	0.87	73.46	46.46	86.79	10H-4, 59-61	87.69	1.62	1.03	57.62	36.35	57.10
3H-5, 143-145	23.43	1.65	1.00	63.01	39.18	64.42	10H-4, 132-134	88.42	1.64	1.04	59.17	36.91	58.50
3H-6, 63-65	24.13	1.62	0.86	74.01	46.81	88.01	10H-5, 57-59	89.17	1.50	0.95	53.29	36.41	57.26
3H-6, 132-134	24.82	1.67	0.99	67.13	41.11	69.80	10H-5, 132-134	89.92	1.43	0.89	52.49	37.57	60.19
3H-7, 55-57	25.55	1.51	0.85	64.10	43.53	77.09	10H-6, 54-56	90.64	1.61	0.98	61.89	39.33	64.83
4H-1, 60-62	26.10	1.65	0.94	69.70	43.17	75.98	10H-7, 57-59	91.50	1.41	0.89	50.86	37.07	58.91
4H-1, 132-134	26.82	1.64	0.89	72.82	45.49	83.44	10H-7, 132-134	92.25	1.62	1.04	57.18	36.14	56.59
4H-2, 58-60	27.58	1.78	1.03	73.30	42.13	72.81	11H-1, 57-59	92.57	1.72	1.06	64.49	38.41	62.37
4H-2, 134-136	28.33	1.58	0.89	67.36	43.72	77.68	11H-1, 132-134	93.32	1.72	1.09	61.27	36.62	57.77
4H-3, 57-59	29.07	1.73	1.00	71.18	42.23	73.10	11H-2, 57-59	94.07	1.68	1.05	61.11	37.36	59.65
4H-3, 131-133	29.81	1.65	0.95	68.45	42.54	74.04	11H-2, 127-129	94.77	1.64	1.02	60.30	37.74	60.62
4H-4, 47-49	30.47	1.60	0.93	64.64	41.49	70.91	11H-3, 57-59	95.57	1.64	0.99	63.54	39.78	66.07
4H-4, 124-126	31.24	1.52	0.88	61.99	41.83	71.92	11H-3, 127-129	96.27	1.72	1.10	60.60	36.12	56.54
4H-5, 57-59	32.07	1.66	0.97	67.38	41.57	71.14	11H-4, 57-59	97.07	1.42	0.79	61.47	44.34	79.66
4H-5, 126-128	32.76	1.50	0.85	63.85	43.55	77.15	11H-4, 127-129	97.77	1.68	1.10	56.75	34.61	52.92
4H-6, 62-64	33.62	1.24	0.70	52.57	43.53	77.08	11H-5, 57-59	98.57	1.65	1.03	60.82	37.77	60.71
4H-6, 134-136	34.34	1.50	0.90	59.08	40.30	67.50	11H-6, 57-59	99.34	1.68	1.04	62.63	38.11	61.58
4H-7, 57-59	35.07	1.51	0.83	67.21	45.50	83.49	11H-6, 132-134	100.09	1.36	0.75	60.00	45.16	82.36
5H-1, 57-59	35.57	1.77	1.06	68.45	39.73	65.92	12H-1, 57-59	102.07	1.69	1.08	59.78	36.21	56.77
5H-1, 132-134	36.32	1.45	0.80	63.42	44.73	80.92	12H-1, 132-134	102.82	1.69	1.10	57.65	34.87	53.54
5H-2, 57-59	37.07	1.62	0.94	66.74	42.25	73.15	12H-2, 57-59	103.57	1.62	1.01	60.12	37.94	61.14
5H-2, 132-134	37.82	1.60	0.95	63.94	40.90	69.22	12H-2, 132-134	104.32	1.63	1.05	56.84	35.64	55.38
5H-3, 57-59	38.57	1.54	0.94	58.70	39.13	64.27	12H-3, 57-59	105.14	1.68	1.07	59.32	36.16	56.64
5H-3, 132-134	39.32	1.46	0.84	61.19	42.84	74.94	12H-3, 133-135	105.90	1.69	1.09	57.82	35.17	54.24
5H-4, 57-59	40.07	1.64	0.98	64.64	40.38	67.74	12H-4, 64-66	106.73	1.62	1.04	56.41	35.62	55.33
5H-4, 132-134	40.82	1.61	0.97	62.86	40.00	66.65	12H-4, 132-134	107.41	1.61	1.00	59.20	37.67	60.45
5H-5, 57-59	41.57	1.68	1.01	65.71	40.10	66.96	12H-6, 57-59	108.62	1.60	1.01	57.07	36.64	57.83
5H-5, 132-134	42.32	1.52	0.83	67.51	45.40	83.16	12H-6, 132-134	109.37	1.51	0.90	59.72	40.48	68.01
5H-6, 57-59	43.07	1.46	0.87	57.91	40.58	68.30	12H-8, 58-60	110.54	1.56	0.97	58.12	38.07	61.48
5H-6, 132-139	43.82	1.60	0.95	63.68	40.77	68.83	12H-8, 128-130	111.24	1.76	1.17	57.73	33.62	50.65
5H-7, 57-59	44.57	1.74	1.03	69.51	40.99	69.46	13H-1, 59-61	111.59	1.42	0.95	45.37	32.84	48.89
6H-1, 57-59	45.07	1.55	0.94	59.59	39.29	64.72	13H-1, 131-133	112.31	1.67	1.02	63.28	38.81	63.44
6H-1, 132-134	45.82	1.72	1.05	65.27	38.97	63.84	13H-3, 56-58	113.28	1.61	0.97	63.03	40.08	66.88
6H-2, 57-59	46.57	1.59	0.95	62.00	40.07	66.85	13H-3, 131-133	114.03	1.39	0.86	51.36	37.91	61.05
6H-2, 132-134	47.32	1.36	0.79	55.46	41.91	72.15	13H-4, 56-58	114.71	1.74	1.37	35.97	21.22	26.94
6H-3, 57-59	48.07	1.51	0.89	60.68	41.24	70.17	13H-4, 131-133	115.46	1.54	1.21	31.63	21.09	26.73
6H-3, 132-134	48.82	1.57	0.91	64.44	42.17	72.92	13H-5, 131-133	116.96	1.66	0.95	69.43	42.91	75.17
6H-4, 55-57	49.55	1.05	0.60	43.91	42.80	74.82	13H-6, 56-58	117.71	1.65	1.03	59.94	37.25	59.36
6H-4, 132-134	50.32	1.68	0.98	67.77	41.38	70.58	13H-6, 131-133	118.46	1.30	0.78	50.77	39.90	66.40
6H-5, 57-59	51.07	1.66	1.01	63.61	39.23	64.54	13H-7, 56-58	119.21	1.49	0.92	54.96	37.90	61.04
6H-5, 132-134	51.82	1.45	0.80	62.86	44.52	80.24	13H-7, 129-131	119.94	1.52	0.90	60.12	40.63	68.42
6H-6, 58-60	52.58	1.42	0.79	61.57	44.52	80.24	13H-8, 56-58	120.71	1.41	0.81	59.02	42.85	74.96
6H-6, 123-134	53.32	1.50	0.87	60.84	41.66	71.41	14H-1, 57-59	121.07	1.50	0.91	57.59	39.25	64.60
6H-7, 57-59	54.07	1.67	0.99	66.39	40.66	68.53	14H-1, 133-135	121.83	1.70	1.07	61.69	37.18	59.19
7H-3, 57-59	56.15	1.66	1.02	62.08	38.39	62.30	14H-2, 57-59	122.64	1.68	1.06	61.22	37.25	59.37
7H-3, 132-134	56.90	1.47	0.90	55.26	38.64	62.98	14H-2, 132-134	123.39	1.61	1.02	56.96	36.36	57.12
7H-4, 57-59	57.65	1.52	0.91	59.36	40.13	67.02	14H-3, 57-59	124.21	1.78	1.29	48.39	27.84	38.58
7H-5, 57-59	59.22	1.54	0.8										

Table 5 (continued).

Core, section, interval (cm)	Depth (mbsf)	Wet-bulk density (g/cm ³)	Dry-bulk density (g/cm ³)	Porosity (%)	Water content (wet wt %)	Water content (dry wt %)
15H-1, 131-133	131.31	1.76	1.16	59.20	34.43	52.52
15H-3, 55-57	133.58	1.65	1.04	60.21	37.31	59.52
15H-3, 131-133	134.34	1.70	1.06	62.75	37.78	60.72
15H-4, 55-57	135.12	1.75	1.18	54.97	32.26	47.63
15H-4, 131-133	135.88	1.51	1.04	46.00	31.27	45.49
15H-5, 56-58	136.74	1.73	1.13	58.46	34.65	53.03
15H-5, 131-133	137.49	1.64	1.03	59.54	37.19	59.21
15H-6, 56-58	138.36	1.48	0.91	55.20	38.32	62.12
15H-6, 131-133	139.11	1.57	0.99	57.29	37.31	59.50
15H-7, 56-58	139.86	1.64	1.02	60.60	37.80	60.77
16H-1, 60-62	140.10	1.44	0.93	49.02	34.97	53.78
16H-1, 131-133	140.81	1.33	0.85	46.77	36.17	56.67
16H-2, 57-59	141.57	1.29	0.79	48.78	38.83	63.47
16H-2, 131-133	142.31	1.54	1.00	52.97	35.26	54.45
16H-3, 60-62	143.10	1.50	0.93	55.09	37.66	60.41
16H-3, 131-133	143.81	1.53	0.94	56.99	38.28	62.02
16H-4, 55-57	144.69	1.56	1.16	39.16	25.72	34.63
16H-4, 130-132	145.44	1.76	1.18	57.11	33.19	49.67
16H-5, 57-59	146.25	1.74	1.15	57.91	34.06	51.65
16H-5, 131-133	146.99	1.68	1.09	57.71	35.26	54.47
16H-6, 57-59	147.78	1.61	1.09	50.68	32.24	47.57
16H-6, 133-135	148.54	1.57	1.02	53.84	35.16	54.24
16H-7, 57-59	149.28	1.68	1.09	57.47	34.98	53.81
17H-1, 57-59	149.57	1.73	1.10	60.98	36.18	56.69
17H-1, 131-133	150.31	1.77	1.15	60.60	35.17	54.24
17H-2, 56-58	151.06	1.73	1.13	58.84	34.86	53.52
17H-2, 131-133	151.81	1.73	1.13	58.42	34.69	53.12
17H-3, 57-59	152.60	1.64	1.03	60.24	37.58	60.21
17H-3, 131-133	153.34	1.73	1.09	62.21	36.88	58.42
17H-4, 56-58	154.19	1.71	1.10	60.17	35.99	56.22
17H-4, 131-133	154.94	1.71	1.09	60.30	36.15	56.62
17H-5, 56-58	155.79	1.67	1.06	59.76	36.69	57.95
17H-5, 131-133	156.54	1.70	1.11	58.05	34.98	53.80
17H-6, 56-58	157.29	1.61	1.04	55.04	35.07	54.01
17H-6, 131-133	158.04	1.63	1.05	56.41	35.42	54.85
18H-1, 53-55	159.03	1.47	0.95	51.01	35.46	54.95
18H-1, 132-134	159.82	1.73	1.11	60.25	35.76	55.66
18H-2, 57-59	160.57	1.74	1.09	63.66	37.46	59.89
18H-2, 132-134	161.32	1.59	1.03	54.53	35.23	54.38
18H-3, 57-59	162.07	1.34	0.87	45.11	34.62	52.95
18H-3, 132-134	162.82	1.68	1.10	56.84	34.65	53.02
18H-4, 57-59	163.65	1.76	1.19	56.10	32.60	48.37
18H-4, 132-134	164.40	1.72	1.13	57.38	34.19	51.95
18H-5, 56-58	165.14	1.08	0.71	36.44	34.47	52.60
18H-5, 132-134	165.90	1.88	1.25	61.12	33.39	50.14
18H-6, 57-59	166.65	1.67	1.12	53.90	33.02	49.31
18H-6, 132-134	167.40	1.49	0.97	50.58	34.85	53.48
18H-7, 37-39	167.95	1.73	1.15	56.33	33.42	50.20
19H-1, 62-64	168.62	1.51	0.94	55.78	37.75	60.65
19H-1, 132-134	169.32	1.76	1.15	59.58	34.70	53.13
19H-2, 57-59	170.09	1.52	0.95	56.11	37.79	60.76
19H-2, 127-129	170.79	1.61	1.02	57.42	36.65	57.84
19H-3, 57-59	171.59	1.58	1.05	51.88	33.72	50.87
19H-3, 132-134	172.34	1.75	1.16	56.99	33.41	50.18
19H-4, 57-59	173.09	1.70	1.11	56.79	34.33	52.27
19H-4, 132-134	173.84	1.58	1.05	51.81	33.63	50.67
19H-5, 57-59	174.65	1.80	1.21	57.61	32.71	48.62
19H-5, 132-134	175.40	1.32	0.84	47.12	36.50	57.48
19H-6, 57-59	176.15	1.51	1.00	49.51	33.67	50.76
19H-6, 131-133	176.89	1.61	1.09	51.20	32.60	48.36
20H-1, 55-57	178.05	1.74	1.08	63.83	37.66	60.42
20H-1, 132-134	178.82	1.66	1.09	55.59	34.40	52.43
20H-2, 57-59	179.57	1.72	1.13	58.27	34.67	53.07
20H-2, 137-139	180.37	1.72	1.12	58.49	34.92	53.66
20H-3, 57-59	181.07	1.74	1.14	57.98	34.17	51.91
20H-3, 132-134	181.82	1.74	1.12	60.46	35.63	55.35
20H-4, 57-59	182.57	1.73	1.15	56.49	33.49	50.34
20H-4, 132-134	183.32	1.73	1.16	55.58	32.90	49.04
20H-5, 57-59	184.07	1.71	1.15	55.49	33.17	49.63
20H-5, 133-135	184.83	1.65	1.01	62.93	39.09	64.17
20H-6, 57-59	185.57	1.77	1.21	54.54	31.63	46.26
20H-6, 132-134	186.32	1.62	1.10	50.43	31.88	46.80
20H-7, 51-53	187.03	1.22	0.88	33.84	28.37	39.60

The following paragraphs will discuss the index properties data illustrated in Figure 22, as the higher resolution of sampling represented in this figure is needed to accurately portray the intermittingly laminated nature of the sediment in Hole 893A.

Below a highly variable zone in Lithologic Subunit IA, which corresponds to laminated beds of diatom nannofossil silty clay and diatom nannofossil silt, water contents and porosities generally decrease downhole. The major exception to this overall trend is a zone of increased variability in water content and porosity, extending from the lower portion of Lithologic Subunit IC to the base of Lithologic Subunit ID (approximately from 105 to 145 mbsf). The variability observed in these properties is generally mirrored by fluctuations in bulk density, which seem to correspond to the presence/absence of laminated sequences, as might be expected. The bulk density data are known to be quite sensitive to the presence of increased amounts of low-density diatom skeletons in the sediment (Hamilton, 1976; Mayer, 1979; Lee, 1982).

A sandy interval within Sections 146-893A-13H-4 and -5 is clearly observed in Figure 22 as a sharp increase in bulk density and by decreases in water content and porosity near 115 mbsf (Fig. 22; also see photo of Core 146-893A-13H). Another example of a sharp increase in bulk density associated with decreases in water content and porosity is observed at the boundary between Lithologic Subunits ID and IE, in the middle of Core 146-893A-16H.

Carbonate content is relatively low (0%-20%) throughout the section, although it is highly variable in Lithologic Subunits IA and ID, and seems to exhibit distinctive increasing/decreasing trends in portions of Lithologic Subunits IC and IE (Fig. 22).

Approximately 4200 digital color images were collected during the 2 wk immediately following splitting and describing of the Site 893 cores. Voids caused by the escape of gas during recovery have been mapped in detail (Table 7) from these images. For purposes of these measurements, a void is defined as an empty region of liner, including any immediately adjacent areas so disturbed as to preclude meaningful measurement of continuous properties (e.g., color reflectance or magnetic susceptibility). Voids smaller than 1 cm in length were ignored. Measurements were made at the center of the core, offsetting to the right of center (upper part of image) when necessary. Precision of measurements was to the nearest 0.5 mm, but messiness of void boundaries usually prevented this level of accuracy.

A revised depth scale has been constructed from which all voids greater than 1 cm long have been deleted (Table 8). Note that the top of each core is arbitrarily assigned the depth recorded by the driller, as shown in the CoreLog data set; however, individual section lengths and depths have been adjusted to eliminate the voids recorded in Table 6. Apparent overlap observed between bottoms and tops of adjacent cores is caused by gas expansion not accounted for by void removal. This new depth scale is to be used to correlate between various proxies, including color logs derived from the images.

BIOSTRATIGRAPHY

Site 893 lies in a water depth of 576.5 m on the floor of the Santa Barbara Basin in a present-day region of highly productive waters resulting from the upwelling of nutrient-rich waters to the west off Point Conception. Throughout the Quaternary, the Santa Barbara Basin has been dominantly under the influence of the cool California Current, which transported cold waters from the higher latitudes of the North Pacific. The basin has also been influenced by the northward transport of warm subtropical waters by the coastal Davidson Current, a process that is intensified during El-Niño/Southern oscillation events. The basin floor at the present time is marked by very low oxygen concentrations.

The late Quaternary planktonic microfossil assemblages of Site 893 largely reflect the glacial/interglacial oscillations of SSTs and associated changes in biogenic productivity. The biostratigraphy of benthic microfossils is primarily controlled by oscillations in bottom-water oxygen concentrations that, in turn, were modulated by gla-

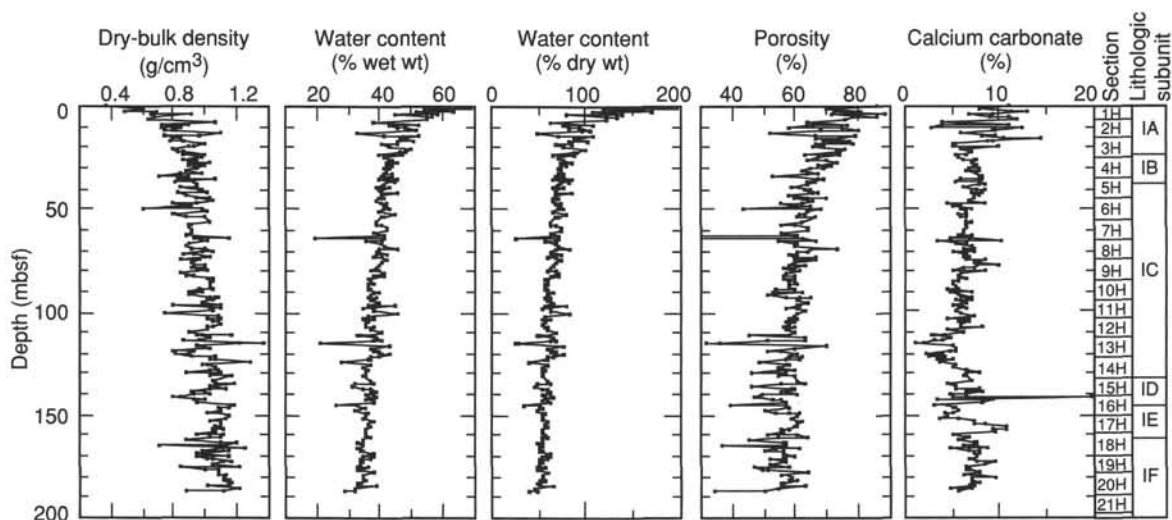


Figure 22. Index properties vs. depth, Hole 893A. Values are calculated from raw data measured on cylindrical sample plugs extracted from cores. Calcium carbonate measurements are provided (F. Rack, unpubl. data) for comparison with index properties. Core and lithologic subunit boundaries are also shown.

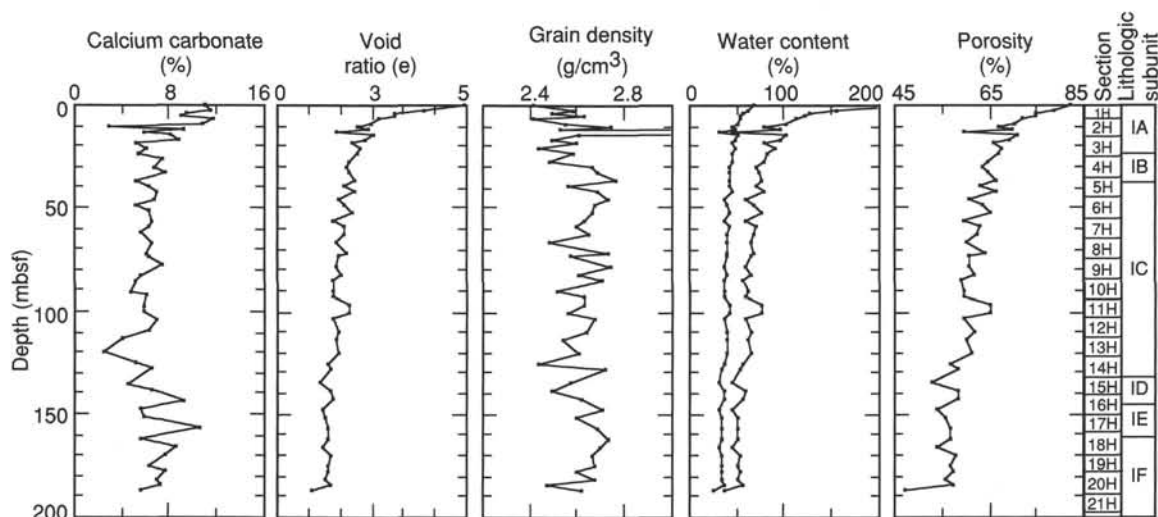


Figure 23. Index properties vs. depth, Hole 893A. Values are calculated from data collected using the Penta pycnometer with helium. Calcium carbonate measurements are provided (F. Rack, unpubl. data) for comparison with index properties. Core and lithologic subunit boundaries are also shown.

cial/interglacial climatic changes. Interglacial episodes are marked by benthic foraminifer assemblages characteristic of very low oxygen concentrations in bottom waters; the glacial episodes are marked by assemblages characteristic of well-oxygenated conditions.

Hole 893A was cored to a depth of 196.5 mbsf, and Hole 893B to a depth of 68.8 mbsf. Site 893 is of latest Quaternary age. Pollen and planktonic foraminifer stratigraphy suggest that Hole 893A extends from the base of Isotope Stage 6 (150,000 ka) to the present day and Hole 893B from within the last glaciation (from about 60,000 yr). A study of cores taken at Hole 893B did not begin until 2 months after the end of Leg 146. Thus, the biostratigraphic information is generalized and limited to observations of smear slides, examinations of coarse (>63 μm) sediment fractions in core-catcher samples, and counts of pollen in core-catcher samples.

A number of microfossil groups occur persistently throughout the sequence including diatoms, silicoflagellates, calcareous nannofossils, benthic and planktonic foraminifers, and radiolarians. Pollen and spores are generally abundant to very abundant throughout. These

faunal and floral groups should be the most useful microfossils for biostratigraphic and paleoenvironmental investigations of the entire sequence. The relative abundances of these major groups change significantly between glacial and interglacial episodes. Other microfossil components that are less persistent and less common include sponge spicules, spatangid echinoid spines, fish debris, micromollusca, dinoflagellates, and ostracodes. Pteropods are largely limited to the uppermost (Holocene) laminated sequences. Microfossils of all types are well preserved throughout most of the sequence. Some assemblages are very finely preserved, especially in the laminated sedimentary intervals.

Planktonic Foraminifers

In spite of the mid-latitude location of 34°N, modern and Holocene planktonic assemblages in the Santa Barbara Basin are cool temperate in character because of the influence of the cool California Current and the upwelling of cool intermediate waters to the west of the California

Table 6. Index properties calculated from Penta Pycnometer data, Hole 893A.

Core, section, interval (cm)	Depth (mbsf)	Volume (% dry wt)	Sediment (wet wt, g)	Sediment (dry wt, g)	Wet wt (g)	Water weight (salt corrected, g)	Salt (calculated wt, g)	Void ratio (e)	Porosity (%)	Water content (% wet wt)	Water content (% dry wt)	Grain density (g/cm ³)
146-893A-												
1H-1, 57-59	0.57	1.23	8.50	2.95	5.52	5.74	0.20	4.91	82.00	67.59	208.53	2.41
1H-2, 58-60	2.08	1.35	8.37	3.47	4.90	5.08	0.18	3.90	78.58	60.69	154.42	2.59
1H-3, 58-60	3.60	1.44	7.81	3.58	4.24	4.39	0.15	3.12	74.83	56.16	128.12	2.50
1H-4, 58-60	5.10	1.42	7.86	3.71	4.15	4.30	0.15	3.10	74.70	54.73	120.89	2.63
2H-1, 57-59	7.07	1.41	6.95	3.40	3.55	3.67	0.13	2.65	71.77	52.91	112.36	2.42
2H-2, 57-59	8.61	1.22	6.01	3.11	2.90	3.01	0.11	2.50	70.60	50.04	100.18	2.55
2H-3, 57-59	10.11	1.79	8.46	4.89	3.57	3.70	0.13	2.08	66.80	43.72	77.68	2.74
2H-4, 57-59	11.62	1.39	6.70	3.52	3.19	3.30	0.12	2.40	69.79	49.28	97.15	2.53
2H-5, 62-64	13.17	1.45	6.98	4.85	2.13	2.21	0.08	1.52	59.69	31.60	46.19	3.36
2H-6, 57-59	14.62	1.43	7.15	3.69	3.46	3.58	0.13	2.55	71.02	50.13	100.53	2.60
3H-1, 64-66	16.64	1.28	6.05	3.20	2.86	2.96	0.10	2.33	69.22	48.93	95.81	2.50
3H-2, 58-60	18.08	1.43	6.39	3.69	2.70	2.80	0.10	1.97	65.64	43.80	77.95	2.59
3H-4, 65-67	21.15	1.78	7.99	4.32	3.67	3.81	0.13	2.16	67.64	47.61	90.88	2.44
3H-6, 63-65	24.13	1.56	7.13	4.02	3.11	3.22	0.11	2.08	66.81	45.16	82.34	2.59
4H-1, 132-134	26.82	1.53	6.59	3.80	2.79	2.90	0.10	1.90	64.84	43.91	78.28	2.49
4H-3, 131-133	29.81	1.50	6.56	3.96	2.60	2.69	0.09	1.80	63.69	41.03	69.59	2.66
4H-5, 126-128	32.76	1.93	8.66	5.14	3.51	3.64	0.13	1.90	64.80	42.04	72.53	2.68
5H-1, 132-134	36.32	1.29	6.08	3.55	2.53	2.63	0.09	2.05	66.48	43.18	75.98	2.76
5H-3, 132-134	39.32	1.62	6.87	4.13	2.74	2.84	0.10	1.76	63.14	41.34	70.47	2.56
5H-5, 132-134	42.32	1.41	6.54	3.78	2.76	2.86	0.10	2.04	66.38	43.79	77.90	2.68
6H-1, 132-134	45.82	1.46	6.23	3.97	2.26	2.34	0.08	1.61	61.02	37.60	60.25	2.73
6H-3, 132-134	48.82	1.46	6.40	3.89	2.51	2.60	0.09	1.79	63.46	40.68	68.59	2.67
6H-5, 132-134	51.82	1.49	6.72	3.94	2.79	2.89	0.10	1.96	65.48	42.95	75.28	2.66
7H-3, 57-59	56.15	2.01	8.19	5.26	2.92	3.03	0.11	1.51	59.53	37.03	58.81	2.63
7H-5, 57-59	59.22	1.67	7.15	4.32	2.83	2.93	0.10	1.76	63.09	40.97	69.41	2.59
7H-7, 57-59	62.22	1.36	5.86	3.60	2.26	2.34	0.08	1.73	62.68	40.00	66.68	2.65
8H-3, 134-136	66.52	1.64	6.52	4.05	2.47	2.56	0.09	1.56	60.42	39.26	64.65	2.48
8H-7, 59-61	71.77	1.51	6.75	4.10	2.65	2.74	0.10	1.82	63.91	40.65	68.50	2.73
9H-1, 56-58	73.56	1.62	6.68	4.16	2.52	2.61	0.09	1.61	61.04	39.04	64.04	2.57
9H-4, 56-58	78.06	1.31	5.55	3.57	1.98	2.05	0.07	1.57	60.50	37.02	58.78	2.74
9H-8, 56-58	82.77	1.48	6.22	3.84	2.38	2.47	0.09	1.67	61.93	39.66	65.73	2.60
10H-2, 132-134	85.32	1.50	6.16	4.03	2.13	2.20	0.08	1.47	58.96	35.78	55.72	2.70
10H-6, 54-56	90.64	1.42	5.63	3.57	2.06	2.14	0.07	1.50	59.48	37.97	61.20	2.52
11H-1, 57-59	92.57	1.61	6.57	4.22	2.35	2.43	0.09	1.51	59.58	37.05	58.85	2.63
11H-4, 57-59	97.07	1.39	6.19	3.63	2.56	2.65	0.09	1.92	65.07	42.81	74.86	2.63
11H-6, 132-134	100.09	1.30	5.73	3.32	2.41	2.50	0.09	1.93	65.22	43.57	77.22	2.57
12H-2, 57-59	103.57	1.60	6.58	4.25	2.33	2.41	0.08	1.51	59.52	36.63	57.81	2.67
12H-6, 132-134	109.37	1.29	5.48	3.41	2.06	2.14	0.07	1.65	61.71	39.06	64.09	2.64
13H-3, 56-58	113.28	1.48	5.98	3.75	2.23	2.31	0.08	1.56	60.40	38.70	63.12	2.54
13H-7, 139-131	119.94	1.42	5.92	3.68	2.24	2.32	0.08	1.64	61.52	39.22	64.52	2.61
14H-3, 133-135	124.97	1.68	6.28	4.10	2.18	2.26	0.08	1.34	56.74	36.02	56.29	2.44
14H-7, 57-59	127.64	1.56	6.36	4.21	2.15	2.23	0.08	1.43	58.25	35.01	53.87	2.71
15H-4, 55-57	135.12	1.89	6.93	4.85	2.08	2.15	0.08	1.13	52.65	31.11	45.15	2.57
15H-6, 56-58	138.36	1.42	5.49	3.53	1.96	2.03	0.07	1.43	58.32	37.01	58.75	2.50
16H-3, 60-62	143.10	1.79	7.21	4.68	2.53	2.62	0.09	1.46	58.78	36.33	57.05	2.62
16H-6, 57-59	147.78	1.60	6.17	4.32	1.85	1.92	0.07	1.19	53.86	31.09	45.11	2.70
17H-2, 131-133	151.81	1.54	5.89	3.98	1.90	1.97	0.07	1.28	55.56	33.47	50.32	2.60
17H-5, 131-133	156.54	1.74	6.90	4.65	2.25	2.33	0.08	1.33	56.65	33.75	50.95	2.69
18H-3, 57-59	162.07	1.86	7.48	5.07	2.41	2.50	0.09	1.34	56.74	33.43	50.22	2.73
18H-5, 132-134	165.90	1.86	7.16	5.01	2.15	2.23	0.08	1.19	53.85	31.11	45.16	2.70
19H-2, 57-59	170.09	1.71	6.85	4.52	2.33	2.41	0.08	1.41	57.98	35.20	54.33	2.66
19H-5, 132-134	175.40	1.70	6.75	4.54	2.21	2.30	0.08	1.34	56.83	34.00	51.52	2.68
20H-1, 55-57	178.05	1.65	6.48	4.29	2.19	2.27	0.08	1.37	57.27	35.08	54.02	2.60
20H-3, 132-134	181.82	1.86	7.30	4.96	2.34	2.42	0.08	1.30	55.95	33.18	49.66	2.68
20H-5, 133-135	184.83	1.73	6.59	4.27	2.31	2.40	0.08	1.38	57.46	36.40	57.23	2.47
20H-7, 51-53	187.03	1.84	6.45	4.81	1.65	1.71	0.06	0.92	47.53	26.45	35.96	2.62

borderland province. The present-day average seasonal surface water temperature range is ~12°C to 17°C. During El Niño/Southern Oscillation episodes, which occur approximately every 7 yr, SSTs rise to ~20°C and subtropical planktonic assemblages are transported to the Santa Barbara Basin.

Interglacial assemblages, like those of the Holocene and Isotope Stage 5, are marked by common to abundant diatoms, calcareous nanofossils, radiolarians, and planktonic foraminifers. The preservation of these groups is excellent in the Holocene and good to excellent in Isotope Stage 5. The pteropods, being constructed of aragonite, are the least well preserved of the calcareous groups. The planktonic foraminifer assemblages are moderately diverse (~15 species). The most abundant species are *Globigerina bulloides*, *Neoglobobulimina dutertrei*, *Neoglobobulimina pachyderma* (dextral coiling), *Globigerina quinqueloba*, and *Orbulina universa*. Uncommon warmer water forms include *Globigerinoides ruber*.

Glacial planktonic microfossil assemblages are quite different from those of interglacial episodes. Most groups exhibit lower taxonomic diversity and lower abundances. Calcareous nanofossils are persistent but rare, whereas diatoms and radiolarians are rare to common. Planktonic foraminifer assemblages are dominated by a single form—*Neoglobobulimina pachyderma* (sinistral)—with a few other species present such as *Globigerina bulloides*. This assemblage is characteristic of the present-day subarctic with temperatures of <10°C. Complete gradations occur between glacial and interglacial assemblages.

Benthic Foraminifers

The benthic foraminifer assemblages of Site 893 exhibit dramatic changes throughout the sequence. Holocene assemblages are clearly dominated by taxa that are typical of very low oxygen environments (especially *Bolivina*, but also *Globobulimina*), whereas assemblages

Table 7. Catalog of voids greater than 1 cm observed in digital images of cores from Site 893.

Top of void within section (cm)	Top of void (mbsf)	Void length (cm)	Top of void within section (cm)	Top of void (mbsf)	Void length (cm)	Top of void within section (cm)	Top of void (mbsf)	Void length (cm)
146-893A-								
1H-4, 120.5	5.70	1.5	6H-2, 126.8	47.25	2.2	9H-7, 31.8	80.86	1.0
2H-1, 13.4	6.63	1.5	6H-3, 68.7	48.16	3.6	9H-7, 73.2	81.27	0.8
2H-2, 71.3	8.73	4.3	6H-3, 85.4	48.32	1.1	9H-7, 90.3	81.44	4.2
2H-3, 33.5	9.84	2.7	6H-3, 115.8	48.63	9.7	10H-1, 0	82.50	3.1
2H-3, 120	10.70	3.3	6H-4, 22.1	49.18	1.8	10H-1, 102.7	83.53	4.3
2H-3, 141.3	10.92	2.1	6H-4, 55.8	49.51	3.4	10H-1, 129.5	83.80	4.0
2H-4, 15.3	11.16	2.3	6H-5, 20.5	50.64	1.7	10H-2, 36.1	84.35	1.2
2H-4, 35.7	11.36	2.2	6H-6, 52.9	52.44	4.9	10H-4, 93.4	86.49	1.0
2H-4, 49.8	11.50	2.3	6H-6, 78.4	52.70	4.4	10H-6, 20.4	88.74	2.2
2H-4, 81.4	11.82	2.0	6H-6, 90.7	52.82	3.7	10H-7, 35.6	89.70	2.0
2H-4, 96.1	11.96	5.3	7H-2, 50.2	54.55	19.5	11H-1, 0	92.00	1.6
2H-5, 8.6	12.58	5.3	7H-2, 78.1	54.83	13.2	11H-1, 81.2	92.81	2.5
2H-5, 23.8	12.74	1.9	7H-2, 96.2	55.01	10.5	11H-1, 97.4	92.97	5.6
2H-5, 56.5	13.06	4.7	7H-3, 7.1	55.61	1.6	11H-4, 35.5	96.81	5.8
2H-5, 64.2	13.14	2.2	7H-3, 21.1	55.75	4.1	11H-4, 102.7	97.49	4.8
2H-5, 73.6	13.23	1.3	7H-3, 52.2	56.06	2.9	11H-4, 111.9	97.58	8.8
2H-5, 103.9	13.54	2.8	7H-3, 67.3	56.21	6.4	12H-1, 46	101.96	10.7
2H-5, 124.1	13.74	1.8	7H-3, 102.4	56.56	9.0	12H-1, 120.2	102.70	5.8
2H-5, 142.9	13.93	2.6	7H-3, 123.6	56.78	7.6	12H-2, 49.8	103.49	3.3
2H-6, 25.8	14.25	3.1	7H-3, 134.3	56.88	2.8	12H-2, 84.5	103.84	5.8
2H-6, 38.4	14.38	2.2	7H-4, 0	57.01	5.8	12H-2, 98	103.97	1.0
2H-6, 65.5	14.65	1.0	7H-4, 30.3	57.31	3.4	12H-3, 20.2	104.76	2.9
3H-1, 46.8	16.47	2.7	7H-4, 43	57.44	4.5	12H-4, 45.9	106.51	5.8
3H-3, 79	19.78	3.1	7H-4, 67.9	57.68	6.5	12H-4, 87.3	106.93	2.5
3H-3, 90.1	19.89	1.0	7H-4, 92.6	57.93	3.9	12H-6, 72.8	108.73	4.6
3H-4, 139.3	21.88	5.4	7H-6, 0	60.05	2.7	12H-6, 84.3	108.85	1.3
3H-5, 35	22.33	2.4	7H-8, 41.1	63.41	4.9	12H-6, 88.2	108.89	9.4
3H-5, 62	22.60	1.8	8H-2, 135.2	65.00	2.6	12H-7, 20.3	109.70	1.1
3H-5, 67.4	22.65	2.1	8H-2, 139.5	65.05	3.7	13H-1, 19.1	111.19	14.1
3H-5, 76.6	22.74	7.4	8H-3, 7.5	65.22	7.3	13H-1, 37.1	111.37	1.0
3H-6, 20.9	23.68	4.7	8H-3, 37.5	65.52	5.9	13H-1, 43.8	111.44	11.0
4H-1, 62.5	26.13	21.7	8H-3, 44.2	65.59	6.2	13H-1, 95.9	111.96	4.6
4H-1, 85.5	26.36	1.3	8H-3, 85.1	66.00	14.9	13H-3, 117.1	113.84	1.1
4H-2, 22.6	27.21	3.9	8H-3, 109.4	66.24	6.3	13H-4, 0	114.16	17.2
4H-2, 50.6	27.49	1.5	8H-3, 126.1	66.41	1.0	13H-4, 29.1	114.45	1.3
4H-2, 124.9	28.24	4.5	8H-3, 135.2	66.50	4.8	13H-8, 34.9	120.47	9.7
4H-3, 70	29.19	2.2	8H-3, 141.2	66.56	3.3	14H-1, 104.2	121.54	3.4
4H-3, 97.1	29.46	3.3	8H-4, 11.9	66.75	6.2	14H-8, 32.2	128.77	1.7
4H-3, 108.8	29.58	2.3	8H-4, 21.9	66.85	6.3	14H-8, 43.5	128.88	1.5
4H-4, 39.8	30.38	2.9	8H-4, 37.9	67.01	10.1	14H-8, 79.8	129.24	1.3
4H-4, 61.8	30.60	9.1	8H-4, 96.3	67.59	2.4	15H-1, 38.4	130.38	27.6
4H-4, 88	30.86	2.7	8H-4, 116	67.79	2.4	15H-1, 75.8	130.76	1.0
4H-4, 104.9	31.03	2.0	8H-4, 130.9	67.94	1.9	15H-2, 28.7	131.78	1.1
4H-4, 130.4	31.29	8.9	8H-5, 118.7	69.26	3.5	16H-1, 14.4	139.64	4.4
4H-5, 69.5	32.18	3.0	8H-6, 79.6	70.36	5.3	16H-1, 21.9	139.72	2.0
4H-5, 80.1	32.29	2.9	8H-6, 128.5	70.85	4.1	16H-1, 32.3	139.82	5.7
4H-5, 108.6	32.57	1.1	8H-7, 5.4	71.11	3.4	16H-1, 50.3	140.00	1.4
4H-5, 113.8	32.62	1.1	8H-7, 10.7	71.16	3.2	16H-1, 87.3	140.37	8.6
4H-5, 116	32.65	1.4	8H-7, 28.3	71.34	4.5	16H-1, 113	140.63	3.1
4H-6, 16	33.13	1.0	8H-7, 52.6	71.58	3.0	16H-1, 134.3	140.84	5.4
4H-6, 68.8	33.66	1.2	8H-7, 118.7	72.24	6.6	16H-2, 117.8	142.18	1.5
4H-6, 106.9	34.04	2.3	8H-7, 136.2	72.42	3.4	17H-1, 7.9	149.08	1.0
4H-6, 128.5	34.26	2.8	8H-8, 4.2	72.58	3.9	17H-1, 9.8	149.10	1.3
4H-7, 6.7	34.55	4.0	8H-8, 12.4	72.66	4.4	17H-3, 79.8	152.82	3.5
5H-1, 99.5	36.00	3.6	8H-8, 36.1	72.90	7.3	17H-6, 84.5	157.51	1.1
5H-1, 108.3	36.08	7.5	8H-8, 65.4	73.19	4.1	17H-6, 86.2	157.52	2.2
5H-1, 120.1	36.20	2.5	9H-1, 60.5	73.61	12.1	17H-6, 95.7	157.62	1.1
5H-2, 3.7	36.53	2.2	9H-1, 75.2	73.75	2.8	18H-1, 54.3	158.55	4.9
5H-2, 18.2	36.67	3.6	9H-1, 116.1	74.16	2.7	18H-2, 23.3	160.23	4.5
5H-2, 29.6	36.78	7.6	9H-1, 128.1	74.28	2.8	18H-4, 45.2	163.53	5.2
5H-3, 76.4	38.72	4.6	9H-1, 134.9	74.35	2.3	18H-5, 57.7	165.15	1.5
5H-3, 91.5	38.87	2.3	9H-2, 37	74.85	3.3	18H-5, 68.9	165.26	1.1
5H-3, 110.7	39.06	2.4	9H-2, 82.2	75.30	4.6	18H-5, 143.3	166.01	1.0
5H-4, 11	39.55	3.7	9H-2, 88.9	75.36	1.6	18H-6, 25.7	166.31	1.5
5H-4, 17.6	39.61	5.0	9H-2, 100.8	75.48	4.7	18H-6, 105.8	167.12	1.6
5H-4, 88.5	40.32	3.9	9H-2, 112.7	75.60	3.7	18H-6, 110.1	167.16	3.3
5H-4, 122.3	40.66	2.1	9H-3, 11.5	76.07	4.8	18H-7, 12.2	167.69	5.8
5H-5, 32.4	41.24	1.9	9H-3, 20.3	76.16	2.0	19H-1, 10.8	168.11	1.0
5H-6, 23.8	42.63	3.4	9H-3, 24.4	76.20	4.6	19H-1, 15.4	168.15	1.5
5H-6, 33.7	42.73	2.2	9H-3, 33.2	76.29	1.2	19H-2, 4.5	169.56	1.3
5H-6, 47.2	42.86	1.5	9H-3, 58.8	76.55	2.3	19H-2, 11.8	169.63	4.8
5H-6, 51.7	42.91	1.0	9H-3, 66	76.62	1.7	19H-2, 42.1	169.93	1.4
5H-6, 69.9	43.09	2.2	9H-3, 80.1	76.76	4.1	19H-3, 28	171.26	1.2
5H-6, 82.3	43.22	6.2	9H-3, 92	76.88	4.3	19H-3, 80.3	171.79	1.4
5H-6, 97.5	43.37	6.8	9H-4, 12.4	77.56	1.8	19H-5, 135.8	175.37	1.0
5H-6, 139.3	43.79	5.4	9H-4, 20.6	77.64	2.0	19H-6, 83.7	176.34	2.9
6H-1, 2.7	44.53	2.5	9H-4, 48.7	77.92	2.1	20H-1, 11.7	177.62	1.1
6H-1, 21.2	44.71	4.4	9H-4, 100.6	78.44	2.7	20H-1, 28	177.78	4.7
6H-1, 43.8	44.94	9.5	9H-4, 120.5	78.64	2.0	20H-1, 110.9	178.61	1.3
6H-1, 70.5	45.21	2.9	9H-4, 128.3	78.72	2.7	20H-1, 117.7	178.68	9.5
6H-1, 97.8	45.48	15.0	9H-5, 60.5	79.53	1.1	20H-3, 41.3	182.41	7.1
6H-2, 10.9	46.09	11.5	9H-7, 5.4	80.59	1.3	20H-6, 103.3	187.52	1.0
6H-2, 31.5	46.30	5.3	9H-7, 17.3	80.71	1.3	20H-6, 116.3	187.65	2.1
6H-2, 104.8	47.03	3.8	9H-7, 19.5	80.73	1.3	20H-6, 124.7	187.73	1.3

Table 7. (continued).

Top of void within section (cm)	Top of void (mbsf)	Void length (cm)	Top of void within section (cm)	Top of void (mbsf)	Void length (cm)	Top of void within section (cm)	Top of void (mbsf)	Void length (cm)
146-893A-			146-893B-			146-893B-		
21H-1, 7.6	187.08	15.4	4H-3, 145.8	25.75	1.2	6H-3, 98.6	44.29	8.1
21H-1, 103.9	188.04	2.0	4H-4, 23.4	26.02	2.6	6H-3, 124.3	44.54	2.3
21H-2, 36.2	188.46	5.2	4H-4, 53.7	26.32	1.0	6H-3, 139.8	44.70	2.4
21H-2, 148.8	189.58	0.6	4H-4, 98.8	26.77	6.3	6H-4, 18.3	44.97	1.1
21H-3, 41.7	190.20	1.7	4H-5, 54.9	27.83	3.4	6H-4, 28.3	45.07	1.2
146-893B-			4H-5, 87.5	28.15	0.8	6H-5, 21.5	46.49	3.6
1H-1, 65.9	0.66	5.4	4H-6, 6.6	28.84	4.0	6H-5, 27.9	46.56	1.3
1H-CC, 7.3	2.19	1.0	4H-6, 18.4	28.96	1.4	6H-7, 12.3	49.39	2.4
2H-1, 0	2.30	7.7	4H-6, 146.3	30.24	2.4	6H-7, 23.3	49.50	1.2
2H-4, 36.3	7.22	1.0	4H-7, 7.4	30.35	1.1	7H-2, 23.1	51.51	2.8
3H-1, 5.7	11.86	4.2	4H-7, 18.5	30.46	4.8	7H-3, 31.8	53.10	4.9
3H-1, 81.8	12.62	6.9	5H-1, 65.1	31.45	11.4	7H-3, 53.6	53.31	4.7
3H-1, 138.8	13.19	5.2	5H-1, 99	31.79	21.0	7H-3, 62.6	53.40	9.6
3H-3, 114.3	15.61	3.8	5H-1, 122.6	32.03	1.4	7H-3, 95.3	53.73	2.9
3H-4, 83.3	17.12	4.9	5H-2, 3.4	32.34	1.8	7H-4, 7.9	54.35	2.9
3H-4, 97.5	17.26	1.8	5H-2, 28.1	32.59	1.6	8H-1, 13.1	59.40	13.7
3H-4, 145.5	17.74	2.2	5H-2, 49.5	32.80	7.5	8H-1, 37.6	59.68	13.5
3H-5, 10.8	17.89	2.8	5H-2, 62.7	32.94	9.1	8H-1, 58.7	59.89	1.1
3H-5, 31.4	18.09	2.7	5H-2, 73.2	33.04	1.8	8H-1, 70.5	60.01	2.0
3H-5, 49	18.27	2.8	5H-3, 52.1	34.33	1.4	8H-2, 35.5	61.15	43.1
3H-5, 54.6	18.32	1.2	5H-3, 133.3	35.14	1.8	8H-2, 88.1	61.67	46.3
3H-5, 61.7	18.39	2.5	5H-3, 135.7	35.16	1.3	8H-3, 62.5	62.91	5.6
3H-5, 79.2	18.57	6.3	5H-4, 55.5	35.85	3.7	8H-3, 124.7	63.54	1.2
3H-5, 93.9	18.72	9.8	5H-4, 85.5	36.15	7.1	8H-4, 4.6	63.82	2.0
3H-5, 114.9	18.93	7.8	5H-4, 95.9	36.25	6.6	8H-4, 21.8	63.99	1.6
3H-5, 130.6	19.08	3.6	5H-4, 119.8	36.49	1.1	8H-4, 43.5	64.21	2.4
3H-5, 141.2	19.19	3.9	5H-5, 19.6	36.98	5.7	8H-4, 83.7	64.61	4.9
3H-6, 19.1	19.45	6.4	5H-5, 61.5	37.40	2.6	8H-4, 128.1	65.06	12.0
3H-6, 53	19.79	9.1	5H-5, 101.6	37.80	4.8	8H-5, 40.4	65.67	24.6
3H-7, 16.3	20.92	1.1	5H-6, 24.1	38.52	2.3	8H-5, 68.5	65.95	1.2
4H-2, 103.4	23.83	1.7	5H-6, 60.2	38.88	3.0	8H-5, 71	65.97	1.1
4H-2, 120.8	24.00	2.4	5H-6, 109.4	39.37	5.3	8H-6, 78.2	67.54	1.4
4H-3, 127.2	25.57	1.5	5H-7, 27.6	40.03	1.4	8H-6, 131.3	68.07	5.4
4H-3, 130.9	25.60	1.1	6H-3, 34.3	43.64	1.8			
			6H-3, 80.3	44.10	11.9			

Note: Voids may be curated empty or filled with styrofoam.

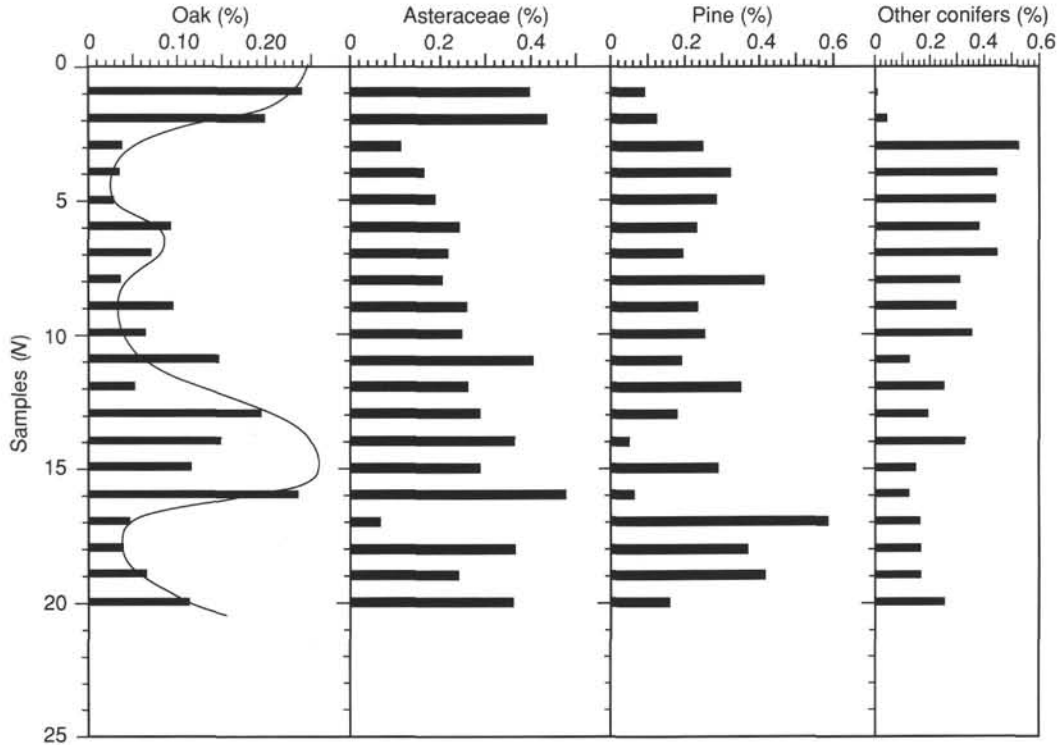


Figure 24. Preliminary pollen data found on examining core-catcher sample from Hole 893A.

Table 8. Depths of tops of sections from Site 893, adjusted by deletion of voids greater than 1 cm.

Core and Section	Depth (mbsf)	Core and Section	Depth (mbsf)	Core and Section	Depth (mbsf)
146-893A-		146-893A-		146-893A-	
1H-1	0	10H-5	88.40	19H-CC	176.65
1H-2	1.48	10H-6	89.88	20H-1	177.50
1H-3	2.99	10H-7	90.67	20H-2	178.84
1H-4	4.50	10H-CC	92.14	20H-3	180.34
1H-5	5.98	11H-1	92.00	20H-4	181.76
1H-CC	6.24	11H-2	93.39	20H-5	183.25
2H-1	6.50	11H-3	94.89	20H-6	184.75
2H-2	8.00	11H-4	96.36	20H-7	186.23
2H-3	9.44	11H-5	97.65	20H-CC	186.76
2H-4	10.86	11H-6	98.41	21H-1	187.00
2H-5	12.22	11H-CC	99.88	21H-2	187.92
2H-6	13.49	12H-1	101.50	21H-3	189.55
2H-7	14.92	12H-2	102.83	21H-4	191.07
2H-CC	15.70	12H-3	104.29	21H-5	192.63
3H-1	16.00	12H-4	105.76	21H-6	194.13
3H-2	17.47	12H-5	107.17	21H-CC	195.24
3H-3	18.97	12H-6	107.63		
3H-4	20.41	12H-7	108.96	146-893B-	
3H-5	21.85	12H-8	109.34	1H-1*	0
3H-6	23.21	12H-CC	110.77	1H-2	1.43
3H-7	24.65	13H-1	111.00	1H-CC	2.07
3H-CC	25.46	13H-2	112.16	2H-1	2.30
4H-1	25.50	13H-3	112.36	2H-2	3.74
4H-2	26.76	13H-4	113.17	2H-3	5.27
4H-3	28.16	13H-5	115.09	2H-4	6.78
4H-4	29.58	13H-6	116.58	2H-5	8.33
4H-5	30.82	13H-7	118.06	2H-6	9.82
4H-6	32.22	13H-8	118.89	2H-7	11.32
4H-7	33.65	13H-CC	119.63	2H-CC	11.87
4H-CC	34.40	14H-1	120.50	3H-1	11.80
5H-1	35.00	14H-2	122.02	3H-2	13.13
5H-2	36.35	14H-3	123.56	3H-3	14.62
5H-3	37.68	14H-4	125.05	3H-4	16.09
5H-4	39.07	14H-5	126.53	3H-5	17.49
5H-5	40.41	14H-6	126.77	3H-6*	18.54
5H-6	41.86	14H-7	126.93	3H-7	19.81
5H-7	43.07	14H-8	128.41	3H-CC	20.34
5H-CC	43.66	14H-9	129.87	4H-1	21.30
6H-1	44.50	14H-CC	130.28	4H-2	22.80
6H-2	45.64	15H-1	130.00	4H-3	24.25
6H-3	46.90	15H-2	131.21	4H-4	25.71
6H-4	48.24	15H-3	132.73	4H-5	27.10
6H-5	49.67	15H-4	134.26	4H-6	28.56
6H-6	51.13	15H-5	135.87	4H-7	29.98
6H-7	52.49	15H-6	137.48	4H-CC	30.73
6H-CC	53.34	15H-7	138.97	5H-1	30.83
7H-1	54.00	15H-CC	139.74	5H-2	31.97
7H-2	54.05	16H-1	139.50	5H-3	33.25
7H-3	55.11	16H-2	140.69	5H-4	34.69
7H-4	56.23	16H-3	142.16	5H-5*	36.00
7H-5	57.56	16H-4	143.80	5H-6	37.36
7H-6	59.03	16H-5	145.33	5H-7	38.73
7H-7	60.49	16H-6	146.85	5H-CC	39.55
7H-8	61.96	16H-7	148.33	6H-1	40.30
7H-CC	62.79	16H-CC	149.18	6H-2	41.80
8H-1	63.50	17H-1	149.00	6H-3	43.30
8H-2	63.65	17H-2	150.46	6H-4	44.52
8H-3	65.08	17H-3	151.99	6H-5	45.99
8H-4	66.07	17H-4	153.54	6H-6	47.43
8H-5	67.22	17H-5	155.11	6H-7	48.93
8H-6	68.68	17H-6	156.60	6H-CC	49.69
8H-7	70.07	17H-7	158.05	7H-1	49.80
8H-8	71.32	17H-CC	158.43	7H-2	51.28
8H-CC	71.96	18H-1	158.50	7H-3	52.75
9H-1	73.00	18H-2	159.95	7H-4	54.02
9H-2	74.25	18H-3	161.40	7H-5	55.48
9H-3	75.55	18H-4	162.98	7H-6*	56.97
9H-4	76.78	18H-5	164.43	7H-7	58.13
9H-5	78.13	18H-6	165.88	7H-CC	58.99
9H-6	79.58	18H-7	167.32	8H-1	59.30
9H-7	79.74	18H-CC	167.74	8H-2	60.49
9H-8	81.12	19H-1	168.00	8H-3	61.09
9H-CC	82.01	19H-2	169.49	8H-4	62.51
10H-1	82.50	19H-3	170.88	8H-5	63.77
10H-2	83.87	19H-4	172.40	8H-6	65.00
10H-3	85.35	19H-5	173.88	8H-7	66.42
10H-4	86.92	19H-6	175.36	8H-CC	67.24

Note: The 3-cm paleontological whole rounds taken routinely from core catchers (CC) and the 10-cm interstitial water whole rounds taken from alternate cores in Hole 893B (denoted by asterisks) are not treated as voids in this compilation, although no material remains in liner.

from glacial maxima (e.g., *Gyroidina*, *Oridorsalis*, *Pullenia*, and *Pyrgo*) are dominated by assemblages typical of well-oxygenated bottom waters. Intermediate assemblages (including *Uvigerina*) are also evident in the core-catcher materials. It should be possible to develop a ranking of benthic foraminifer assemblages from those characteristic of very low to high oxygenated bottom waters in the Santa Barbara Basin. Studies of these assemblage changes during the late Quaternary will form a useful foundation for many other investigations, especially those related to organic carbon preservation and alteration and sedimentary environments. For example, abundant assemblages of *Bolivina* spp. are commonly associated with distinctly laminated sediment intervals, whereas well-oxygenated benthic assemblages are associated with sediments that are nonlaminated and homogenized.

Benthic foraminifer assemblages associated with sand layers are typically transported from shelf (neritic) and upper slope (upper bathyal) environments.

Pollen Assemblages

Pollen samples are dominated by oak in interglacial episodes and conifers in glacial episodes (Fig. 24). Conifer-dominated assemblages lack coastal redwood (*Sequoia*) and western hemlock. This indicates that the conifers that dominated the coastal areas of Santa Barbara during glacial episodes were not simply southern biogeographic extensions of the coastal redwood forests of present-day northern California and Oregon.

REFERENCES*

- Baumgartner, T.R., Ferreira-Bartrina, V., Cowen, J., and Soutar, A., 1991. Reconstruction of a twentieth century varve chronology from the central Gulf of California. In Dauphin, P., and Simoneit, B. (Eds.), *The Gulf and Peninsular Province of the Californias*. AAPG Mem., 47:603-616.
- Baumgartner, T.R., Michaelsen, J., Thompson, L.G., Shen, G.T., Soutar, A., and Casey, R., 1989. The recording of interannual climatic change by high-resolution natural systems: tree-rings, coral bands, glacial ice layers, and marine varves. In Peterson, D.H. (Ed.), *Aspects of Climate Variability in the Pacific and the Western Americas*. U.S. Geol. Surv., Geophys. Monogr., 55:1-14.
- Baumgartner, T.R., Soutar, A., and Ferreira-Bartrina, V., 1992. Reconstruction of the history of the Pacific sardine and northern anchovy populations over the past two millennia from sediments of the Santa Barbara basin, California. *Calif. Coop. Oceanic Fisheries Invest. Rep.*, 33:24-40.
- Bernhard, J.M., and Reimers, C.E., 1991. Benthic foraminiferal population fluctuations related to anoxia: Santa Barbara basin. *Biogeochemistry*, 15:127-149.
- Brandma, D., Lund, S.P., and Henyey, T.L., 1989. Paleomagnetism of Late Quaternary marine sediments from sediments from Santa Catalina basin, California continental borderland. *J. Geophys. Res.*, 94:547-564.
- Douglas, R., 1981. Paleocology of continental margin basins: a modern case history from the borderland of Southern California. In Douglas, R., Gorsline, D., and Colburn, I. (Eds.), *Depositional Systems of Active Continental Margin Basins*. Soc. Econ. Paleontol. Mineral., Pacific Sect., Short Course, 121-156.
- Drake, D.E., Kolpack, R.L., and Fischer, P.J., 1972. Sediment transport on the Santa Barbara-Oxnard shelf, Santa Barbara Channel, California. In Swift, D.J.P., Duane, D.B., and Pilkey, O.H. (Eds.), *Shelf Sediment Transport*: Stroudsburg, PA (Dowden, Hutchinson, and Ross), 307-331.
- Dunbar, R.B., 1981. Sedimentation and the history of upwelling and climate in high fertility areas of the Northeastern Pacific Ocean [Ph.D. dissert.]. Univ. of California, San Diego.
- , 1983. Stable isotope record of upwelling and climate from Santa Barbara basin, California. In Thiede, J., and Suess, E. (Eds.), *Coastal Upwelling, its Sediment Record. Part B: Sedimentary Records of Ancient Coastal Upwelling*: New York (Plenum) 217-246.

* Abbreviations for names of organizations and publication titles in ODP reference lists follow the style given in *Chemical Abstracts Service Source Index* (published by American Chemical Society).

- Emery, K.O., and Hülsemann, J., 1960. The relationships of sediments, life and water in a marine basin. *Deep-Sea Res. Part A*, 165–180.
- Enfield, D.B., and Allen, J., 1980. On the structure and dynamics of monthly mean sea level anomalies along the Pacific Coast of North and South America. *J. Phys. Ocean.*, 10:557–578.
- Eppley, R.W. (Ed.), 1986. Plankton Dynamics of the Southern California Bight. *Lect. Notes Coastal Estuarine Stud.*, 15.
- Fleischer, P., 1972. Mineralogy and sedimentation history, Santa Barbara Basin, California. *J. Sediment Petrol.*, 42:49–58.
- Grant, C.W., 1991. *Distribution of bacterial mats (Beggiatoa spp.) in Santa Barbara Basin, California: a modern analog for organic-rich facies of the Monterey Formation* [M.S. thesis]. California State Univ., Long Beach.
- Hamilton, E.L., 1976. Variations of density and porosity with depth in deep-sea sediments. *J. Sediment. Petrol.*, 46:280–300.
- Heusser, L.E., 1978. Marine pollen in Santa Barbara, California: a 12,000 year record. *Geol. Soc. Am. Bull.*, 89:673–678.
- Hickey, B.M., 1992. Circulation over the Santa Monica–San Pedro Basin and Shelf. In Small, L.F. (Ed.), *Progress in Oceanography*: Oxford (Pergamon Press), 37–115.
- Imbrie, J., and Kipp, N.G., 1971. A new micropaleontological method for paleoclimatology: application to a late Pleistocene Caribbean core. In Turekian, K.K. (Ed.), *The Late Cenozoic Glacial Ages*: New Haven (Yale Univ. Press), 71–181.
- Junger, A., 1979. Northern Channel Islands, California. Miscellaneous Field Studies. *U.S. Geol. Surv.*, Map MF-991.
- Keigwin, L.D., and Jones, G.A., 1990. Deglacial climatic oscillations in the Gulf of California. *Paleoceanography*, 5:1009–1023.
- Kennedy, J.A., and Brassell, S.C., 1992a. Molecular records of twentieth century El-Niño events in laminated sediments from the Santa Barbara basin. *Nature*, 357:62–64.
- , 1992b. Molecular stratigraphy of the Santa Barbara basin: comparison with historical records of annual climate change. *Org. Geochem.*, 19:235–244.
- King, R., Banerjee, S.K., Marvin, J., and Ozdemir, O., 1982. A comparison of different magnetic methods for determining the relative grain size of magnetite in natural materials: some results from lake sediments. *Earth Planet. Sci. Lett.*, 59:404–419.
- Kolpack, R.L., 1971. Oceanography of the Santa Barbara Channel. In Kolpack, R.L. (Ed.) *Biological and Oceanographical Survey of the Santa Barbara Channel Oil Spill 1969–1970* (Vol. 2): Los Angeles (Allan Hancock Found., Univ. of Southern California), 90–180.
- Lange, C.B., Berger, W.H., Burke, S.K., Casey, R.E., Schimmelmann, A., Soutar, A., and Weinheimer, A.L., 1987. El Niño in Santa Barbara basin: diatom, radiolarian, and foraminiferan responses to the 1983 El Niño event. *Mar. Geol.*, 78:153.
- Lange, C.B., Burke, S.K., and Berger, W.H., 1990. Biological production off southern California is linked to climatic change. *Climate Change*, 16:319–329.
- Lee, H.J., 1982. Bulk density and shear strength of several deep-sea calcareous sediments. In Demars, K.R., and Chaney, R.C. (Eds.), *Geotechnical Properties, Behavior, and Performance of Calcareous Soils*. ASTM Spec. Tech. Publ., 777:54–78.
- Lund, S.P., Gorsline, D.L., and Henyey, T.L., 1992. Rock magnetic characteristics of surficial sediments from the California continental borderland. *Earth Planet. Sci. Lett.*, 108:93–107.
- Lutze, G.F., 1964. Statistical investigations on the variability of *Bolivina argentea* Cushman. *Contrib. Cushman Found. Foraminiferal Res.*, 15:105–116.
- Mayer, L.A., 1979. Deep sea carbonates: acoustic, physical, and stratigraphic properties. *J. Sediment. Petrol.*, 49:819–836.
- McGowan, J.A., 1984. The California El Niño. 1983. *Oceanus*, 27:48–51.
- Namias, J., 1969. Use of sea-surface temperature in long-range predictions. WMO Technical Note 103. In *Sea-Surface Temperatures*. World Meteorological Organization, 247:1–18.
- Pisias, N.G., 1978. Paleooceanography of the Santa Barbara basin and the California Current during the last 8000 years. *Quat. Res.*, 10:366–384.
- , 1979. Model for paleoceanographic reconstructions of the California Current during the last 8000 years. *Quat. Res.*, 11:373–369.
- Reimers, C.E., Lange, C.B., Tabak, M., and Bernhard, J.M., 1990. Seasonal spillover and varve formation in the Santa Barbara Basin, California. *Limnol. Oceanogr.*, 35:1577–1585.
- Schimmelmann, A., Lange, C.B., and Berger, W.H., 1990. Climatically controlled marker layers in Santa Barbara basin sediments, and fine-scale core-to-core correlation. *Limnol. Oceanogr.*, 35:165–173.
- Schimmelmann, A., Lange, C.B., Berger, W.H., Simon, A., Burke, S.K., and Dunbar, R.B., 1992. Extreme climatic conditions recorded in Santa Barbara basin laminated sediments: the 1835–1840 *Macoma* Event. *Mar. Geol.*, 106:279–299.
- Schimmelmann, A., and Tegner, M.J., 1991. Historical oceanographic events reflected in $^{13}\text{C}/^{12}\text{C}$ ratio of total organic carbon in Santa Barbara basin sediment. *Global Biogeochem. Cycles*, 5:173–188.
- Sholkovitz, E.R., and Gieskes, J.M., 1971. A physical-chemical study of the flushing of the Santa Barbara Basin. *Limnol. Oceanogr.*, 16:479–489.
- Sholkovitz, E.R., and Soutar, A., 1975. Changes in the composition of the bottom water of the Santa Barbara basin: effect of turbidity currents. *Deep-Sea Res. Part A*, 22:13–21.
- Soutar, A., 1975. Historical fluctuations of climate and bioclimatic factors as recorded in varved sediment deposits in a coastal sequence. *Proc. WMO/IAMAP Symp. Long-term Climatic Fluctuations*. World Meteorological Organization, 421:147–158.
- Soutar, A., and Crill, P.A., 1977. Sedimentation and climatic patterns in the Santa Barbara Basin during the 19th and 20th centuries. *Geol. Soc. Am. Bull.*, 88:1161–1172.
- Soutar, A., Johnson, S.R., and Baumgartner, T.R., 1981. In search of modern depositional analogs to the Monterey Formation. In Garrison, R.E., and Douglas, R.E. (Eds.), *The Monterey Formation and Related Siliceous Rocks of California*. Spec. Publ.—Soc. Econ. Mineral. Paleontol., Pacific Sect., 123–148.
- Thornton, S.E., 1981. Suspended sediment transport in surface waters of the California Current off southern California: 1977–78 floods. *Geo-Mar. Lett.*, 1:23–28.
- , 1984. Basin model for hemipelagic sedimentation in a tectonically active continental margin: Santa Barbara Basin, California continental borderland. In Stow, D.A.V., and Piper, D.J.W. (Eds.), *Fine-grained Sediments*. Geol. Soc. Spec. Publ. London, 15:377–394.
- Weinheimer, A.L., Carson, T.L., Wigley, C.R., and Casey, R.E., 1986. Radiolarian responses to recent and Neogene California El Niño and anti-El Niño events. *Palaeogeogr., Palaeoclimatol., Palaeoecol.*, 53:3–25.

Ms 1461R-024

NOTE: For all sites drilled, core-description forms (“barrel sheets”) and core photographs can be found in Section 3, beginning on page 53.